


5-2014

Analysis of Environmental Influences on Dressed Stone Decay: a Case Study of Tafoni Development on a Hewn Djinn Block in Petra, Jordan

Kaelin M. Groom

University of Arkansas, Fayetteville

Follow this and additional works at: <http://scholarworks.uark.edu/etd>

 Part of the [Cultural Resource Management and Policy Analysis Commons](#), [Geography Commons](#), and the [Geomorphology Commons](#)

Recommended Citation

Groom, Kaelin M., "Analysis of Environmental Influences on Dressed Stone Decay: a Case Study of Tafoni Development on a Hewn Djinn Block in Petra, Jordan" (2014). *Theses and Dissertations*. 2306.
<http://scholarworks.uark.edu/etd/2306>

This Thesis is brought to you for free and open access by ScholarWorks@UARK. It has been accepted for inclusion in Theses and Dissertations by an authorized administrator of ScholarWorks@UARK. For more information, please contact scholar@uark.edu, ccmiddle@uark.edu.

Analysis of Environmental Influences on Dressed Stone Decay:
A Case Study of Tafoni Development on a Hewn Djinn Block in Petra, Jordan

Analysis of Environmental Influences on Dressed Stone Decay:
A Case Study of Tafoni Development on a Hewn Djinn Block in Petra, Jordan

A thesis submitted in partial fulfillment
of the requirements for the degree of
Master of Science in Geography

by

Kaelin Groom
University of Colorado Denver
Bachelor of Arts in Geography, 2012

May 2014
University of Arkansas

This thesis is approved for recommendation to the Graduate Council

Dr. Thomas Paradise
Thesis Chair

Dr. John Dixon
Committee Member

Dr. George Sabo III
Committee Member

Abstract

Petra, Jordan captivates tourists and researchers with its dramatic sandstone cliffs, Nabatean, Roman, Byzantine and Roman architecture, and rich cultural heritage. However, increasing tourism in the valley is exacerbating stone degradation and complicating heritage management. This research analyzed environmental influences on dressed stone decay via tafoni development and evaluating cell evolution on an isolated hewn feature, known as Djinn Block X. Resembling other sandstone blocks found in the area, this irregular sandstone monument exhibits faces ranging in size from 2.5m by 3.5m to 3.9m to 4.2m (29m perimeter). Protruding features, incisions along the top, and a large platform attached to the northern face suggests this monument was ritualistic or unfinished.

Over twenty morphometric and micrometeorologic variables were measured for the ten largest and smallest tafoni cells per face. Data were examined and analyzed statistically, photographically, and cartographically. A mirrored-value-aspect matrix was created to reveal statistical relationships between aspect and detailed measurements including cell depth, average diameter, estimated volume, surface temperatures, ambient temperature, and humidity. Results supported field observations displaying greatest decay on the southern and northern faces with r^2 values as high as 0.157 at 144°N for cell volume (total material lost). Moreover, morphometric data exhibited episodic spikes in cell growth, both by depth and diameter, supporting a possible threshold response explanation. These findings challenge steady-rate decay models and represent major implications for rock decay and tafoni research, as well as cultural stone assessment. Furthermore, Geomorphologic research such as this provides policy-makers information necessary to improve conservation efficacy for crucially sensitive heritage sites.

Keywords: *tafoni, threshold response, Petra, Djinn Block X, cultural stone decay, sandstone*

©2014 by Kaelin Groom
All Rights Reserved

Table of Contents

| | | |
|-------|--|-----|
| I. | Introduction | 1 |
| II. | Site Setting | 5 |
| | a. Hashemite Kingdom of Jordan | 5 |
| | b. The Lost Kingdom of Petra | 8 |
| | c. Nabatean Monuments and Architecture | 16 |
| III. | Literature Review | 27 |
| | a. Geomorphologic Theory and Weathering | 27 |
| | b. Regional Geomorphology | 37 |
| | c. Geomorphology and Cultural Resources Management | 40 |
| IV. | Methods | 44 |
| | a. Aspect as Proxy for Insolation and Environmental Conditions | 44 |
| | b. Tafoni Morphometry and Micrometeorology | 45 |
| | c. Assumptions and Limitations | 47 |
| V. | Results and Analysis | 51 |
| | a. Tafoni Morphometry Analysis | 51 |
| | b. Microenvironments and Micrometeorology | 55 |
| VI. | Discussion | 61 |
| | a. Insolation and Rock Decay Patterns | 61 |
| | b. Microclimate, Environment, and Aspect | 71 |
| | c. Tafoni Morphometry and Threshold Modeling | 77 |
| VII. | Conclusions and Implications | 91 |
| VIII. | References | 96 |
| IX. | Appendices | 110 |

Chapter One: Introduction

Hewn from colorful sandstone cliffs, the ruined city of Petra, Jordan hosts an extensive array of Nabatean-Roman-Byzantine-Crusader monuments representing rich local and regional cultural heritage and is, regrettably, in perpetual risk of decay. International notoriety of this ancient city, especially after gaining the prestigious designation *UNESCO World Heritage Site* in 1985, has dramatically increased tourist activity, making it one of Jordan's most visited historic sites (PTN 2013). Unfortunately, intense foot traffic through the valley threatens to exacerbate stone degradation faster than heritage management can allocate appropriate resources to arrest decay (Paradise, 2005, 2010). Multidisciplinary in nature, effective stone conservation depends on a functional symbiotic relationship between cultural resource management and geomorphologic researchers (Dorn et al., 2008; Allen & Groom, 2013)(Figure 1.1). Rock decay, or weathering, analyses on cultural stone can provide management with material evidence needed to optimize conservation policies while also giving researchers the unique opportunity to

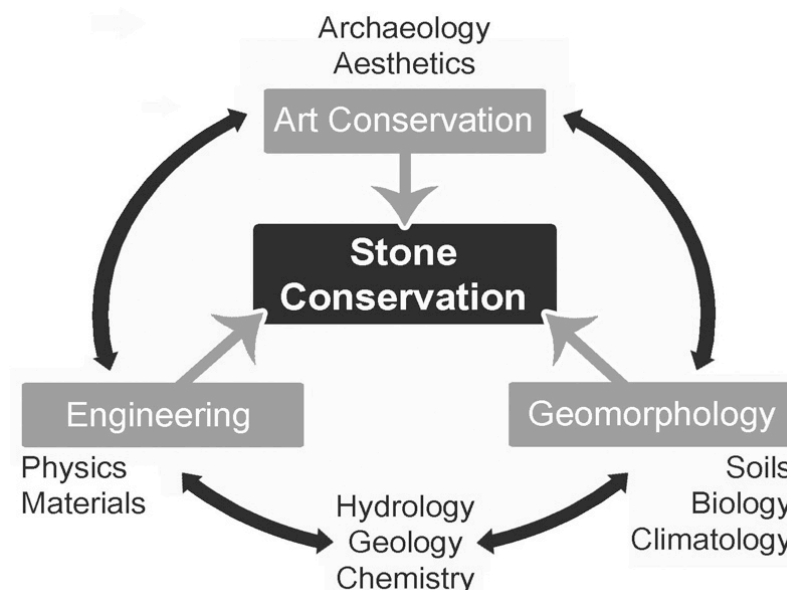


Figure 1.1 – Graphic showing the interdisciplinary nature of stone conservation. Diagram modified from Pope et al. (2002).

work within contextually controlled parameters not available for unaltered “natural” stone (Pope et al., 2002). Employing this collaborative model in Petra, this research investigated tafoni development as a proxy for overall deterioration on an isolated hewn monument, Djinn Block X, with the following objectives:

- *Determine aspect-dependent (insolation) patterns of cultural stone decay*
- *Assess environmental influences on the development of cavernous decay*
- *Develop an empirically-based threshold model for tafoni evolution*

The complexity of cultural stone decay requires a quantifiable surrogate measure, therefore specific rock decay features known as tafoni, or cavernous decay, were chosen due to their polygenetic nature. Physical (e.g. Mol & Viles, 2010), chemical (e.g. McBride & Picard, 2000), and biological (e.g. Mottershead et al., 2003) decay processes have all been associated with tafoni formation, so cell development suggests at least one of these processes is impacting the substrate. Therefore, measurements of tafoni cell morphometry, distribution, and environmental characteristics could be used to quantify the severity of multiple, possibly simultaneous, processes deteriorating Djinn Block X, and as an extension, the city of Petra.

While geomorphologic methods and techniques cannot directly prevent the deterioration of cultural stone, they can identify primary causes of decay and provide policy-makers the information required to strategically distribute conservation resources and concentrate efforts where they are needed most. For instance, advanced understanding of insolation patterns and the recognition of spatial and environmental disparity of rock decay allows stone conservators and heritage management to effectively identify monuments at greater risk (Paradise, 1999; Smith et al., 2008; see also Figure 1.1). Also, architects may consider placement and exposure in regards to longevity and conservation when designing monuments and landmarks (Smith et al., 2008;

Doehne & Price, 2010). In fact, geomorphologic studies have worked in tandem with heritage management for a number of cultural sites including rock art (e.g. Allen & Groom, 2013), temples (e.g. Achyuthan et al., 2010), historic buildings (e.g. Mottershead et al., 2003), and even multiple studies in Petra (e.g. Paradise, 1999, 2010), including a preliminary study of surface recession on Djinn Block X (Paradise, 2013).

The multifaceted construction of this research benefits cultural heritage management through empirical environmental analyses to better distribute conservation efforts, but also contributes to geomorphologic knowledge by revealing morphometric patterns in tafoni development. Tafoni genesis investigations are often segregated into physical (e.g. Mol & Viles, 2010) and chemical processes (e.g. McBride & Picard, 2000; Sunamura, 1996), but the two are not necessarily discretely separable (e.g. Brandmeier et al., 2010; Paradise, 2012). This research provides additional justification, including threshold modeling, for a multi-process approach to the investigation of this still enigmatic decay phenomena. In addition, measured cell interior volumes serve as an estimation of total material lost as well as a comparable representation of age, accepting the assumption that space is equivalent to time (i.e. larger cells are older cells)(Schumm, 1979). This added temporal component is critical for modeling cell initiation, growth, and general tafoni evolution.

Furthermore, morphometric data exhibit periodic spurts in growth possibly supporting threshold modeling for tafoni evolution. Existing models include linear (e.g. Huinink et al., 2004), non-linear exponential (e.g. Sunamura, 1996), log-normal (e.g. Norwick & Dexter, 2002), and S-shaped (e.g. Sunamura & Aoki, 2011), but none of these consider the concepts of thresholds beyond initiation lag times. Paradise (1999) identified compositional thresholds in sandstone weathering within the city of Petra but not specifically related to tafoni. Elaborating on

these studies, this research applied threshold response theory to tafoni evolution to create a visual model of growth using empirical data collected from Djinn Block X in Petra, Jordan. While this model is non-mathematical, its significance rests in representing a new approach to tafoni development and threshold-based stages of decay.

Overall, this study outlines the geographical and morphometric concepts involved in tafoni development on Djinn Block X as a case study for overall cultural stone decay in Petra, Jordan. After describing the importance of the study site's physical and cultural landscape interaction, an in-depth review of relevant literature is offered, including:

- *Geomorphologic Theory and Weathering*
- *Regional Geomorphologic Research*
- *Geomorphology and Cultural Resource Management*

An explanation of field and data collection methods are then offered, followed by an outline of statistical, photographic, and cartographical techniques employed. After which, meaningful relationships are quantitatively identified and their significances discussed in detail, incorporating assumptions and limitations. Finally, a succinct conclusion addresses the innovation of this study's threshold-based tafoni genesis model and potential morphometric research applications to cultural stone decay and heritage management efficacy.

Chapter Two: Site Setting

The ancient city of Petra, Jordan represents a unique field study location. Factors such as its extended occupational history, intricate stone dressings, and distinct petrology contribute to cultural stone deterioration but also provide context for comprehensive studies of rock decay phenomena, such as tafoni and cavernous decay. In the case of Petra, examination of broader environments and historic backgrounds illuminates the complexity of the city. This subchapter discusses the various scalar, temporal, and geographical elements influencing the “Rose Red City” and the degradation of its irreplaceable sandstone monuments.

2.1 Hashemite Kingdom of Jordan

Sharing its borders with Saudi Arabia to the south and east, Iraq and Syria to the north, and Israel and the West Bank to the west, Jordan occupies roughly 89,200 squared kilometers in the northwestern neck of the Arabian Peninsula (Al-Jaloudy, 2006)(Figure 2.1). With a steadily



Figure 2.1 – Political map of the Hashemite Kingdom of Jordan and surrounding countries. Modified from Paradise (2013). Cartography by K. Groom (2013).

growing population the sprawling capital city of Amman, once the Classical city Philadelphia, represents a cultural, economic, and political hub of the nation. Jordan's landscapes, both cultural and physical, have unique attributes influencing tourism, heritage management, and cultural stone decay.

2.1.1 Cultural Geography of Jordan

Formally established in 1946, the Hashemite Kingdom of Jordan is a parliamentary monarchy currently ruled by King Abdullah II and his wife Queen Rania. As a former British mandate, Jordan has enjoyed relative stability in a notoriously unsettled part of the world. The massive influx of Palestinian, Iraqi, and Syrian refugees over the past decades has, however, put a considerable strain on the Jordanian government and economy. Fortunately, the country has attempted to incorporate this new population into everyday workings through resettlement projects and international funding (Chatelard, 2010).

Since gaining independence in the aftermath of World War II, the Jordanian economy has enjoyed constant growth and development, primarily concentrated in agriculture, industry, and services. New technologies in irrigation and advanced water conservation methods have allowed Jordan to establish a fairly healthy agriculture sector (Ramrez et. al., 2009). Large industries have also flourished in the kingdom, particularly around mineral petroleum refining (Jaber et. al., 2001). Jordan has scarce natural resources but compensates through symbiotic relations with their heavy oil-producing neighbors.

Jordan's limited resources necessitate the development of a service-based market. Consisting mainly of government, transportation, communication, financial services, and tourism, the service vector dominates the economy earning an estimated 72% of the kingdom's

GDP (MoIT & UNCTAD, 2003). In 1997, the kingdom approved the Charter of the Jordan Tourism Board and effectively began promoting itself as a tourism center in the Middle East. However, Jordan's popular destinations, like Petra, now have economies overwhelmingly dependent on tourism. While UNESCO involvement has helped maintain some historic integrity, it also promotes the prime tourist destinations in the Middle East and draws visitors from all reaches of the world. This popularity increases funding but the constant influx of people can have profound and often detrimental impacts on monuments (e.g. Paradise, 1995; Heinrichs, 2008) and rock decay remains a serious concern for resource management and the Jordanian Department of Antiquities.

2.1.2 Physical Geography of Jordan

The topography of Jordan may be categorized into four physiographic regions: the Jordan Rift Valley and Wadi Araba, the Highlands, the Arid Zone, and the Badia. Extending from Lake Tiberius (Galilee – Kinneret) to the Gulf of Aqaba, the deep Jordan Rift Valley and Wadi Araba represents the western border of the Arabian Plate (Figure 2.2). While the Wadi Araba, south of the Dead Sea, is extremely arid and deserted, the Jordan Rift Valley to the north is the country's primary agricultural region with Mediterranean climate characteristics and steady surface and ground-water supplies. Tectonic uplifting created the Highlands just East of the rift valley, a geologically diverse landscape including the Ajloun mountain range, the hills of Ammon and Moab, along with the Edom Mountains. The southern and eastern plains flatten into the desert Arid Zone and Badia with sporadic sandstone inselbergs and exposed Precambrian igneous basements, like those found in the Wadi Rum UNESCO World Heritage/Natural Site (Bender, 1975; Osborn & Duford, 1981).

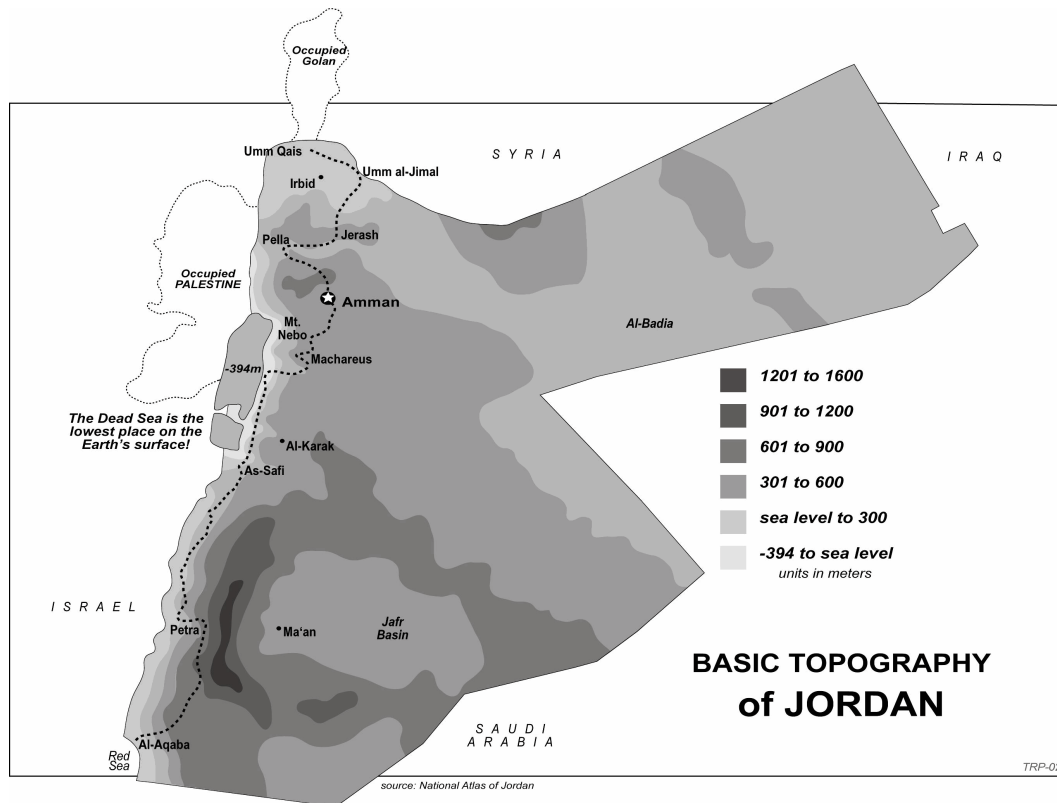


Figure 2.2 – Map of the basic topography of Jordan. Note the highlands surrounding Petra in the southwestern region of the country leading to the Wadi Araba (Paradise, 1999).

Product of the variability of Jordan’s geology and climate, the kingdom hosts a myriad of soil taxonomies and great groups depending on the moisture regimes in which they develop. The two prominent moisture regimes in Jordan are xeric and torric (or aridic), however, the relatively wetter xeric moisture regimes are restricted to the northern regions of the Jordan Rift Valley. The soils found across Petra are aridisols created under torric conditions (Al-Qudah, 2001).

2.2 The Lost Kingdom of Petra

Located at 30.3286° N and 35.4419° E, the city of Petra lies in the mountainous region on the western skirts of the Wadi Araba leading into the eastern desert. The vacant monuments hewn into the cliff faces and built in the valley represent a long occupational history only made

possible by the steep protective cliffs and unique environment (Figure 2.3). Cultural resources management in Petra must keep a delicate balance between conserving its irreplaceable landmarks while simultaneously promoting tourism and international participation. Therefore, both physical *and* cultural characteristics of the city relate to cultural stone decay and its influences.

2.2.1 History of Petra

While there is discussion that Petra is the lost biblical land of Edom, the first recorded occupants were the Nabateans beginning around 580 B.C. (Browning, 1973). Theirs is also the primary culture associated with city, often called The Lost Kingdom of the Nabatean Empire. Originally nomadic, Nabateans were the first to hew tombs, living quarters, and monuments into the cliff faces. In order to sustain permanent residence, they engineered ingenious waterways and systems consisting of dams, cisterns, weirs, and piping throughout the city to maintain water

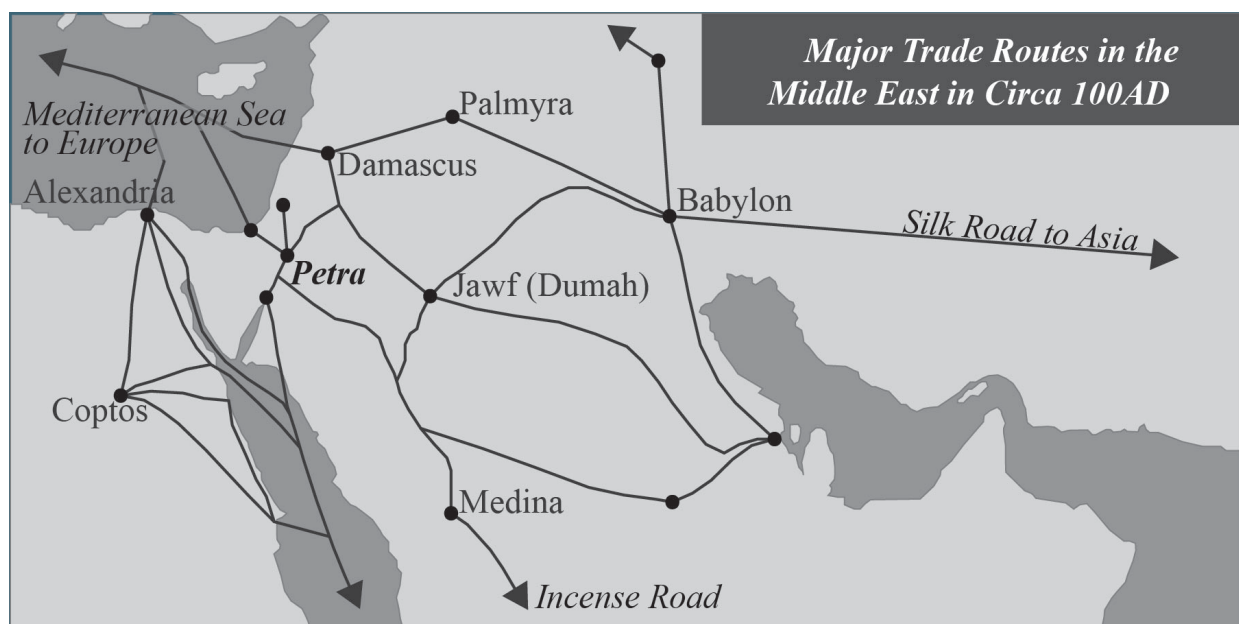


Figure 2.4 – Map of Trade routes throughout the region during the height of the Nabatean Empire showing Petra's central trade location. Cartography by K. Groom (2013).

supply, many of which can still be found today (Ortloff, 2005). City walls were also erected for added security, though the steep cliffs and narrow passes also lent the city a natural safety. With the promise of water and protection, Petra became a vital stop for caravans and traders traversing the brutal Arabian Desert and the city thrived as a central trade hub (Figure 2.4).

Eventually, a number of cultures and ethnicities became integrated into the city and this social nexus is evident in the Hellenistic influences on Nabatean art and architecture. Despite the Nabateans' lack of military strength, they were able to maintain independence well into Roman annexation through bribes and politics. It wasn't until 106 CE that the Romans claimed the Nabatean Empire as their own "Arabia Petrea" and the city was redesigned to fit Roman standards (Fiema, 2003). The city continued to flourish under the Romans and during the height of Petra's Roman occupation there were upwards to 30,000 people living in the city in this new client status within the expansion of the Roman Empire (Fiema, 2003).

With the gradual northern shift of major trade routes to Roman cities like Jerash and Palmyra and increasing sea trade around the Arabian Peninsula, Petra's economy slowly began to weaken until 363 CE, when a massive earthquake, possibly followed by a catastrophic flood, devastated the city (Paradise, 2012). Afterwards, it is unclear how many people remained in Petra but a few Byzantine structures and architectural influences suggest at least some degree of human activity, as is evident by the free standing Byzantine church discovered in the main valley in 1991 (Fiema et al., 2001). Some scholars claim Petra was actually the seat of a Byzantine Bishopric (Browning, 1973) and several monuments were modified to fit Christian needs, such as the Urn Tomb's conversion to a church (Paradise, 2010). Then, in 1095 CE, Pope Urban II initiated the first crusade and within five years the Crusader Kingdom was fairly well established in the region with Petra sitting on its eastern border. Strategically situated, occupancy of Petra

benefited military purposes but was limited to only a few forts in the area, primarily the mountain fort Al-Habis within the main valley and the larger fortress of Al-Wu'aira nearby (Hammond, 1970). With the fall of the Crusader Kingdom in 1191 CE, Petra fell into obscurity (Browning, 1973).

Lost to the western world, Petra lay in waiting for several centuries until 1812 when it was rediscovered by Swiss explorer Johann Ludwig Burckhardt (1784 – 1817). Although his writings on the city weren't officially published in Europe until 1829 (Browning, 1973), word of his discovery spread quickly and by the 1820s other explorers and artists were already traveling to the grand city. Early representations of Petra by artists such as David Roberts (1796 – 1864) and Léon de Laborde (1807 – 1869) produced during these first visits are now considerably valuable, often selling for several thousands of dollars at auction (Christie's Auctioneers)(Figure 2.5). Visitors to Petra remained minimal for decades, limited by access, funds, and social and political instability in the region (Browning, 1973). A major turning point for Petra came December 1985: inscription into the United Nations Educational, Scientific, and Cultural Organization's (UNESCO) World Heritage Conservation program. Nominated by the



Figure 2.5 – Examples of David Roberts' artwork from Petra: El Deir, Petra, 1839 (left) and Conference of Arabs at Wady Moosa, Petra, 1839 (right)(United States Library of Congress, 2014).

International Council on Monuments and Sites (ICOMOS) as an irreplaceable archaeological site, Petra gained the esteemed distinction “Cultural Heritage Site” during the World Heritage Committee’s Ninth Ordinary Session (whc.unesco.org). This has given Jordan the resources and prestige to both maintain and promote Petra as a cultural resource, effectively turning the once lost Nabatean Capital and its gateway town of Wadi Musa into the country’s most visited tourist attraction with nearly a million visitors in 2010 (PNT 2013).

Although Petra had been forgotten by the western world, it is unlikely that it was ever completely deserted, as local nomadic Bedouins sought shelter in the ruins and made use of the water entrapments left from grander days (Russell, 1993). Primarily goat herders and temporary farmers, the Bedouins usually live in easily transported goat hair tents but the stone sanctuary of Petra was a welcomed retreat (Simms & Russell, 1997). A few tribes in particular, the Beduls, Amarine, and Nawafleh, have intimate relationships with Petra, inhabiting the valley and surrounding regions long before Burckhardt arrived (Simms & Russell, 1997). However, the site’s induction in the UNESCO World Heritage program and the subsequent tourism boom dramatically impacted the Beduls’ way of life. No longer permitted to live in the valley, the Beduls were relocated to the government-built town of Umm Sayhoun on a plateau above Petra proper (Bienkowski & Chlebik, 1991). The forced transition from a nomadic to sedentary lifestyle has been complicated, and the settlement has limited grazing land for goats or other traditional livestock (Angel, 2011). Later installments of roads leading back to Petra allow local Bedouins and Jordanians a livelihood of selling souvenirs, refreshments, and guided tours (Russell, 1993).

2.2.2 Physical Geography of Petra

Often called “The Valley of the Crescent Moon”, the dramatic Valley of Petra has a distinctive curve that resembles a crescent when seen from above. At an elevation of 900-1000m above sea level, Petra is in the transition zone between the more temperate Highlands and the harsh desert of the Wadi Araba. Petra’s climate can be categorized as a Mid-Latitude Dry Semiarid Steppe, specifically a *BSk* in the Köppen Classification, although the cool, wet winters and hot, dry summers often resemble a Mediterranean climate (Cordova, 2007). In Petra, average temperatures range from 6°-12°C in the winter months to 15°-32°C in the summer with less than 130 mm average annual precipitation (Jordanian Meteorological Division, 1971)(Figure 2.6). Repeated theft of monitoring equipment has discouraged the collection of any current long-term meteorological data.

As part of the Northern Araba Drainage Basin, Petra is located in a valley surrounded by steep sandstone cliffs fed by slender canyons (siqs) and a myriad of wadis, or ephemeral streams, that run through the city center (Figure 2.3). Prone to flash floods, the namesake Wadi Musa is dangerous during storms and many precautions are taken during rainier winter seasons, especially in the narrow entrance of the Bab As-Siq, where 20 tourists drowned in a major flashflood in 1963 (Al-Weshah & El-Khoury, 1999). In fact, it has been speculated that Petra has experienced one or more catastrophic flood events in recent history, as indicated by large flood deposits discovered significantly above known water channels (Paradise, 2010). Other major drainages in Petra include the eastern Wadi ed-Mataha and Wadi Turkmaniyya from the north. Numerous other smaller wadis weave throughout the valley, which, with the aid of water

entrapments and dams, allowed people to reside in the city for several hundreds of years (Browning, 1973).

However, the most noticeable physical characteristic of Petra is also one of the most alluring: its striking sandstone cliffs. Along with the eclectic architecture and hewn monuments, the unique geology mesmerizes visitors and researchers alike. Displaying some of the oldest exposed sandstone on earth, Petra exists at the contact of two siliciclastic components of the Ram Group: the Cambrian Umm Ishrin Sandstone at the base and the Ordovician Disi Sandstone above. The Umm Ishrin Formation is a quartz arenite with cross-bedded components of siltstone and mudstone, feasibly representing the fringe of a fluvial system (Makhlouf & Abed, 1991). The Umm Ishrin is also responsible for the famous “rose red” color found in the city, although its color ranges from red to salmon, chocolate, or a deep mustard yellow. Continuing the culinary descriptors, the distinctively white or cream-colored Disi Formation is the “icing on top”.

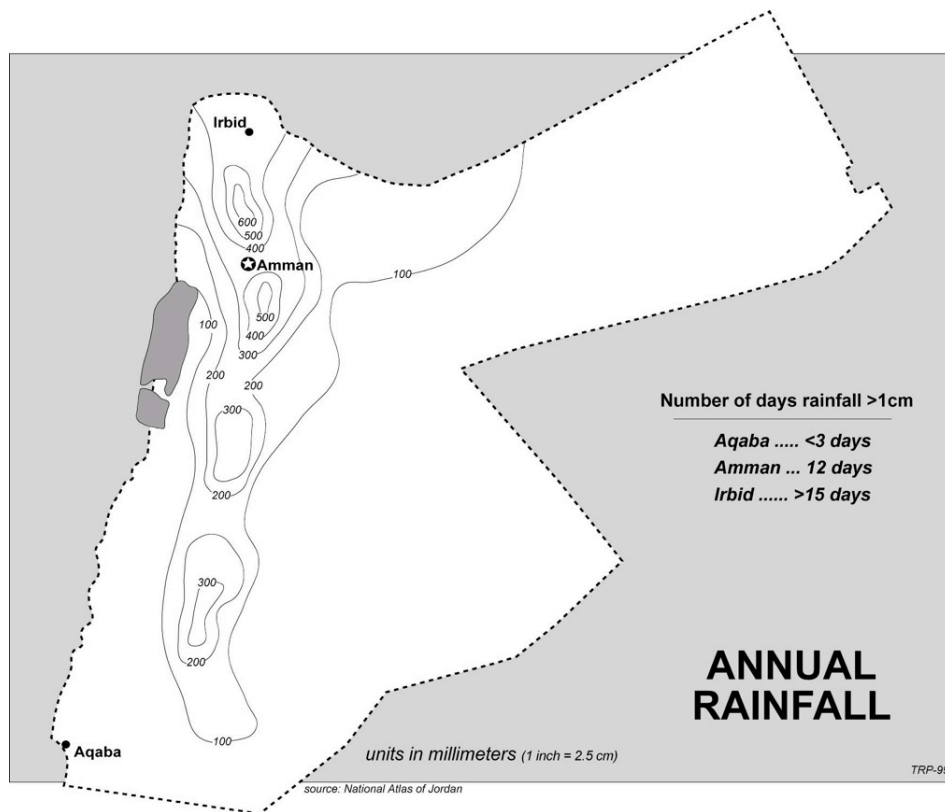


Figure 2.6 – Map showing the average annual precipitation in Jordan (Paradise, 1999).

Significantly coarser, the Disi Sandstone lacks horizontal cross bedding and was deposited in a braided stream environment among numerous dunes and sandbars (Nairn & Alsharhan, 1997). The fairly uniform Disi across Jordan is more inconsistent in Petra due to irregular and unconforming contact with the as-Shara Limestone above the Bedouin village, Umm Sayhoun, and Wadi Musa (Figure 2.7).

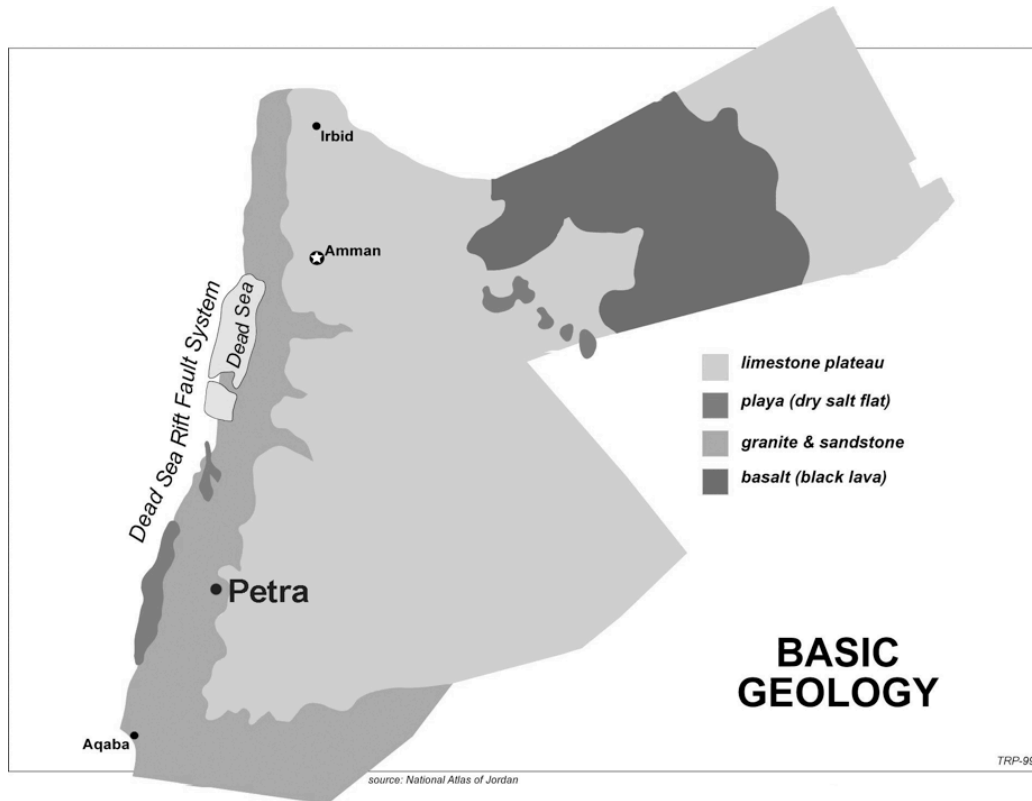


Figure 2.7 – Map of the basic geology of Jordan. Note Petra’s location on the edge of the limestone plateau mixing with granite and sandstone (Paradise, 1999).

2.3 Nabatean Monuments and Architecture

Inhabiting Petra for over 400 years, the Nabatean Empire created some of the most recognized tombs, facades, and monuments in the valley, each displaying distinctive Nabatean architectural styling and stone dressings (Tholbecq, 2007). Some of the earliest archeologists in Petra have tried identifying typological groups for Nabatean monuments (e.g. Brünnow & von

Domaszewski, 1904; Kennedy, 1925), but the most common design elements include central doorways, often framed by two half columns or pilasters, and the presence of decorative crowstep patterns, adopted from Assyrian architecture (Bounni, 1999). Some of the more famous monuments in Petra matching this architectural style include the Urn Tomb, the tomb of the Roman Soldier, tomb of Sextius Florentinus, and the western face of the Temenos gate near Qasr al-Bint al-Faroun (Tholbecq, 2007). Iconic landmarks such as al-Khazneh (the Treasury) and al-Deir (the Monastery) created during this era include Nabatean elements (i.e. capitals) but also display Hellenistic and Roman design influence in their characteristic pedestals and intricate stonework, exemplifying the city's eclectic population and relations with neighboring civilizations (Taylor, 2007; Tholbecq, 2007)(Figure 2.8).



Figure 2.8 – Images of famous monuments in Petra exhibiting the eclectic Nabatean style with heavy Roman and Hellenistic influence: al-Deir (left) and al-Khazneh (right). Photographs by K. Groom (2013).

Even simple monuments with no decorative stonework can be associated with the Nabatean Era through stone dressings: masonry methods to flatten and finish stone surfaces. Common stone dressings at the time included abrasive (e.g. scraping or rubbing) or percussion (e.g. hammer and chisel) techniques, each leaving a discernible surface texture (Taylor, 2007).

The most characteristic Nabatean stone dressings, frequently found on interior or flat surfaces, are diagonal lines ranging from 15° to 45° from the vertical created with fine point or, more likely, toothed chisels (Taylor, 2007)(Figure 2.9). In some case, these diagonal grooves are in a slight curve the length of an average human arm, suggesting the chisel was repeatedly dragged along the surface to create the dressing (i.e. abrasive) instead of using a hammer (i.e. percussion). Quite often, the slanted pattern is repeated in the opposite direction to create the distinctive herringbone pattern seen throughout the city, which is regularly used to identify Nabatean Era surfaces and contextually date monument construction (Paradise, 2005, 2013).



Figure 2.9 – Examples of Nabatean stone dressings: Close up of herringbone dressing on Djinn Block X (left) and a large dressed surface near the opening of the Siq (right). Photographs by K. Groom (2013).

2.3.1 Nabatean Djinn Blocks

Among Petra's many Nabatean monuments are djinn blocks: large hewn cubes found throughout the valley, with unknown purpose or meaning (Figure 2.10). The Arabic name for these cubes, *sahreej*, means cistern or reservoir, but there is little indication the blocks are hollow or designed to store water (Taylor, 2007), although many are found near water sources (Browning, 1973). Rumored to have legendary connections with djinn, or impish genies, some locals justify the blocks' Arabic name by explaining they were created to imprison evil or

mischievous spirits. Others believe the djinn blocks are merely decorative monuments in the shape of the Nabatean god Dushara or goddess al-Uzza, often represented as cubes or blocks throughout the valley (Browning, 1987). Alternatively called tower tombs, these cubes are also considered to be freestanding tombs or tomb markers, as they resemble other cube tombs made of clay found elsewhere in the Nabatean Empire (Tholbecq, 2007). There is also speculation that some of these blocks might have had some kind of built superstructure containing a burial chamber, but little evidence of such structures remains (Browning, 1973).



Figure 2.10 – Images of the more famous djinn blocks near the opening of the Siq. Note the Hellenistic characteristics of the block on the left. Photographs by K. Groom (2013).

Although there are over thirty djinn blocks recorded throughout Petra, their degree and style of decoration varies (Taylor, 2007). Some djinn exist as plain cubes with no more than flat Nabatean stone dressing while others exhibit Assyrian, Cavetto, and even Hellenistic inspired carvings, including quintessential Nabatean crowsteps (Taylor, 2007). Nearly all djinn blocks are cube-shaped with equal dimensions, though some are taller than wide. The most famous blocks mark the entrance of the Bab as-Siq, the main entrance into Petra, and the Snake Monument, south of the city center. These particular monuments exhibit typical Assyrian and Cavetto-style decorations and crowns, leading some scholars to believe they are among the earliest tombs in Petra (Taylor, 2007). One of the blocks at Bab as-Siq is much more decorated than the others

with multiple pilasters and distinctive Hellenistic horizontal crowns on each of the four walls, which could have mounted darker or more colorful stone decorations at some point (Browning, 1973).

2.3.2 Djinn Block X

The djinn block addressed in this study, Djinn Block X, is an isolated irregular hewn monument located above the three primary djinn blocks at entrance of the Bab as-Siq (Figure 2.11). It has been termed Djinn Block X because it was excluded from Brünnow and von Domaszewski's famous 1909 record of every monument in Petra, assigning each a defining number. While it's not a cube like the others, the sides are mostly orthogonal to the ground and flat, face a distinct aspect, and exhibit indicative Nabatean herringbone stone dressing, contextually placing construction of the monument to roughly 2000 years ago, contemporary with the other djinn blocks (Paradise, 2013). The block resembles an oblong cube with unevenly sized faces, a protruding feature on the eastern side, and a large flat ledge attached to the northern face (Figure 2.12). Therefore, each analyzed aspect was actually composed of one or

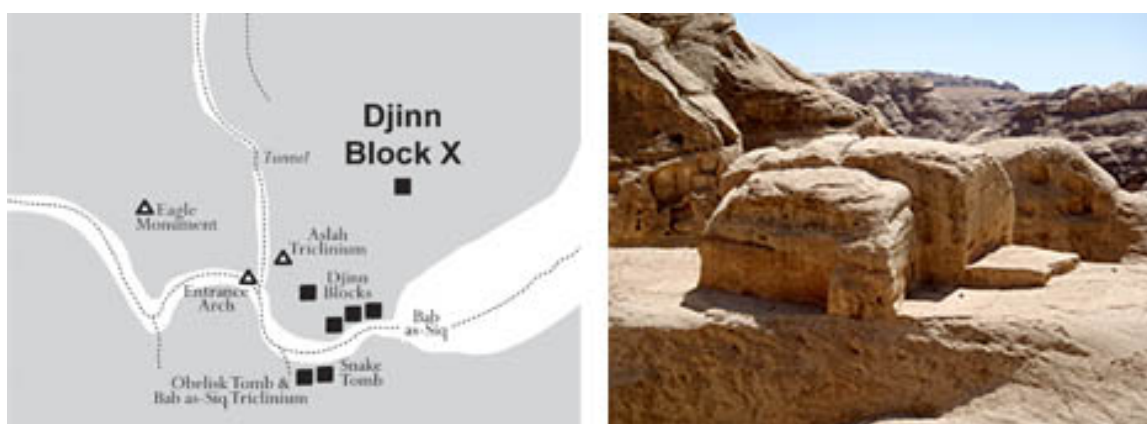


Figure 2.11 – Cropped section of the map of Petra from Taylor (2007) with the location of Djinn Block X (left) and an image of the block from the east (right). Groom (2013).

more distinct panels. This research concentrated on decay features limited to vertical surfaces so the top of the block was omitted and only the sides of the northern ledge were assessed.

The northern face (328°N) includes three panels: A large square wall, the front face of the ledge/step, and the sidewall of the jutting feature on the eastern face (Figure 2.13). The primary square face is approximately 3.5m wide, 2.7m tall on the left side, and 2.2m on the right. This face is heavily pitted with extensive lichen overgrowth on the uppermost section. There is also some evidence of vandalism on this panel (i.e. engraved signatures and initials). The second panel is the front face of the large platform and measured 2.9m wide and 0.36m tall. There are a

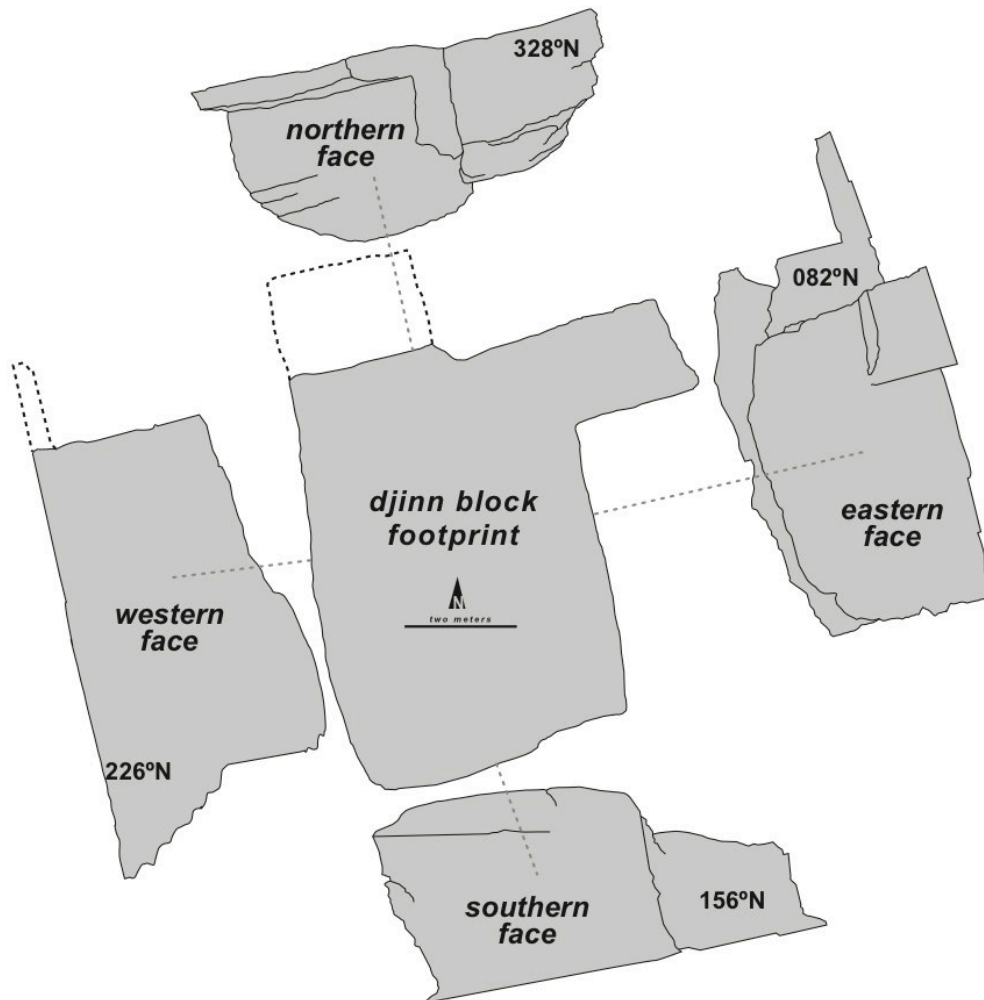


Figure 2.12 – Diagram of Djinn Block X showing the four major faces (Paradise, 2013).

couple patches of lichen development on this surface but the majority of this panel shows significant decay. The third, and final, panel encompassed in the northern aspect is the sidewall of an oddly shaped protrusion from the eastern face. Its base width measures roughly 2.9m, although the top width is only 2.4m, and it is 1.6m tall on the left side and 1.8m on the right. There is an oblong cavity on this panel displaying karren-like features, suggesting water flows through the feature regularly. There is also a large tafoni cell on the far left corner of this panel that has broken through to the eastern face.



Figure 2.13 – Images of the northern face on Djinn Block X (left) and the large cavity obviously impacted by water runoff (right). Photographs by K. Groom (2013).

The western face (226°N) is one large continuous surface but for this research it was divided into two different panels because of a slight curve and to maintain accuracy during the raw count, as there is significant tafoni development on this aspect (Figure 2.14). The first panel includes a sidewall of the northern ledge, measuring 3.6m tall by 1.6m long, and a portion of the large wall 3.5m in length, 3.1m tall on the far left, and 3.5m at the junction with the next section. There is considerable flaking and other sandstone-related weathering phenomena along the base of this panel and an overall rougher texture on the upper portions. There are also lichen colonies and cyanobacteria possibly acting as stabilizing agents on areas lacking tafoni development. The

second panel for the western aspect is a continuation of the curved wall 3.7m long, 3.5m at its shortest (where it meets the first panel), and 3.9m at its tallest on the far right side. The majority of tafoni cell development on this panel formed in linear patterns, indicating lithological influences on cell distribution. There is one cluster of larger cells that run parallel with a fissure down the center of the panel that could be due to advanced decay from water runoff, similar to the large cell on the northern face.



Figure 2.14 – Images of the western face of Djinn Block X (left) and intense small tafoni development (right). Note the 3cm Nabatean potsherd for scale. Photograph by K. Groom (2013).

The southern aspect (156°N) is composed of two panels: a primary square wall and the other sidewall of the eastern protrusion. The main face measures 4.2m wide, 3.5m tall on the left side, and 3.1m on the right. Observationally, this face is the most heavily decayed with the most indiscrete cell development and the beginning stages of what appears to be drapery formation along the base (Figure 2.15). This is also one of the only surfaces on the djinn block to exhibit extensive case hardening and dark desert varnish coating. The second panel is much smaller, only measuring 0.8m wide and 1.3m tall. The small size and overall lack of tafoni development, aside from a single large cavity, lead to this panel's ultimate omission from the statistical and morphometric analysis.



Figure 2.15 – Images of the southern face of Djinn Block X (left) and the large isolated cavity on the small excluded southern panel (right). Photographs by K. Groom (2013).

Although the eastern face (082°N) technically consists of three panels, only two were included in this research for safety reasons. The first panel is the primary eastern face to the south of the protrusion, measuring roughly 4.4m wide, 2.9m tall on the shorter left side, and 3.9m tall at its tallest right at the edge of the protrusion. There is minimal tafoni development on this section, although there is considerable flaking present and formation of large spalls that might detach in the near future. There is also more evidence of case hardening and thicker rock coatings, including dark desert varnish, on this section. The second assessed panel is a small vertical wall (2.3m by 1.3m) on the other side of the protrusion and the last sidewall of the northern ledge (0.4m by 2.1m). There are more tafoni cells on this portion of the eastern aspect (Figure 2.16). It fits within the corner between the eastern protrusion and northern ledge, so advanced decay could be due to the area acting as a wind trap and/or human activity, denoted by fire residue/damage at the base and graffiti/vandalism near the center of this panel. The third technical panel, the front face of the protrusion, was excluded from the research entirely because it is precariously positioned at the ledge of a steep ravine and inaccessible without climbing equipment.



Figure 2.16 – Images of the eastern face of Djinn Block X (left) and advanced flaking and case hardening at the contact between the Umm Ishrin and Disi formations on this face (right). Photographs by K. Groom (2013).

The irregular shape and elevated isolation of Djinn Block X might explain its absence from several monument surveys taken throughout the valley (Paradise, 2013). Previous studies of the block suggest it may be a quarry remnant converted to a djinn block, due to its proximity to evidence of stone removal from adjacent cliff faces; an unfinished djinn block suggested by deep grooves along the top of the monument and the protruding section on the eastern face; or a ritualistic site attributable to the prominent northern ledge (Paradise, 2013). At 1022m above sea level, this block is 20m above the entrance road and the highest known djinn block in elevation.

Djinn Block X is geologically unique as well. While most monuments in Petra are composed of either the Umm Ishrin or the Disi sandstones, Djinn X contains both due to its elevated location. There is a distinct contact running through the center of the monument with Disi on the bottom and an interdigitated lens of Umm Ishrin and Disi on top (Figure 2.17). This is contrary to the rest of the valley, as well as neighboring regions, where both formations are exposed as the Disi sandstone formation is younger and *above* the darker, older Umm Ishrin (Nairn & Alsharhan, 1997). This suggests a geologic unconformity in the substrate where Djinn Block X is located, as material from the older Umm Ishrin mixed with the younger Disi

sandstone during lithification, resulting in the interdigitation present today. The Umm Ishrin and Disi sandstones have relatively similar compositions of siliceous sand clasts but differences in carbonate levels and iron constituents in their matrices cause a greater weathering susceptibility in the Disi than the more resilient Umm Ishrin (Paradise 1999, 2005). This disparity is plainly evident on Djinn Block X, as the majority of decay is confined to the lower formation, including a stark difference of tafoni distribution. The less weathered upper section contains significantly more lichen and lithobiont growth, along with case hardening and thicker rock coatings, particularly on the southern and eastern faces.

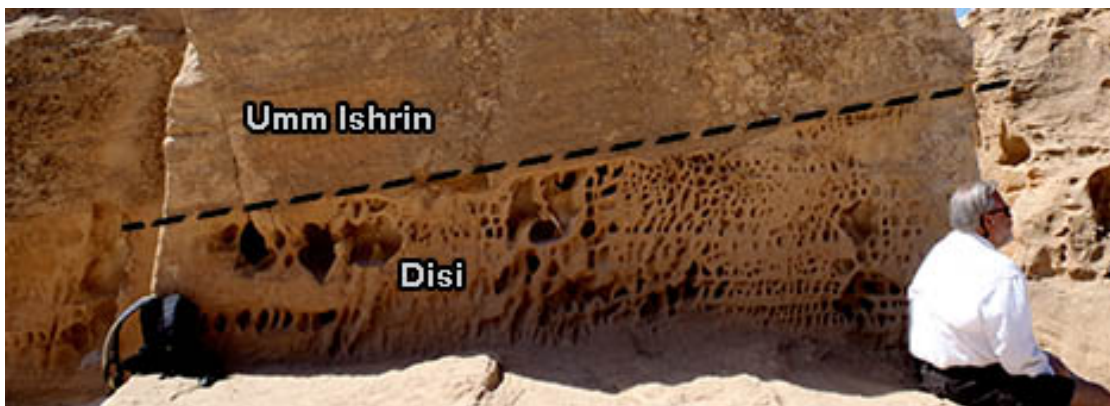


Figure 2.17 – Image displaying the obvious differences in decay between the Umm Ishrin and Disi sandstone formations on the northern face. Photograph by K. Groom (2013).

Chapter Three: Literature Review

Examining prior research and literature on tafoni development and rock decay in Petra, Jordan can provide insight into broader investigations and applications in architectural deterioration and cultural heritage management. To establish a holistic scientific framework for this research, this literature review is divided into three thematic subchapters: theory, geography, and multidisciplinary application. First, general and specific geomorphologic praxis is discussed, including the academic dichotomy of intrinsic and extrinsic rock decay processes, polygenetic research perspectives for cavernous weathering, and threshold response theory. Then, an introduction to regional research is provided, encompassing the city of Petra as well as its wider geographical setting. Finally, relevant techniques and geomorphologic applicability in the analyses of dressed stone deterioration and cultural resource management is outlined.

3.1 Geomorphologic Theory and Weathering

Essentially, geomorphologic research illuminates the complexity of forms and processes continually transforming landscapes. In fact, in the late 1800s geomorphology was defined as “the study of the morphology of Earth’s surface” (de Margerie, 1886). Scholars have measured the Earth’s physical characteristics as a means to empirically examine their surroundings and understand concepts of decay operating outside the human time frame. Ancient Greek and Roman scholars such as Herodotus (484 – ca. 425BC), Aristotle (384 – 322BC), and Strabo (ca. 64BC – 20AD) speculated on the creation of landforms, changing of the scenery, and the driving forces behind the Earth’s surface, often with impressive insight and accuracy (Martin & James, 1993). In modern literature, landscape change is quantified through the analysis of morphometry, the measurement of form and shape. This includes everything from measuring surface recession

(Paradise, 1999; Inkpen & Jackson, 2000) and analyzing surface moisture (Mol & Viles, 2012), to evaluating weathering forms and dimensions (McBride & Picard, 2004) and examining grus and other detached weathering debris (Mustoe, 1983). This subchapter examines some of the different scales, forms, and theories in geomorphologic research. Although this research study focuses on sandstone decay exclusively, studies of other lithologies nonetheless contribute beneficial information and are therefore included.

3.1.1 Arid Land Geomorphology

Climatic influences on landscape change have been evident for generations, especially within the scope of morphology (Chorley, 1957), and each climate contains unique forms, processes, and interrelationships. Arid environments are no exception. Sporadic precipitation events, prevalent aeolian processes, and sparse vegetation are a few features that mark the world's deserts. In terms of research, arid geomorphology is a well-recognized and explored topic, as evident by the multitude of books (e.g. Parsons & Abrahams, 1994; Thomas, 2011), reviews (e.g. Tooth, 2007), and special journal issues (e.g. Fryberger & Goudie, 1981; Bullard, 2006). The emphasis of arid lands geomorphology can range from aeolian forms and processes like dune formation (Goudie, 2002) and the interrelationships of environmental change and the formation of rock varnishes (Liu & Dorn, 1996), to the pedogenesis of aridisols, patterned ground, and desert pavements (Dixon, 2009).

The unique environmental features of arid land geomorphology are reflected in common research parameters and concerns. Arid lands studies have included such variables as intense shifts in diurnal surface temperatures (Kerr et al., 1984; Jenkins & Smith, 1990), the presence and formation of rock varnishes and desert pavements (Smith, 1988), diurnal ambient

temperature and climatic variations (McFadden et al., 2005), and perpetual environmental stresses (Warke, 2007). These iconic desert characteristics can lead to a number of natural and anthropogenic hazards that have been the focus of many geomorphologic studies, including intense salt-driven destabilization of building material and engineered structures (Goudie & Viles, 1997), geologic and hydrologic hazards for urban settlements in desert environments (Webb et al., 2013), flashflood vulnerability of super arid regions (Magilligan & Goldstien, 2011), and paleoflood evidence for ancient disasters in desert environments (Paradise, 2012).

The depositional formation of many arid lands also concentrate a significant amount of sandstone research to deserts and other arid environments (Young et al, 1992). Sandstone specific studies can range from analyses of groundwater movement and hydrogeology in arid environments (Mahmod et al., 2013) and the influences of cyanobacteria on sandstone surface change (Büdel et al., 2004) to wider formation examinations and explanations for grand sandstone landscapes such as the Land of Standing Rocks in Canyonlands National Park in southern Utah (Nicholas & Dixon, 1986) and the Wadi Rum UNESCO World Heritage Site (Goudie et al., 2002).

3.1.2 Rock Decay and Weathering

Where geomorphology assesses landscape change in a broader scope, the discipline of weathering and rock decay concentrates on the breakdown and deterioration of stone that essentially *drives* landscape change (Price, 1995). Traditionally called *weathering*, rock decay is actually the result of many different processes and variables; so to avoid the misconception that the *weathering* of stone is caused by *weather* many scholars within the field prefer the more accurate designation of *rock decay* (Hall et al., 2012; Dorn et al., 2013). Additionally, although

they are often erroneously used interchangeably, rock decay and erosion are distinctively different processes. Rock decay is the deterioration of the stone in situ where erosion describes the transportation of decayed material. While the specialized field of rock decay focuses on the causes and effects of stone deterioration, past and current research is often divided by two major ideological and process dichotomies: the importance of intrinsic versus extrinsic variables to stone stability/weakness and the effectiveness of physical (e.g. spalling and salt crystallization) versus chemical (e.g. dissolution and matrix disaggregation) driver of decay.

The inner workings of the relationship between intrinsic (internal) and extrinsic (external) variables in geomorphology and rock decay have been debated for years. G.K. Gilbert (1843 – 1918) defined landscape change in terms of shear strength and shear stress and observed “solidity is not absolute but relative” (Gilbert & Dutton, 1880). This viewpoint is applicable in rock decay research by ‘shear strength’ referring to intrinsic variables like lithification and mineralogy; where ‘shear stress’ represents extrinsic variables such as environmental setting, climate, and anthropogenic activity. Rock decay studies on intrinsic variables include identifying geologic matrix thresholds for sandstone surface recession (Paradise, 1995), the role of preexisting subsurface salts in the disintegration of granite (Bradley et al., 1978), and the impacts of core softening and interior stone destabilization (Conca & Rossman, 1985). Other studies analyzing the extrinsic variables range from assessing climate and morphometry (Chorley, 1957) and the impacts of thermal heating and cooling (Warke et al., 1996) to differences in decay rates depending on geographic and climatological location (Inkpen & Jackson, 2000).

The second major dichotomy in rock decay research is the divide between physical and chemical decay processes. Physical decay involves the mechanical breakdown of stone, and research centers around factors like salt crystallization causing flaking and exfoliation (Bradley

et al., 1978) and the movement of subsurface moisture movement as a destabilizing agent (Mol & Viles, 2010). On the other end of the spectrum, the well-established field of geochemistry has been evaluating the chemical breakdown of rocks for decades (Krauskopf & Bird, 1967). Like physical processes, chemical decay hypotheses predominantly address salt and moisture as key components, except in different functions, at dissimilar scales, and often not as self-contained variables. Chemical rock decay research analyzes variables like corrosion on eroded material (Butler & Mount, 1986) and the stabilizing or deteriorating effects of different rock coatings and varnishes (Campbell, 1999).

While these two processes are virtually always studied separately, directly comparing physical and chemical hypotheses to determine supremacy is misguided, as both function at discretely separate scales: physical decay analyzes breakdown from the granular scale or larger (e.g. McBride & Picard, 2000), where chemical decay examines mineral alteration at a molecular scale (e.g. Dixon & Thorn, 2005). The illusion of superiority of one over the other merely represents scalar bias in the geomorphologic community. Further, this scalar discrepancy implies both processes can affect stone materials simultaneously and reinforces the concept of polygeneous decay (e.g. one process initiating another, chemical leading to physical)(e.g. Young, 1987).

Intimately tied to geomorphology, weathering and stone deterioration processes and patterns also vary geographically and climatologically (Pope et al., 1995). In fact, rock decay in arid environments is still a major topic of academic discussion. Studies range from the multidimensional role of salt weathering in hot deserts (Wellman & Wilson, 1965; Cooke, 1979) and laboratory simulations of salt-induced decay (e.g. Smith & McGreevy, 1983), to examinations of the stabilizing or deteriorating effects of rock coatings and desert varnish (e.g.

Dorn & Oberlander, 1982; Staley et al., 1992), along with some of the original work involving cavernous weathering and tafoni development (e.g. Bryan, 1928; Blackwelder, 1929).

3.1.3 Tafoni and Cavernous Decay

Tafoni and cavernous rock decay have been well documented for over 3,500 years (Boxerman, 2005), however their formation wasn't a topic of scientific discussion until the mid-1800s (Darwin, 1839; Dana, 1849), sharply increasing in quantity and geographic span later in the 20th Century. While tafoni remain the primary focal point, publications on the topic vary dramatically from qualitative observations (Bryan, 1928; Tschang 1974), modeling temporal cell growth (Sunamura, 1996; Norwick & Dexter, 2002), detailed laboratory investigations (Rodriguez-Navarro et al., 1999; McBride & Picard, 2004), and complex multidisciplinary field analyses (Martini, 1978; Brandmeier et al., 2010). Also, the variability in size, shape, and distribution of these phenomena has resulted in a wide range of names including alveoli, stone lace, honeycombing, caverns, pitting, and so forth, with a general understanding that each term is size dependent (i.e. "alveoli" only applies to small cells). However, there is no established scale or universally accepted distinction between terms and, therefore, for this thesis "tafoni" (singular: tafone) is considered non-scalar and used exclusively throughout the rest of the document.

Geographically, tafoni research was originally concentrated in North America (Bryan, 1928; Blackwelder, 1929, etc.) and remained there until a scientific boom in the 1960s. By the late 1970s studies began to emerge from Antarctica (Calkin & Cailleux, 1962; Prebble, 1967), Southern Australia (Dragovich, 1969; Winkler, 1979), Hong Kong (Tschang, 1974), Northwest Sahara (Smith, 1978), and Italy (Martini, 1978). By the end of the 20th Century the regional

scope of research had expanded into the United Kingdom (Pye & Mottershead, 1995), Japan (Matsurkura et al., 1989; Suzuki & Hachinohe, 1995), Spain (Sancho & Benito, 1990; Mellor et al., 1997), Northern Ireland (McGreevy, 1985), Scotland and Southern Greece (Kelletat, 1980), and Finland (Kejonen et al., 1988), with more studies from U.S. (e.g. Butler & Mount, 1986), Antarctica (e.g. Conca & Astor, 1987), and Australia (e.g. Twidale & Sved, 1978). The reach has even gone as far as Mars (Rodriguez-Navarro, 1998). Through the 21st Century the breadth of studies expanded into Jordan (Viles & Goudie, 2004), South Africa (Mol & Viles, 2010), and Southern India (Achyuthan et al., 2010), along with continuing work in previously mentioned locations (e.g. McBride & Picard, 2004).

The diverse geographic distribution of tafoni is reflected in their diverse geologic and environmental landscapes. The phenomena have been examined on various lithologies: intrusive granite and gneiss (e.g. Dragovich, 1969), volcanic tuff (e.g. McBride & Picard, 2000), slightly metamorphosed conglomerate (Martini, 1978), sedimentary sandstone (e.g. Grantz, 1976) and limestone (e.g. Rodriguez-Navarro et al., 1999), and even manmade materials like cement (Pestrong, 1988). Climatologically, tafoni have been discovered in a multitude of settings including, but not limited to, coastal (e.g. Suzuki & Hachinohe, 1995), sub-zero deserts (Selby, 1979), river basins (Sancho & Benito, 1990), and both arid and semi-arid deserts (Wilhelmy, 1964). The range of host landscapes, both physical and climatological, inhibits adopting any one universal process hypothesis and instead suggests a complex relationship between formation processes and lithology, location, and environment.

Despite considerable academic attention, primary cell formation processes still remain enigmatic. Countless hypotheses have been presented, and the process dichotomy between chemical and physical decay mechanisms emerged fairly early, led by Blackwelder (1929) and

Bryan (1928), respectively. Notwithstanding certain works suggesting integrated physio-chemical contributors (Young, 1987, Kejonen et al., 1988) and an early recognition of necessary collaboration (Mustoe, 1983), the two processes are typically researched separately. Biologic decay has also been mentioned in tafoni studies (Andre & Hall, 2004) but remains largely disassociated with formation and was omitted in this research. There are commonalities between physical and chemical tafoni evolution research, mainly crucial variables like salt (e.g. Bradley et al., 1978; Winkler, 1979) and water (e.g. Mol & Viles, 2010), but the specific roles of these elements vary per process paradigm and substrate. Physically, pressure from subsurface salt crystal growth is a widely accepted rock deterioration mechanism (Wellman & Wilson, 1965; Birot, 1968). Moisture is also considered a predominant factor in mechanical decay, whether as a transport agent of salts and other minerals (e.g. Mustoe, 1983) or breakdown through internal water migration and expansion (e.g. Conca & Astor, 1987). In relation to tafoni, many studies proclaim the physical influences of salt and moisture fundamental to cell formation (e.g. Mustoe, 1982; French & Guglielmin, 2000). The specifics of these factors, however, have been explored by comparing salinity and water movement with various extrinsic variables.

Rates of salt movement and crystal accumulation, signifying cell development, have been associated with multiple characteristics, and studies positively correlate cavity formation with factors such as extended wetting and drying cycles (e.g. Huinink et al., 2004), elevated evaporation rates of surfaces perpendicular to prevailing wind patterns (Rodriguez-Navarro et al., 1999), and deposition and migration of crystalline salts and calcites via precipitation (McBride & Picard, 2000). Each study supports a general pattern: some selected climatic factor determines the addition or evaporation of moisture, which in turn dictates the deposition and

concentration of salt crystals furthering cavernous decay. McBride and Picard (2004) have also determined that these processes are exacerbated in material with high porosity and permeability.

Water movement through stone, independent of salt materialization, has also been identified as a physical stone deterioration mechanism. Tafoni formation have been directly associated with hydro-geomorphological processes like ice-induced micro fracturing (Kejonen et al., 1988; French & Guglielmin, 2000) and joint-dependent water migration (Conca & Astor, 1987). More recently, Mol and Viles (2010) associated wetter internal moisture regimes with decreased stone hardness and, thus, increased decay. They applied the same techniques to tafoni cells and similar processes appear to influence cell development (Mol & Viles, 2011). However, even these studies note a fundamental recognition of interrelationships with chemical processes.

Principle chemical processes applied to cell development include salt-induced dissolution of silica (Young, 1987), core softening (Conca & Rossman, 1985), and the formation of iron casings and case hardening (Campbell, 1999). In tafoni evolution, most chemical processes merely condition, not directly deteriorate, the host material for the formation of physical decay features such as exfoliation (Blackwelder, 1929), flaking (Dragovich, 1967), and granular disintegration (McGreevy, 1985; Mottershead & Pye, 1994).

While the importance of this codependence has been known for years (Martini, 1978), it has not been until recently that tafoni research has begun incorporating processes from multiple schools of thought (e.g. Brandmeier et al., 2010). For example, Pope et al. (1995) aptly describes these complex interrelations in the terms of synergy. Likewise, Paradise (2012) illustrates the variance of principle driving mechanisms in cavernous rock decay, but also highlights the interconnectedness of those processes depending on lithology and environmental setting. In fact, it is this multivariate nature that makes tafoni development a justifiable representation of overall

stone stability and decay. Turkington and Phillips (2004) utilize this concept of polygenicity to create a model for stone instability feedback systems that is non-dependent on specific formation processes. The same research thrust can be applied to assessing overall cultural stone decay in the hewn city of Petra, Jordan. Where Turkington and Phillips (2004) modeled this polygenetic nature, this thesis sought to analyze empirical data in addressing the factors of tafoni development as a surrogate for dressed stone deterioration in Petra, Jordan.

3.1.4 Threshold Response in Rock Decay Research

While not conventionally applied to rock decay, the concept of thresholds has been present in geomorphologic research for years (Schumm, 1979). Thresholds are abrupt shifts in a system responding to gradual levels of energy. These exist in the natural world exemplified by dew points and quantum mechanics, but also in the built environment with forms such as structural collapse and dam failures. Within geomorphology, threshold patterns have been observed in landscape change like arroyo development (Graf, 1979), mass wasting (Carson, 1971), and complex drainage systems and erosion (Schumm, 1973; Schumm & Kahn, 1972). In fact, the introduction of geomorphologic thresholds helps define and model many non-linear processes found in landscape evolution (Phillips, 2006). As these examples demonstrate, geomorphologic threshold research is primarily confined to weathering-limited, often fluvial, processes and pedogenesis (Muhs, 1984).

Although they represent different stages of decay, weathering and pedogenesis are intimately interrelated and several thresholds discussed in pedogenesis research may be applicable to rock decay. For instance, distinctions between intrinsic (Chadwick & Chorover, 2001) and extrinsic (Ewing et al., 2006) thresholds in pedogenesis literature may reflect

corresponding thresholds in weathering by substituting soil chemistry with lithology and mineralogy. Analyzing surface recession in sandstone, Paradise (1999) was the first to identify thresholds in a weathering-focused study. This thesis collaborates with these findings and also applies geomorphologic thresholds to tafoni evolution and development.

3.2 Regional Geomorphology

Before discussing the connections of geomorphologic research and cultural resource management, this review first examines preexisting geomorphologic research in the region to establish locational and scalar context and research lacunae. Beginning at a wide regional scope and progressively narrowing focus to the city of Petra, this subchapter assesses geomorphologic research conducted throughout the Middle East and North Africa, then within the Hashemite Kingdom of Jordan, and finally the archeological UNESCO World Heritage Site: Petra.

3.2.1 Research in the Middle East and North Africa

The Middle East and North Africa represent a disproportionately small percentage of arid geomorphology research. Existing research is generally utilitarian in nature. Due to regional tectonic activity, much of the geomorphologic research in the Middle East focuses on seismic susceptibility (e.g. Cong & Mitchell, 1999; Ambraseys et al., 2005), natural or anthropogenic hazards (Seber et al., 1997), and considerable attention on climate change (e.g. Grove, 1980; Drake & Bristow, 2006). In fact, much of the climatic research from the region is conducted in the Sahara desert, including regional geomorphic responses to climate change during the Pleistocene and Holocene (Bull, 1991), the evolution of the Sahara desert as a response to increasingly arid conditions (Grove, 1980), and simulations of abrupt vegetation shifts in the Sahara during the mid-Holocene (Claussen et al., 1999).

In terms of general rock decay of the region, many studies remain focused on urban or economic applications like analyses of concrete breakdown and longevity (Fookes & Collis, 1976; Fookes et al., 1981), examinations of building materials (Crowder & Amjad Ali, 1985), or petroleum-targeted research (e.g. Song et al., 2000; İşcan et al. 2006). Other continued research themes from landscape-scale to weathering-scale in the region include direct and indirect effects of climate change on building stone material (Viles, 2002), different techniques for assessing cultural stone decay to improve heritage management (Viles et al., 2011), and the comparison of simulated salt weathering in natural and laboratory settings (Goudie, 1993).

3.1.2 Research in Jordan

Geomorphologic research in the Hashemite Kingdom of Jordan varies from desertification (Louke & Schmidt, 2007) to natural radioactivity (Al-Okour et al., 2013) but largely centers attention on the decay of its cultural stone monuments and iconic desert landscapes. Such landmarks include the Cambrian and Ordovician sandstone inselbergs of Al-Quwayra near Wadi Rum (Viles & Goudie, 2004), the Great Temple in the capital city of Amman (Paradise, 1998), and, of course, the primary tourist attraction: the lost city of Petra (Paradise, 1995, 2002). Interdisciplinary collaboration between geomorphologists and archeologists is essential to the survival of these historic sites (Pope et al., 2008).

Evidence of this research cooperation can be found in the recently designated UNESCO World Heritage Site of Wadi Rum. Earning a dual designation as a Natural *and* Cultural Heritage Site, Wadi Rum boasts impressive inselbergs of the Disi and Umm Ishrin sandstones perched on an exposed Precambrian granite basement, and an array of petroglyphs and Thamudic inscriptions (Migón, 2009). Geomorphologic research in Wadi Rum includes assessing the

formation of large footslope debris ramps (Migón et al., 2005), geographic comparisons of sandstone formations composed of ancient sedimentary basins (Migón, 2009), and even an academic plea for international recognition of the value and inherent fragility of desert landscapes within cultural resource management (Goudie & Seely, 2011).

3.1.3 Research in Petra

The ancient city of Petra boasts an elaborate array of carved and constructed sandstone monuments from several well-known civilizations including Nabatean, Roman, Byzantine, and Crusader. Each occupational period contributed their own distinct styles, architecture, and building methods to the existing infrastructure, creating the unique multifaceted metropolis that hypnotizes tourists and researchers alike. The obvious historical significance of the city has invariably attracted countless archeologists from local (e.g. Al-Bashaireh & Hodgins, 2011) and international agencies and universities (e.g. Acevedo et al., 2001; Ortloff, 2005). Similarly, the myriad of stone structures also endorses geomorphologic research with a variety of foci, including: evaluating conservation techniques (Al-Saad & Abdel-Halim, 2001; Wedekind & Ruedrich, 2006), assessing restoration methods (Bani-Hani & Barakat, 2006), quantifying physical impacts of tourism (Franchi et al., 2009; Paradise, 2010), rock-fall hazard assessments (Delmonaco et al., 2013), and even uncovering evidence for past catastrophic events (e.g. Russell, 1980; Paradise, 2012).

While this spectacular stone city inspires researchers from all disciplines, including geomorphology, empirical studies of sandstone decay and tafoni development in the city are rare (Paradise, 1995; Heinrichs, 2008). In fact, the city is perforated with cavernous decay features and yet only a handful of studies have addressed tafoni formation locally in Petra (Gomez-Heras

et al., 2012; Paradise, 2013). This paucity limits local and international heritage management understanding and, moreover, efficacy of resource allocation and conservation policies.

3.3 Geomorphology and Cultural Resource Management

The interdisciplinary applications of geomorphologic methodology are endless, including cultural and heritage resource management (Pope et al., 2002; Smith et al., 2008). Humans have an inherent fascination with the past and its perceived immortality. But while portable artifacts like books and paintings can be preserved in artificially controlled environments, immobile relics like permanent monuments and building façades remain susceptible to environmental degradation. With the establishment of international conservation projects, such as the UNESCO World Heritage Program, stability and deterioration analyses of historically significant landmarks has become of global importance (Pope et al., 2002). While geomorphologic tools and methods cannot prevent the inevitable deterioration of such landmarks, specific application can provide heritage management with the necessary information to strategically allocate conservation efforts and resources to arrest further decay (Dorn et al., 2008; Allen & Groom, 2013). Rock decay research also benefits from this collaboration with an extension of potential research opportunities, as advocated by Smith et al. (2005), as long as they remain within the methodological limitations of heritage management policies.

3.3.1 Cultural Stone Decay Research

Researching historic stonework provides additional information unavailable for natural surfaces in traditional geomorphologic research. Whether explicit (e.g. Mottershead et al., 2003)

or contextual (e.g. Paradise, 1995; Norwick & Dexter, 2002) this information allows researchers to estimate baseline surfaces for recession studies (Paradise, 1999) and specific rates of decay to validate models (e.g. Sunamura, 1996) or assess environmental change (Inkpen & Jackson, 2000). A known date of exposure also provides credence to direct comparisons of deterioration in different environments (e.g. Achyuthan et al., 2010), of varying ages (e.g. Mottershead, 1997), and repeated measurements to assess temporal changes (e.g. Thornbush & Viles, 2008). While most of these studies could be conducted on natural (non-worked) stone, definitive results and conclusions would be controversial due to uncertainties and necessary assumptions.

Another unique trait of geomorphologic research on dressed stone includes the often dressed, uniform surfaces, which mimic laboratory-type conditions but in a real-world context, which permit unique opportunities for discrete aspect and insolation analyses (Warke et al., 1996; Paradise, 2002). While solar insolation is often disregarded as a direct agent of decay (Blackwelder, 1933; Reiche, 1950), it is indirectly associated with accepted weathering processes such as thermal expansion (Ollier, 1963) and hygric expansion (Weiss et al., 2004). Aspect and insolation have also been applied as surrogate measures for micro-environmental influences (Warke & Smith, 1998). In the context of Petra, Jordan, the establishment of an original date of exposure and surface orientation permits credible comparative examinations of degradation and aspect among otherwise ambiguous surfaces (Paradise, 1999, 2002).

However, potential research on cultural stone is restricted, as it must adhere to a series of limitations set forth by protective heritage management agencies. While there have been urgent appeals for the inclusion of rock decay research (Burns, 1991), the sensitive nature of heritage management strictly inhibits invasive or destructive investigations, significantly limiting traditional geomorphologic methodology, which typically includes some form of sample

retrieval using coring or rock hammers. For this reason, nonintrusive methods must be adapted to provide holistic representations of deterioration via observational and extrinsic variables (Smith et al. 1992) without compromising historic integrity and context. Another limitation is contextual and self-evident: the distribution, quantity, and quality of dressed stone are confined to territories of human activity or occupation. This often excludes harsh or inhospitable environments like the Polar Regions or hyper-arid deserts, where settlements are reduced to scattered and sporadic oases. Current stone decay research mimics this pattern by concentrating in humid, temperate, or coastal environments and largely overlooking dressed stone in arid environments, like Petra, Jordan.

3.3.2 Tafoni Research on Cultural Stone

Despite the methodological limitations, utilizing cultural stone can be very advantageous to cavernous decay research, especially within heavily weathered and inconsistent mature cells. Within tafoni research, there are often temporal complications as natural baseline exposures and rates of decay can be difficult to determine. To bypass this obstacle, researchers generally use cell size as a surrogate to age, assuming larger cells are older cells, but accurate dates and growth rates remain vague. There have been a few attempts to create equations (Matsurkura & Matsouka, 1991; Sunamura & Aoki, 2011) and models (Boxerman, 2005) for rates of tafoni development, but the consensus is that cell deterioration is irregular and extremely case-sensitive, thus making general age estimations problematic. This uncertainty can be averted when working with cells on datable surfaces. In fact, there have been a number of cavernous decay studies conducted on anthropogenic structures such as temples (Achyuthan et al., 2010), Anasazi and Mormon stone houses (Norwick & Dexter, 2002), artificial seawalls (Pestrong, 1988), and historic buildings

(Mottershead et al., 2003). Most of these studies, however, mirror the environmental preferences of dressed stone research and focus on regions of extended human occupation, generally dismissing desert settlements.

Nevertheless, studies of tafoni on dressed surfaces in arid settings have not been completely neglected (e.g. Norwick & Dexter, 2002) since the dearth of desert weathering research presents ample opportunities for unique and original analyses. In the southern Jordanian desert, Paradise (2013) observed an unconventional southern-heavy distribution of tafoni development on an isolated hewn block in the city of Petra, and hypothesized solar flux to be a factor.

Incorporating the complexities of cavernous cell formation, solar thermal weathering, and cultural stone decay, this thesis utilizes supplementary empirical data from the same hewn monument in Petra, Jordan to corroborate an informational paucity – to verify insolation as a contributing element to tafoni genesis, and thus dressed stone deterioration, in arid environments and its implications for effective cultural heritage management.

Chapter Four: Methods

Dressed stone structures like the djinn blocks offer unique opportunities for rock decay (weathering) research. Contextually datable surfaces allow the creation of a false datum to analyze total surface recession (Paradise 1999, 2013), but this is not the only advantageous characteristic of Djinn X. While not a regular cube like its more recognizable counterparts throughout Petra, Djinn X's faces are still relatively uniform in each compass direction, providing ideal 360° positioning for aspect and insolation analyses. Also, its isolated and slightly elevated location limits human interaction and the potential for significant anthropogenic decay, although there is minimal vandalism (e.g. fire residue and carved initials) on the northern face. The remoteness of Petra as a whole also removes certain elements such as urban or industrial air pollution as contributing factors, leaving only lithographic and environmental conditions as key decay mechanisms. In this subchapter, before addressing key assumptions and limitations, research parameters and methods are outlined and discussed.

4.1 Aspect as Proxy for Insolation and Environmental Conditions

In attempt to avoid the proclaimed over-simplicity and singularity of rock decay research in desert environments (Smith, 2009), this research embraces the complexity of environmental conditions by using aspect and tafoni as proxies for insolation and rock decay respectively. The polygeny of tafoni development represents intricate chemical, physical, and biological breakdown within the substrate and therefore offers a multifaceted proxy for general rock deterioration. Individual environmental influences of rock decay, such as insolation, are difficult to identify discretely, but can be holistically quantified via aspect (Williams & Robinson, 2000; Brandmeier, 2010). Warke & Smith (1998) revealed dissimilarities in rates of deterioration

between direct (solar) and indirect (laboratory oven) heating, thus validating the importance of exposure and insolation. Paradise (2013) used aspect discontinuity to analyze the impacts of insolation on the same Djinn Block X, but focused on surface recession rates, and restricted tafoni measurements to a single transect around the monument.

4.2 Tafoni Morphometry and Micrometeorology

Obtaining comprehensive measurements of each tafone on Djinn X was logistically problematic, as there are well over 2500 discrete cells, so a maximum variation sampling strategy was employed (Patton, 2005). The ten largest and ten smallest cells per face were measured in detail, within instrument capability, to examine the dimensional extremes of tafoni development as well as observe the differences between the smallest (assumed youngest) cells with larger (assumed oldest) cells. The block was initially divided into nine faces but one precariously abuts a steep drop and was excluded for safety purposes. The few cells on this face were noted but not measured nor included in the analysis. As this thesis analyzes environmental influences on stone decay, the data consist of two components: cell morphometric dimensions and interior/exterior micrometeorologic readings (Figure 4.1).

For most accurate estimation of cell volume (i.e. representing total mass of decayed material), multiple dimensions were recorded and then averaged. Depth, longest axis, shortest axis, vertical axis, and horizontal axis were all measured in centimeters via a *Staedtler® Mars®* field ruler. For visored cells, when the interior cell is larger than the opening, additional interior measurements were documented. Other physical characteristics like lichen overgrowth, cyanobacteria, flaking or spalling, and case hardening were also documented. A series of raw counts of all cells was also conducted to establish base measures for comparison. Every cell was

Dimensional and Meteorological Measurements

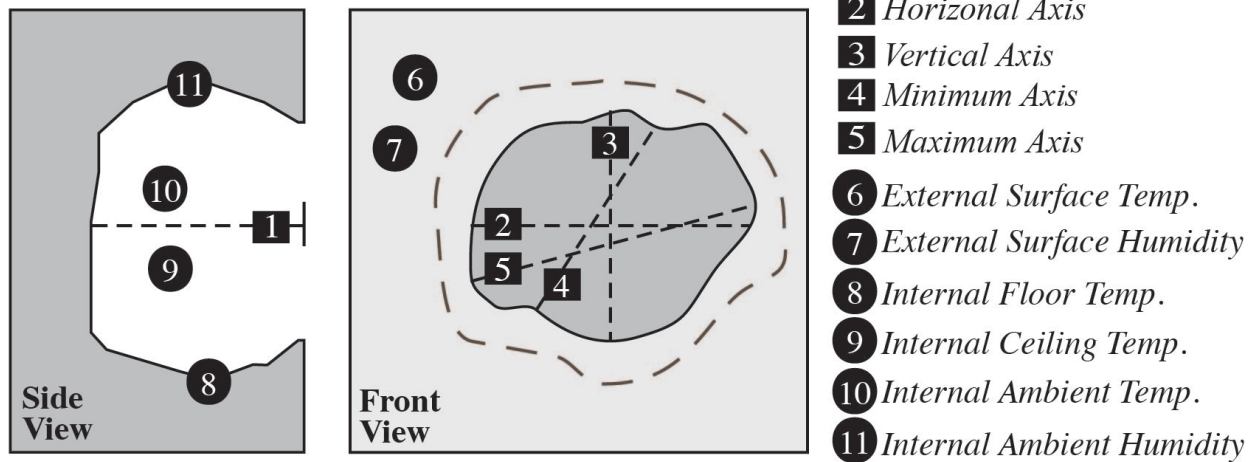


Figure 4.1 – Diagram showing all the morphometric and micrometeorological measurements for a single tafone. Note the square markers represent physical dimensions and the circle markers represent environmental readings. Diagram by K. Groom (2014).

tallied and categorized into four discrete size ranges (< 2cm, 2-3.9cm, 4-5.9cm, ≥ 6cm) for both depth and average diameter.

Paradise (2013) advocated insolation influenced wetting and drying as well as heating and cooling cycles as causes for advanced decay so micrometeorological measurements were also taken for each recorded cell. Ambient temperature and humidity within the tafoni and approximately 15cm outside the cells were measured with a Dwyer® TH-series thermo-hygrometer (+/- 5% relative humidity and +/- 1.5°C accuracies). Internal and external temperatures and humidity have been analyzed in the past (e.g. Dragovich, 1969) but not in relation to aspect and insolation. In addition, surface temperatures were recorded for cell ceilings, cell floors, and external surfaces directly outside the openings with an Oakton® Mini-IR Thermometer (+/- 2°C accuracy). Time of day was also noted with each measurement to maintain perspective and prevent continuity errors. After collection, the detailed morphometric and micrometeorological measurements and their corresponding notes and additional facts were

entered into a Microsoft Excel™ worksheet for calculations and analysis. A spreadsheet was also created for the raw cell counts as supplementary information.

Based on these parameters, this thesis uses tafoni development as a proxy to investigate insolation as a contributing element to cultural stone decay on a hewn djinn block in Petra, Jordan via these steps:

1. *Define panel extents and determine aspect for each face*
2. *Record discrete count of total cells per panel for comparison*
3. *Document observations of unique physical characteristics (e.g. lichen growth)*
4. *Measure cell morphometry of the 10 largest and 10 smallest tafoni per panel*
5. *Collect internal and external micrometeorological readings of same cells*

4.3 Assumptions and Limitations

Before any detailed analysis, assumptions and limitations must be discussed. First, as is the case with many historic stonework analyses, this research assumes all surfaces under consideration were hewn at the same time and were originally flat without any preexisting cavities or discrepancies. Other more well known djinn blocks in Petra display decorative pediments and other ornaments, but Djinn X is not fully orthogonal in dimension and appears to have been left unfinished in parts with no evidence of decorative embellishments and, therefore, original hewn surfaces are assumed to have been even.

Second, there has not been any significant human interference with natural decay mechanisms (i.e. quarrying or removing material post-construction) or abrasion from periodic flash floods that plague the region. The elevated position of djinn block isolates it from the heavy

tourist traffic and flood pathways in the Bab Al-Siq. Any anthropogenic deterioration would come from curious Bedouin goat herders and only to a minimal effect.

Third, the environmental conditions are relatively the same now as they were at the time of construction. While there is evidence of climatic fluctuations throughout Southern Jordan and Israel (Lucke et al., 2005) it can be assumed that any effects of these changes on weathering rates average out over the last two millennia and are negligible within a human-scale timeframe.

Fourth, this research works under the assumption that the maximum/minimum sampling style provides an accurate and holistic representation of all tafoni cells on the monument. There are over 2500 discrete cells present on Djinn Block X and it was logistically impossible to record every cell in detail.

The last assumption is inherent in tafoni and cavernous decay research: that larger cells indicate older cells (Schumm, 1979). As exact cell initiation and growth rates are so inconsistent from study to study, common practice uses size as a proxy to age (e.g. Sunamura, 1996). In the case of Djinn X, since all surfaces are assumed to be contemporary, and fairly young from a geologic perspective, age becomes less important than rates of initiation and deterioration. There are a few models of cell development (e.g. Boxerman, 2005; Paradise, 2013) but this research assumes larger cells represent later stages of decay, which may or may not correlate with age. In any instance, the dated surface stipulates a maximum cell age of 2000 years.

Along with these assumptions, there are also several logistical and methodological limitations. To begin with, a few cells that might have qualified as minimum or maximum were precariously located and, therefore, omitted from the data set for safety reasons. Also, minimum dimensions and micrometeorological readings do not accurately represent the absolute smallest cells, as they were limited to openings of 1.5 cm in diameter or larger in order to insert the

nozzle of the pen hygrothermometer. Smaller cells were abundant on Djinn X but internal and external readings would be too minute to discern any useful information.

Finally, as both a limitation and assumption, this research recognizes that the micrometeorological readings are static and do not indicate microclimatic patterns or any conditional changes over time. These data were obtained throughout different times of day and significant comparisons are both scale and time dependent. While the instruments are fairly

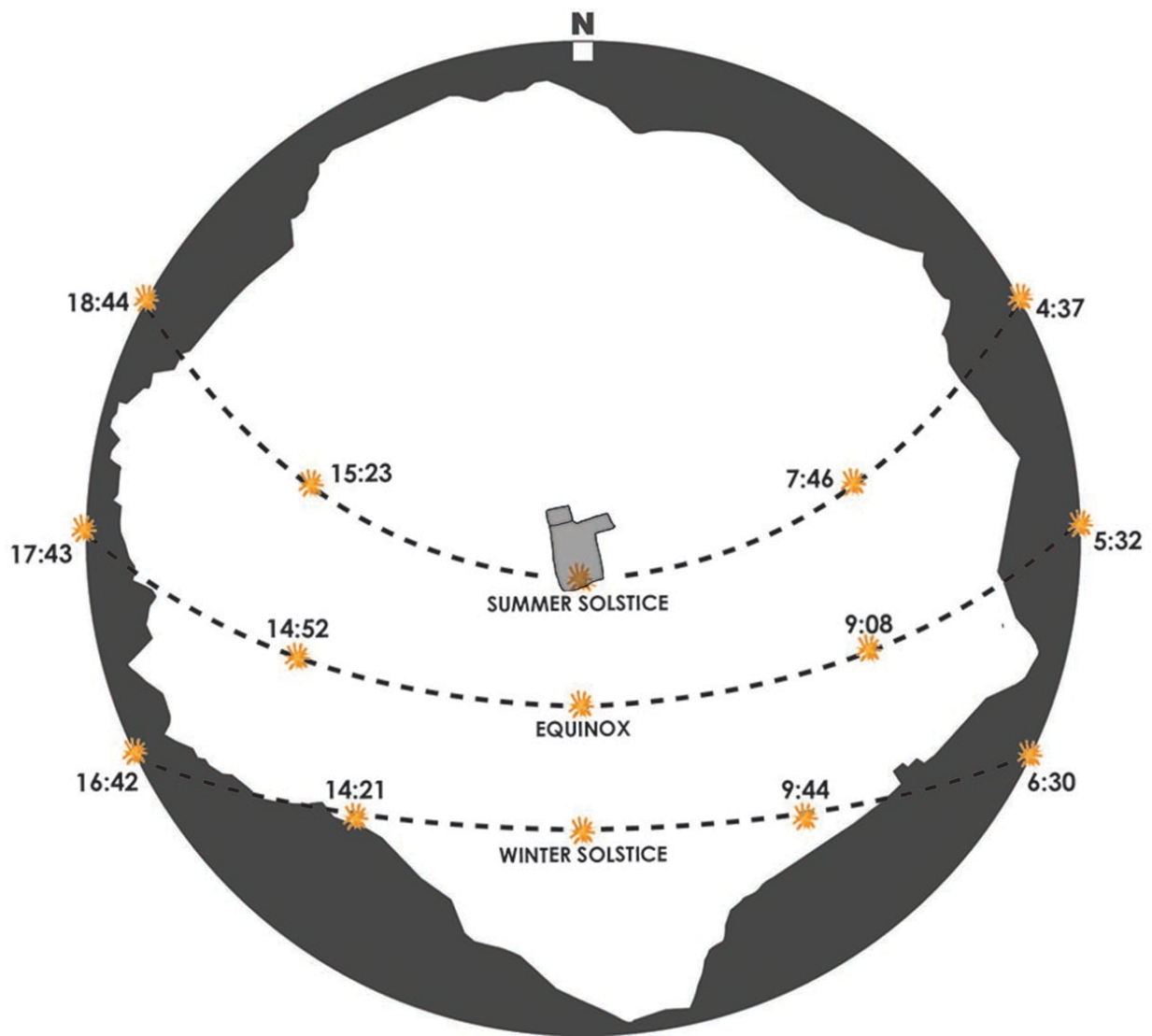


Figure 4.2 – Horizon diagram for Djinn Block X. Note that even during the summer and winter solstices there is very little direct sunlight on the northern face and the southern face always receives at least some direct insolation. Paradise (2013).

precise, discontinuity in physical collection controls limits the potential for accurate comparisons. Nonetheless, each face was assessed under conditions that reflect those most common to that particular face (Figure 4.2). The southern face was the only face not measured in the shade. However, this merely mirrors the fact that, actually, there is no shade on the southern face as it is exposed to direct sunlight throughout the entire day. Inversely, The northern face doesn't receive any direct sunlight and the eastern and western faces only get minimum sunlight during the day so they were all measured in the shade. Also, it is recognized that many of the micrometeorological differences between internal and external readings are minute and fall well within the window of error of the thermo-hygrometer, but the use of statistics illuminate meaningful relationships despite any potential data conflicts. As with all preliminary research, a certain level of uncertainty is permissible. Nevertheless, temporal and accuracy discrepancies will be considered and noted during analysis and discussion.

Chapter Five: Results and Analysis

This research analyzed three primary components: morphometry analysis, micro-environmental conditions, and their interrelationships with insolation and aspect. All three are inherently correlated but each component required specific calculations to divulge any significant relationships and patterns. Therefore, the analyses of each topic are discussed separately before providing a comprehensive assessment in the subsequent discussion chapter. In addition, both statistical and distributional analyses were conducted to provide more holistic results, as some relationships between aspects and the morphometric and micrometeorological parameters were better divulged on a non-linear logarithmic curve and, therefore, skewed when assessed purely statistically.

5.1 Tafoni Morphometry Analysis

This thesis study evaluated the shape, size, and distribution of decay forms, specifically, tafoni cells in Petra, Jordan. Since insolation and environmental influences were the primary independent variables, each cell's dimensions and aspects were paired throughout the analysis. Ultimately, the morphometry section contained two separate subdivisions: overall cell morphometry and the influences of aspect (insolation) on decay. Both components utilized the detailed measurements but to different degrees and for different purposes. It should be noted, though, that while all 156 detailed measurements were included in the cell morphometry analyses, the aspect and insolation assessment only used the ten maximum and ten minimum cell values per aspect to ensure an even distribution of cell measurements.

5.1.1 Tafoni Cell Dimensions and Calculations

Since most tafoni cells, including those found on Djinn Block X, do not develop homogeneously (Mustoe, 1983), several dimensions were measured to insure the most accurate representation of each cell. Measurements were then averaged to obtain a single value to represent that cell during statistical calculations, as analyzing each measurement would be tedious and not as indicative to the cell as a whole. Depth represents the z-axis and only required a single measurement at the center of each cell so no additional modifications were needed. However, the horizontal, vertical, maximum, and minimum axes were averaged per cell for a single diameter value to avoid confusing cell values (i.e. one value per cell instead of four values per cell that could be mistaken as other cells). Both these horizontal/vertical and maximum/minimum relationships were considered when calculating the tafone volume, representing the volume of total material lost. Assuming the cell opening is the largest circumference of the cell, volume was calculated as half of an ellipsoid using the following equation:

$$v = \frac{\frac{4}{3}\pi(r_1r_2r_3)}{2}$$

Where r_1 represents depth divided by two, r_2 is the minimum axis divided by two, and r_3 represents maximum axis divided by two. The volume was calculated again using the horizontal and vertical axes instead of the minimum and maximum axes. The two volumes were then averaged for statistical and graphical analyses. An ellipsoid equation was used instead of a spherical model because the majority of cells on Djinn Block X are non-spherical and the ellipsoid model allowed more flexibility between length and height. Also, it was divided in half to accommodate the cell openings as the largest diameter of the cell, as was the case in most recorded tafoni on Djinn Block X.

Before evaluating how insolation and environmental conditions influence the development of tafoni cells on Djinn Block X, the general method and patterns of decay must first be analyzed. Depths, average diameters, and volumes were all examined graphically in relation to increases in volume, as a surrogate for age, and in relation to each other to evaluate morphometric relationships. Recognizing the possible auto-correlation between these variables, the purpose was not to establish causality but to assess the degree to which both depth and diameter influence the growth of the cells. The gap between the minimum and maximum cell values was so extreme that the two subsets were graphed separately for the best visual representations. These analyses were then cross-referenced with raw cell counts and distribution on Djinn X to assess tafoni evolution and potential models of decay.

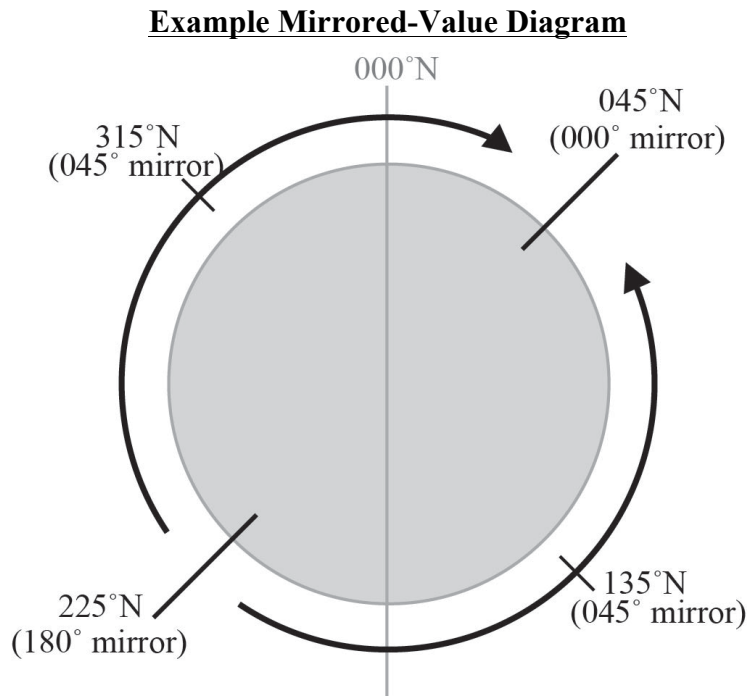


Figure 5.1 – Diagram demonstrating the mirrored-aspect values for the example of 225°N.

Mirrored-Aspect Values for Djinn Block X

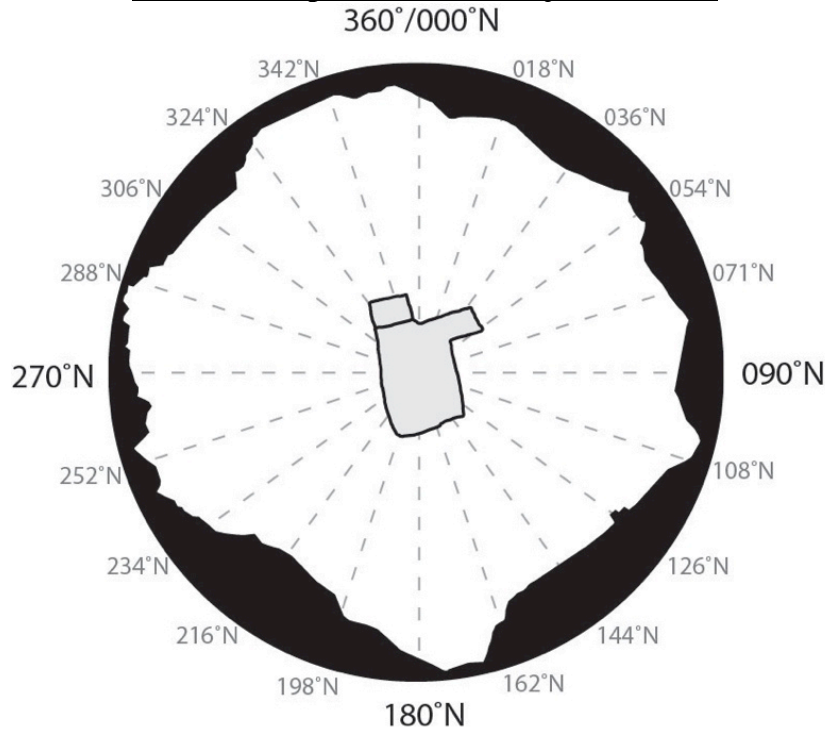


Figure 5.2 – Horizon diagram modified from Paradise (2013) to show the location of all mirrored-aspect values in relation to Djinn Block X.

5.1.2 Morphometry and Aspect

Solar flux (insolation) impacting Djinn Block X has previously been estimated in annual mega-joules per square meter using conventional calculations (Paradise, 2013) and range between 175 MJ/m^2 on the northern faces up to 3050 MJ/m^2 on the southern aspects. For that reason, the morphometric data collected for this thesis was categorized to match these pre-existing aspects and insolation values to avoid unnecessary duplication in the statistical analysis.

However, as aspect values increase past 180° towards 360° statistical significance is skewed. Therefore, a mirrored-value matrix was created where aspect values increased from 000° to 180° back down to 000° (see example in Figure 5.1). Then, to find aspects with the greatest influences on cell development, twenty mirrored values were created starting at 000°N and

increasing every 18° until 342°N (Figure 5.2). In the matrix, the mirrored value is represented by 180° with values decreasing in both directions to the opposing value replaced by 000°. Then the new corresponding values for each face's 360° aspect value were recorded in a new morphometric Excel™ spreadsheet until there were twenty unique spreadsheets, one for each mirrored value. Once this was completed, the coefficient of determination (R-squared) was calculated between aspect and different dimensions of cell development using the following relationship:

- *Independent Variable: Aspect from Mirrored Value Matrix*
- *Dependent Variables: Cell Depth, Average Diameter, and Average Volume*

Counter intuitive to field observations, initial correlations were weaker than expected. The only parameter to show significant relationships with aspect was depth: r^2 values ranging from 0.076 to 0.101 around 071°N to 126°N. Suspecting a cancelling effect in the advanced decay of both the northern and southern faces, the statistical analysis was split into two data sets. The first set excluded the northern (328°N) cell dimensions and the second set excluded the southern (156°N) cell dimensions, essentially analyzing the data as two half circles instead of a full 360 degrees. This revealed several more significant correlations for both depth and volume, though diameter remained generally insignificant. For the northern data set (i.e. omitting southern values), the most significant correlation for depth was $r^2 = 0.130$ at 108°N and for volume $r^2 = 0.157$ at 324°N. The southern data set displayed different patterns with the most significant R-squared values of depth $r^2 = 0.123$ at 216°N and a volume $r^2 = 0.076$ at 342°N.

5.2 Microenvironments and Micrometeorology

The second principal component of this research concerned microenvironments and their connection with aspect and tafoni cell development/stone decay. Similar to the morphometric data, when compared to aspect and insolation, the micro-environmental data were categorized to match the aspect values for Djinn Block X established by Paradise (2013) to maintain analysis consistency when compared to preexisting insolation values. Once all three variables (surface temperature, ambient air temperature, ambient humidity) were entered into the morphometric spreadsheets and mirrored-value aspect matrices, the differences between internal and external values were calculated for each microclimatic variable, noting that positive values indicated warmer and/or more humid conditions inside the cell compared to outside, and negative values meant cooler and/or dryer, while near-zero values indicate equal conditions.

Micrometeorologic difference values (internal minus external) varied between the largest and smallest cells so each dataset is considered discrete and, therefore, discussed and compared to each other as stand-alone entities. Both distributional and statistical analyses were conducted to determine which, if any, microclimatic variables correlate with aspect and cell morphometry to significant degrees. Distributional analysis assessed the relationships among the micrometeorological conditions and aspect locations on Djinn X, however, most difference values are well below instrumental accuracies ($\pm 2.0^{\circ}\text{C}$ surface temperature, $\pm 1.5^{\circ}\text{C}$ ambient temperature, and $\pm 5.0\%$ humidity), therefore pure distributional analyses are feasibly subject to instrument error and not discretely reliable. To counter potential instrumental-caused uncertainties, statistical analyses were also conducted to reveal significant associations. To address influence without neglecting the positive/negative relationships between aspect and microenvironment conditions, both correlation coefficients (r) and coefficients of determination

(r^2) were calculated, where r divulges positive and negative correlations with aspect, and r -squared establishes the degree of aspect's influence on the absolute values of difference. Furthermore, as no independent or dependent variables could be confidently identified between the morphometric and micrometeorological parameters, only simple correlation tests were performed to identify meaningful positive or negative relationships between these variables.

5.2.1 Surface Temperature

During data collection, three separate surface temperatures were measured per cell: external surface within 1cm of the cell opening, the cell ceiling, and the cell floor. Once entered into the morphometric spreadsheet, the cell ceiling and floor values were averaged to determine an overall internal surface temperature, which was used to calculate the surface temperature difference value.

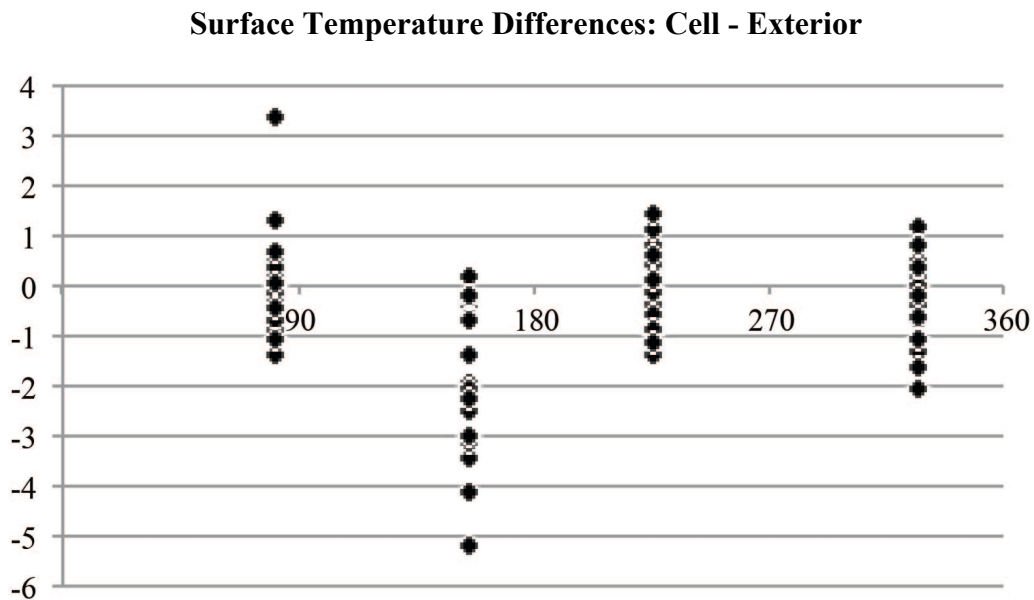


Figure 5.3 – Graph displaying the temperature differences between interior and exterior measurements per aspect. Note the values below 0.00 represent cooler interior temperatures and values above 0.00 represent warmer interior temperatures relative to exterior temperatures.

Distributionally, surface temperature showed the tightest statistical association with morphometry among the environmental variables, though only fairly weak correlations exist (depth $r = -0.370$ and diameter $r = -0.414$). When compared to aspect, however, more stark patterns and relationship become apparent (Figure 5.3). Statistically, basic relationships remain relatively weaker with the most significant correlations of $r = 0.383$ from 000°N and $r = -0.413$ at 162°N with determination coefficients peaking near $r^2 = 0.171$ at 162°N .

5.2.2 Ambient Temperature

Another micro-environmental variable assessed was ambient air temperature within and without each tafoni cell. Before analysis, the difference between internal and external cell temperature was calculated. Again, a negative value signifies a cooler internal temperature than the external temperature and positive values denote warmer internal conditions. Then, similar to surface temperature, this value was compared to both morphometry and aspect.

In terms of morphometry, the relations appear nonlinear and statistically unrelated with r -values ranging from depth $r = 0.032$ and diameter $r = -0.051$. Graphical examination did not reveal any other note-worthy relationships. Correlations with aspect are slightly more meaningful but still fairly weak with peak r -values around $r = -0.186$ at 126°N and $r = 0.186$ at 288°N and an insignificant greatest level of influence near 126°N ($r^2 = 0.035$). Graphical representation was scattered and did not show as clear of a pattern as surface temperature.

5.2.3 Ambient Humidity

The last micro-environmental element examined was internal and external ambient humidity. The difference between internal and external humidity was calculated the same way as

ambient temperature except positive values mean a higher internal humidity and negative values indicate dryer internal conditions. These values were also compared to morphometric and aspect variables via simple linear correlations and graphical interpretation.

There appear to be some weak correlations between humidity and the morphometric variables. Statistically, humidity related to depth with an $r = 0.134$, diameter with $r = 0.183$, and volume with $r = 0.143$. Scatter plots did not show any other substantial patterns in terms of morphometry. Regarding aspect, the clearest statistical correlations were found to range from $r = -0.245$ at 162°N and $r = 0.245$ at 306°N . These correlation values are technically considered weak and the aspect to humidity relationship is not as stark graphically as aspect to surface temperature but still noteworthy (Figure 5.4). Influence is equally as weak with the highest r^2 -values of $r^2 = 0.060$ at 162°N and again at 306°N .

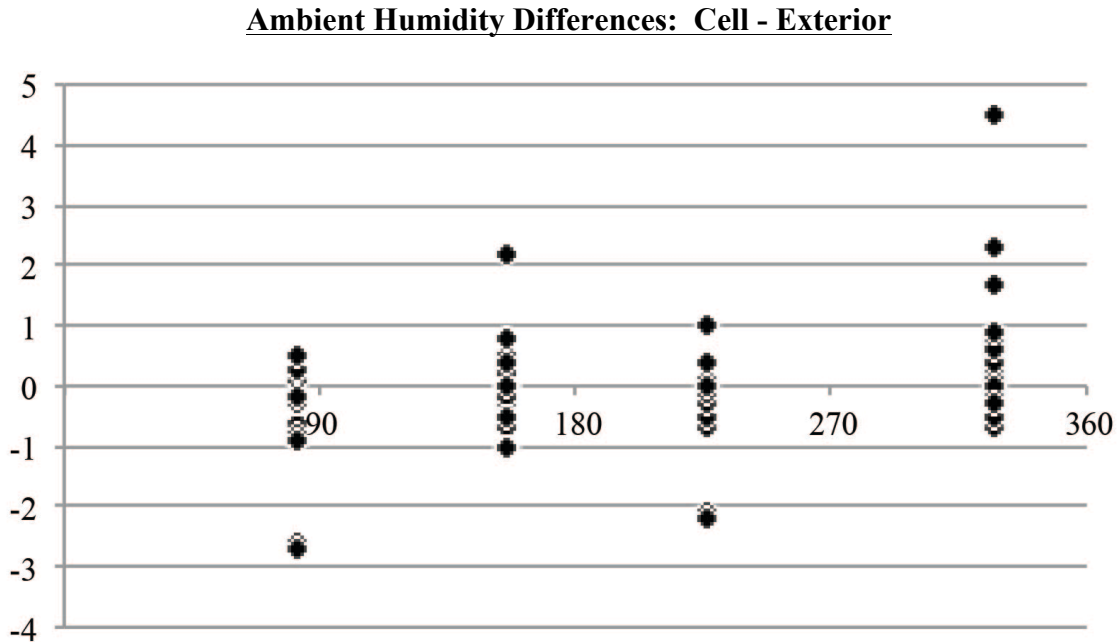


Figure 5.4 – Graph displaying the humidity differences between interior and exterior measurements per aspect. Note the values below 0.00 represent lower internal humidity and values above 0.00 represent higher internal humidity relative to exterior readings.

The findings of this research revealed that each morphometric and micrometeorological variable resulted in statistically varied degrees of influences on tafoni cell formation, and therefore dressed stone decay measured through linear modeling. Morphometrically, diameter remained fairly insignificant, even after the data were separated into northern and southern sets, where as the depth r^2 -values reached as high as 0.130 at 108°N (east southeast) and 288°N (west northwest) in the northern data set. Volume displayed the greatest connection with aspect with a peak r^2 -value of 0.157 at 144°N (southeast) and 324°N (northwest) for the northern data set, suggesting up to 15.7% of cell formation (i.e. stone deterioration) is due to insolation and other aspect-dependent stresses. The preliminary micrometeorological analysis identified surface temperature as the most relevant microclimate variable in terms of aspect (peak $r^2 = 0.171$ at 162°N) and morphometry (depth $r = -0.370$ and diameter -0.414).

Chapter Six: Discussion

The major thrusts of this research dealt with environmental influences on rock decay (weathering) and the morphometry of tafoni evolution on a hewn monument in Petra, Jordan through the analysis of three morphometric and three micrometeorological characteristics measured from a series of selected tafoni cells. Statistical, graphical, and cartographical analyses revealed complex associations among the variables. The discussion of these interrelationships was broken into three foci: (a) morphometric patterns and cell distribution related to aspect, and thus insolation, (b) micrometeorological measurements and their relationship to aspect and cell development, (c) tafoni evolution and decay. This study investigated tafoni growth modeling based on existing cells, distribution of the decay phenomena, and threshold theory.

6.1 Insolation and Rock Decay Patterns

Surface recession patterns and rates of decay on Djinn X have been already attributed to differences in insolation (Paradise, 2013), but this thesis research expounds upon this to include the influences of insolation on tafoni development, as a surrogate for comprehensive stone decay. Multiple detailed morphometric dimensions (depth, longest axis, shortest axis, horizontal axis, and vertical axis) were averaged and used to calculate three primary characteristics: cell depth, average diameter, and estimated volume. Measuring all 2500+ cells on the block was problematic and therefore, following a greatest variation sampling method, the ten largest and ten smallest cells per face were measured. The large numerical difference between the largest and smallest cells skewed initial analyses and required separate examination, but most display similar patterns despite scale and, therefore, they are discussed individually and as a set.

6.1.2 Aspect and Depth

Corresponding with field observations, the quantitative analysis of tafoni depth and aspect (i.e. insolation) displayed clear distributional relationships on Djinn Block X.

Morphometric assessments are based on the categorized raw count and field observations while statistical analysis employed the mirrored aspect value matrix and the detailed measurements organized to fit insolation values from Paradise (2013).

Morphometrically, the highest concentration of deeper cells was found mainly on the northern and southern faces, but the deepest cells were on the northern (52.8cm) and western (36.5cm) faces. Although these values represent outliers in the dataset, average depth values per face reflect the same pattern with the deepest cells on the northern (22.5cm) and western

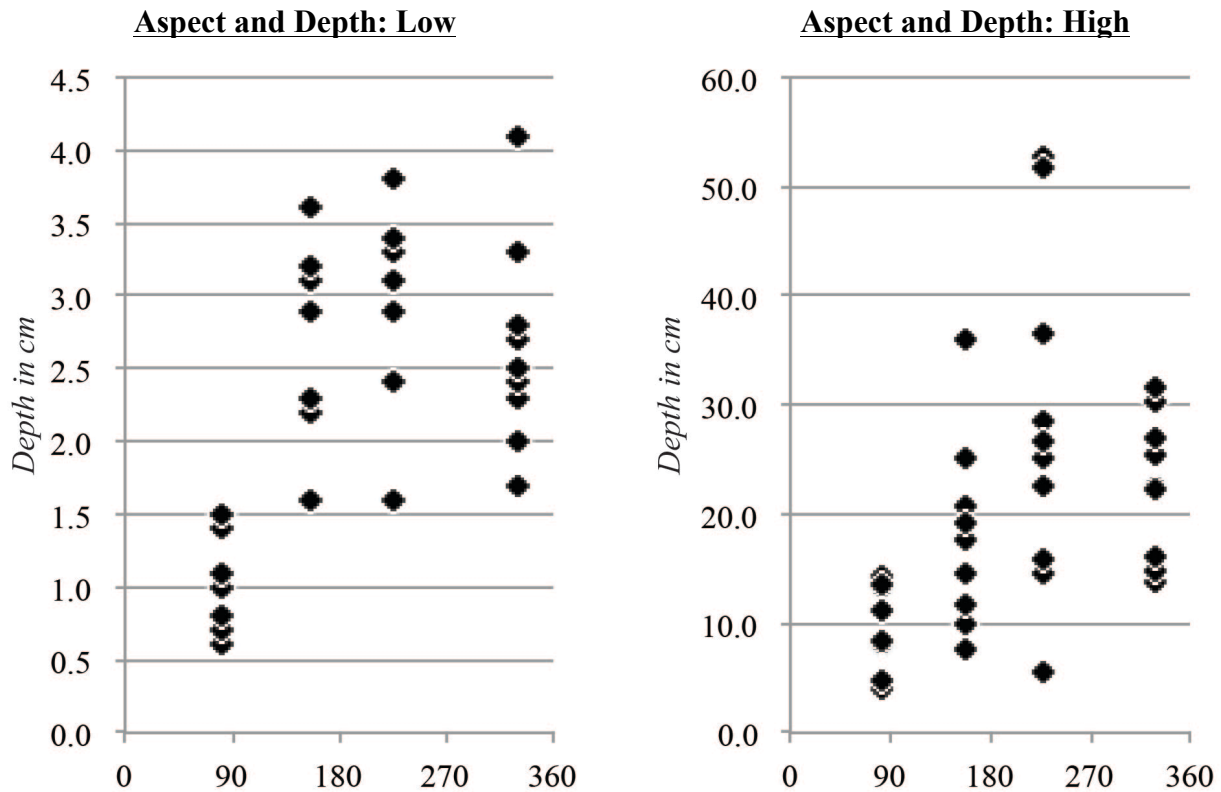


Figure 6.1 – Graphs showing the high and low depth value distribution in relation to aspect. Note the different scales to the left of the graphs.

(17.3cm) faces (Figures 6.1). However, cell depths were measured from the back wall to the lip of the opening so cell depths are not necessarily equivalent to surface recession as some cells have developed on already receded surfaces, such as those found on the heavily decayed southern face. Therefore, had depth been measured to an original surface false-datum, like Paradise (1999, 2013), the southern face would display significantly deeper cells. Inversely, the shallowest cells (less than 2cm deep), which are much more abundant on Djinn X, are concentrated on the eastern and western faces (Figure 6.3), with the shallowest cells, both measured (0.6cm) and averaged (1.2cm), on the eastern face. These findings correspond with

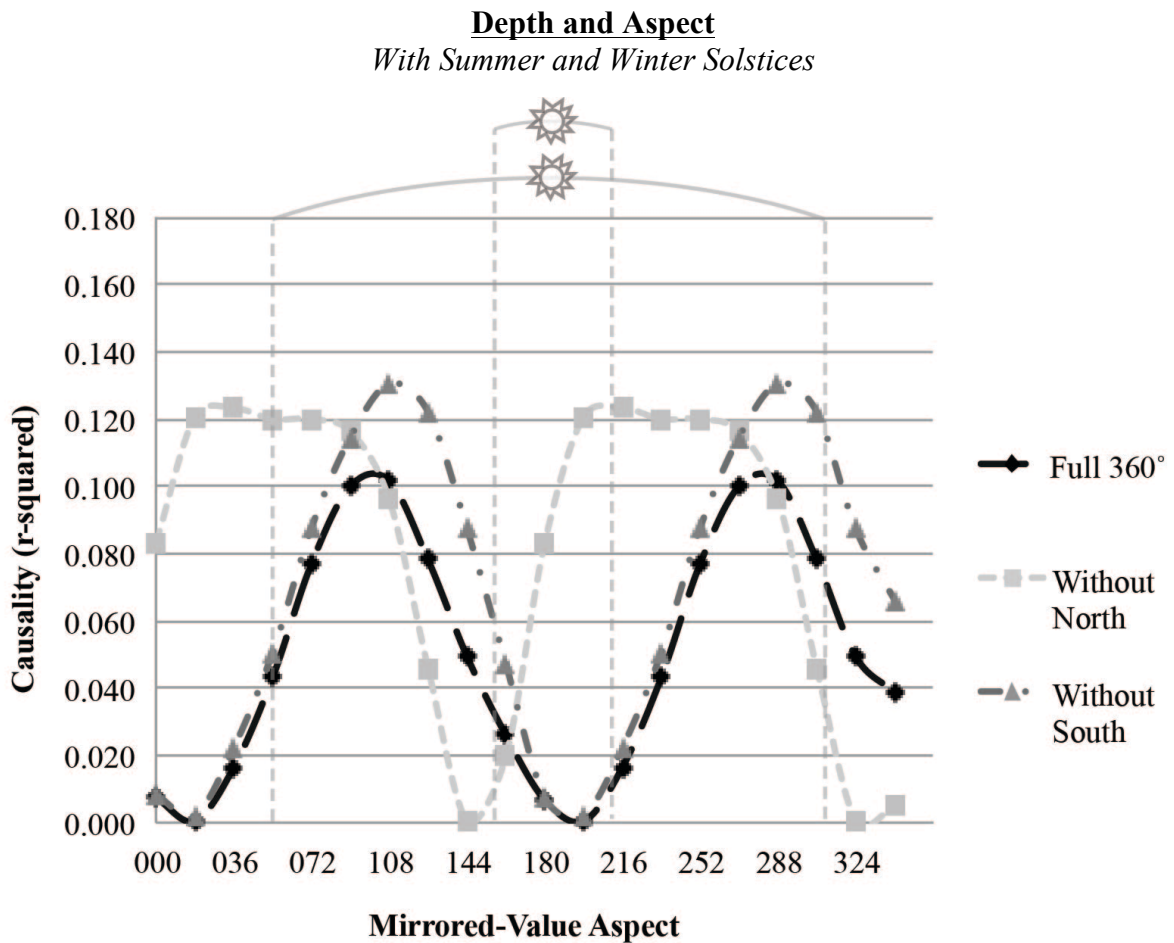


Figure 6.2 – Graph showing the depth r-squared values for the three mirrored-aspect matrices. Note the block receives significantly more direct sunlight during the summer (bottom sun) as opposed to winter (top sun).

surface recession patterns in Paradise (2013), which claimed the southern and northern faces have the highest rates of decay, 120-220 mm/millennia and 105-110 mm/millennia respectively.

Statistically, the analysis of depth and aspect revealed different patterns, particularly among the three mirrored value ranges: full 360°, excluding southern values, and excluding northern values (Figure 6.2). When all faces were examined (i.e. the full 360°) there were only weak correlations peaking around $r^2 = 0.102$ at 108°N (east) and again at 288°N (west). This suggests that the highest percentage of cell growth (on the z-axis) due to insolation, or other aspect dependent variables, is on the east and west faces, which are contrary to morphometric and distributional field observations. When the southern depth values were excluded from the

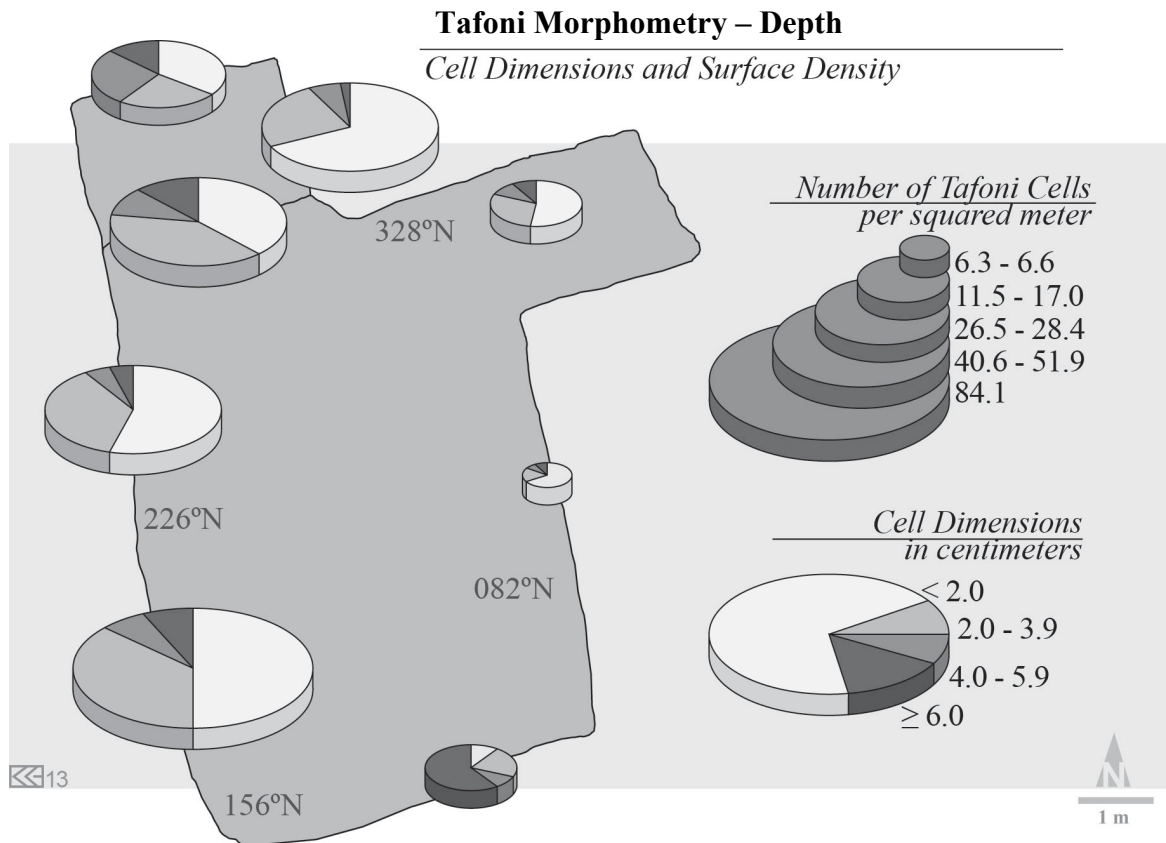


Figure 6.3 – Footprint of Djinn Block X showing the raw count of cells per panel categorized by size for depth. Note the most common cell depth is less than 2cm. Groom (2014).

matrix, the correlations were slightly higher and followed a similar pattern but with much steeper slopes leading up the strongest $r^2 = 0.130$ at 108°N and 288°N , signifying a sharper increase in insolation/aspect influence on decay. Contrariwise, when the northern values were excluded, the entire curve shifted several degrees and displayed a much different pattern. Significant correlations peaked around $r^2 = 0.123$ at 036°N and again at 216°N , but remain high between 018°N to 072°N (north northeast quadrant) and 198°N to 252°N (south southwest quadrant). This configuration of north/south dominance is more congruent with field observations and previously established patterns of decay focused on the northern and southern aspects (Churchill, 1982).

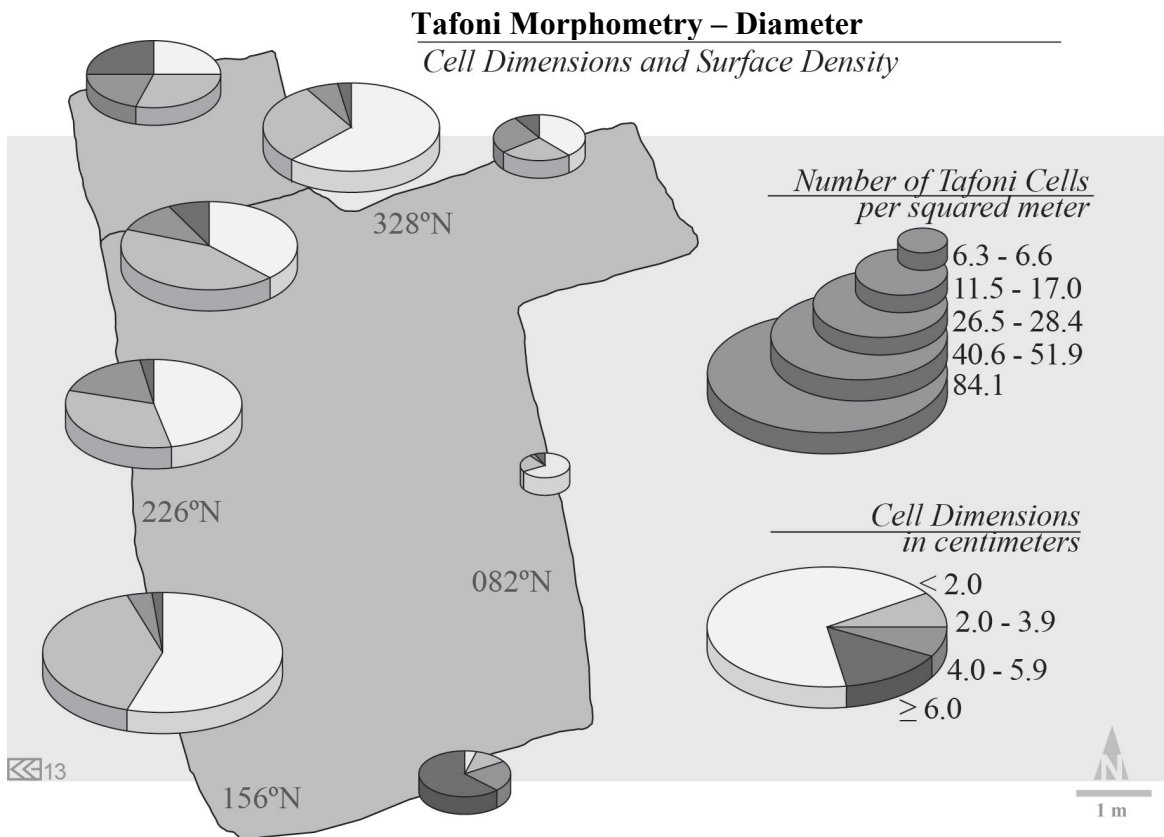


Figure 6.4 – Footprint of Djinn Block X showing the raw count of cells per panel categorized by size for diameter. Note the different cells sizes for the southern face. Groom (2014).

6.1.3 Aspect and Diameter

Morphometric, distributional, and statistical analysis between diameter and aspect reveal significant relationships distinctly different than those between aspect and depth. As before, the morphometric and distributional assessments utilize the detailed measurements of the ten largest and ten smallest cells as well as the categorized raw counts while the statistical analysis encompasses the mirrored value aspect matrix and the aligned morphometric values.

Morphometrically, there is a significantly higher concentration of larger (wider) cells on the southern face, followed by the northern face (Figure 6.4). The largest measured (81.5cm) and average (27.8cm) cells are also located on the southern face. Many of the larger cells show evidence of coalescing, when two or more cells merge to create one larger tafone (Mustoe,

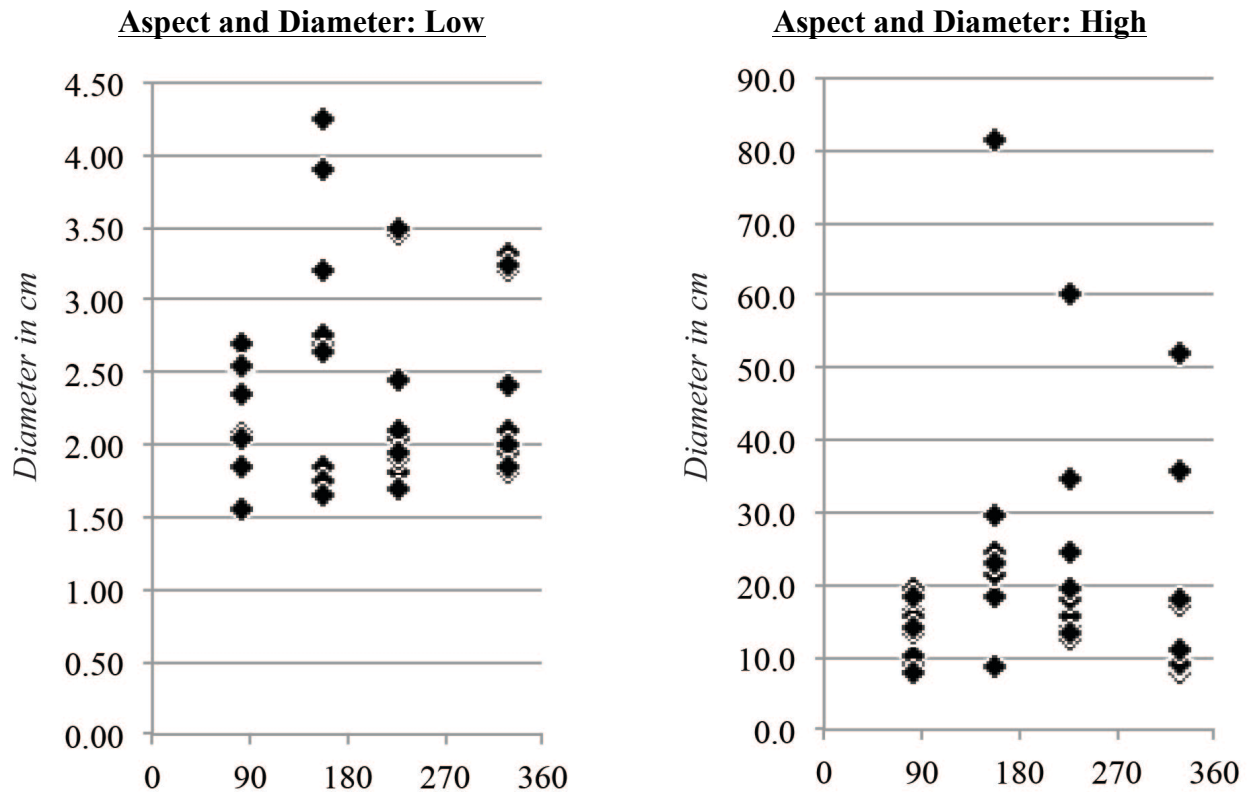


Figure 6.5 – Graphs showing the high and low diameter value distribution in relation to aspect. Note the different scales to the left of the graphs.

1983). The largest cells on both the southern and northern faces are outliers but the southern face displays significantly more coalescing and indiscrete (broken floors, ill-defined cell boundaries, or otherwise difficult to measure) cell expansion than any other face. The smaller (narrower) cells were heavily concentrated on the eastern and western faces with the smallest measured (1.6cm) and average (1.8cm) cells on the western face. Even though the smallest cells measured were not necessarily the smallest cells on the block, as the thermo-hygrometer couldn't accommodate any cell smaller than 1.5cm in diameter, the western face had abundant cells right at this threshold, as reflected by the minimum-size data set (Figure 6.5).

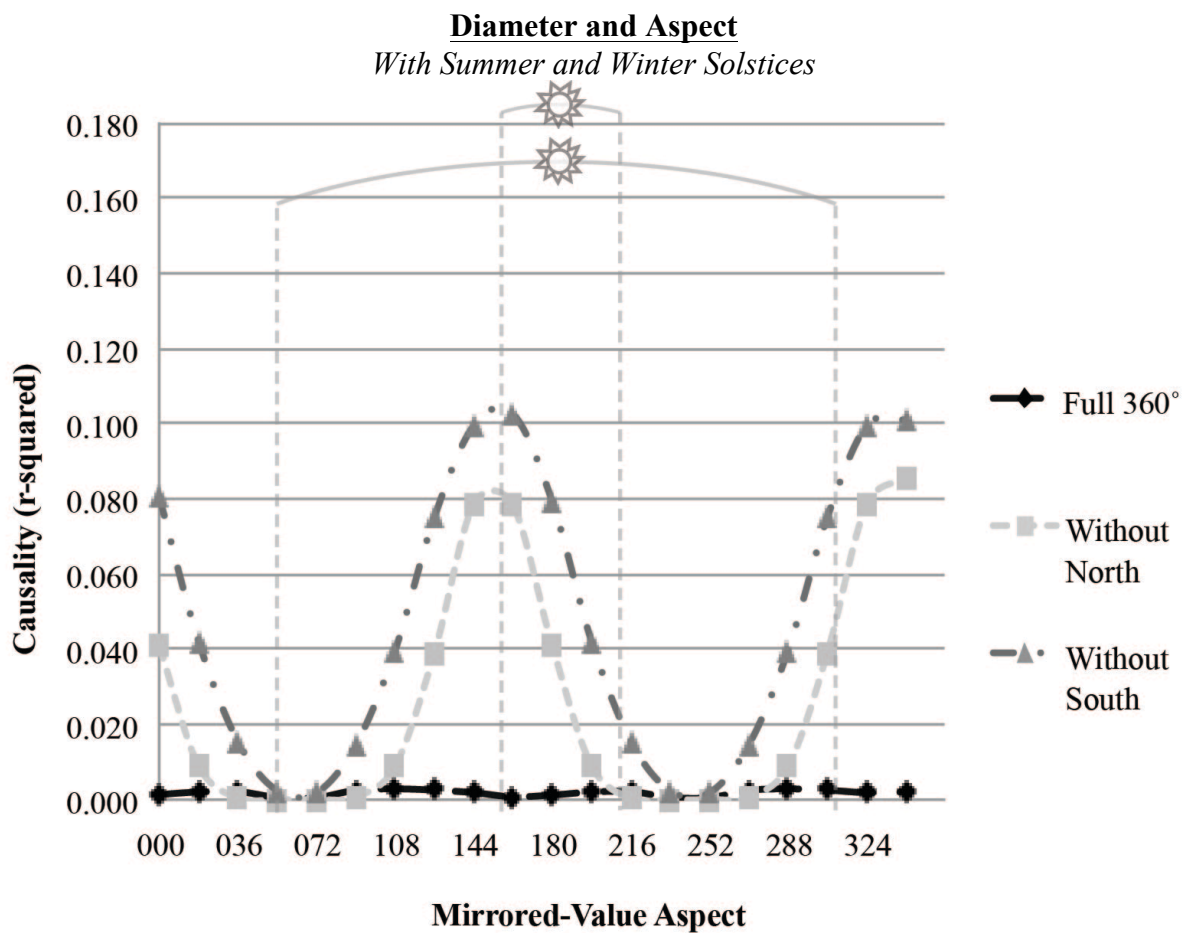


Figure 6.6 – Graph showing the diameter r-squared values for the three mirrored-aspect matrices. Note the block receives significantly more direct sunlight during the summer (bottom sun) as opposed to winter (top sun).

The statistical analysis of diameter versus aspect shows a distinct pattern among the three mirrored value matrices data sets (Figure 6.6). The initial 360° matrix revealed almost zero correlation and very little distinction between mirrored values aside from slight correlations at 090°N (due east) and 270°N (due west). The northern (i.e. without south) and southern (i.e. without north) data sets, however, demonstrate higher correlations at 144°N to 162°N (south southeast) and again from 324°N to 342°N (north northwest). The stark difference between the separated data sets and the 360° evaluation supports the hypothesis that the heavily decayed northern and southern faces were having a cancelling effect in the statistics. The northern data set has the strongest correlation with $r^2 = 0.103$ at 162°N and $r^2 = 0.101$ at 342°N. The southern data set follows the same path but with slightly weaker relationships peaking around $r^2 = 0.078$ at 162°N and $r^2 = 0.086$ at 342°N. This north/south pattern is dissimilar from the 360° and southern depth correlations but is more consistent with field observations of more heavily decayed northern and southern faces.

6.1.4 Aspect and Volume

As a compilation of multiple variables, volume has its own unique relationships with aspect. Since the values are a result of multiple calculations and alterations, any statistical analyses may not be as reliable as measured variables like depth, but are still relevant and provide valuable information. Furthermore, volume can be used to represent total material lost, similar to Mol and Viles (2012), so volume morphometric examinations focus on the differences and similarities between depths' and diameters' distributions and how they interact in relation to total stone decay and aspect. Therefore, both the morphometric and statistical analyses were

conducted using the same techniques as depth and diameter, although resulting significances are different.

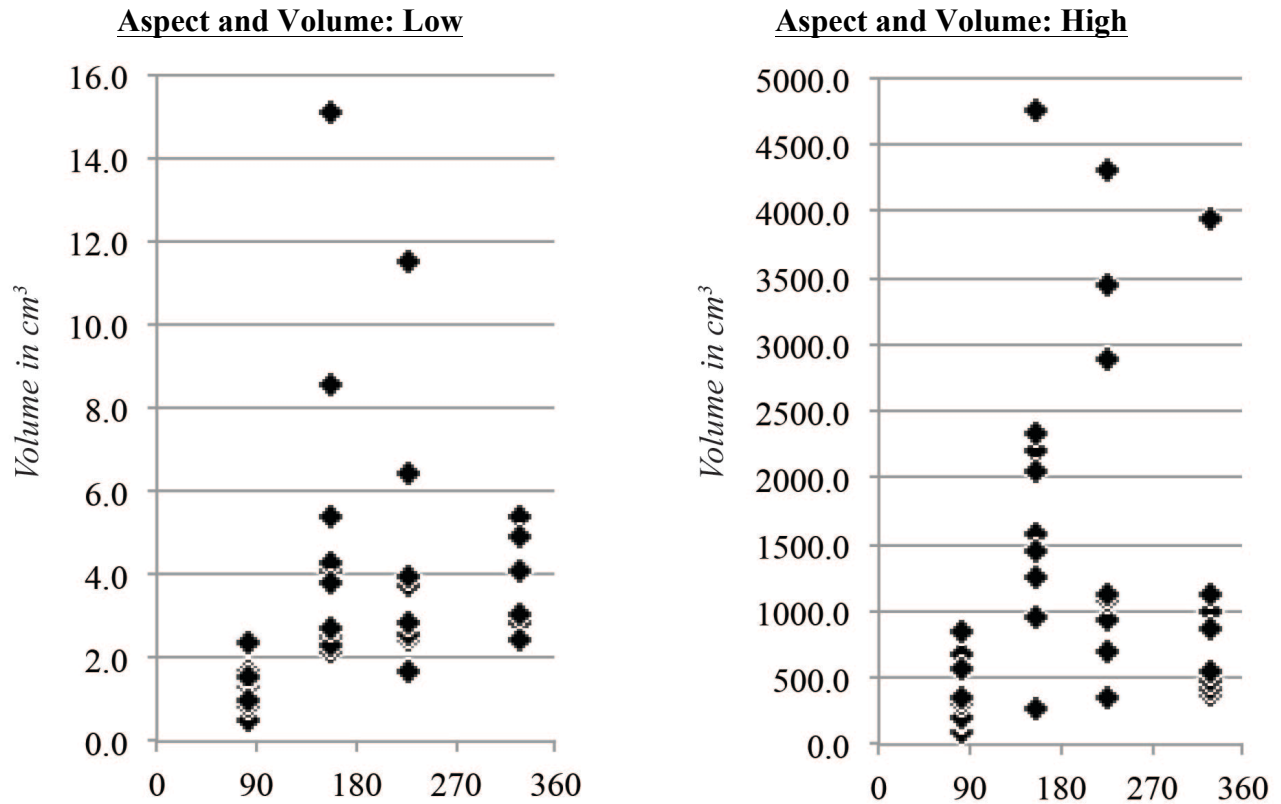


Figure 6.7 – Graphs showing the high and low volume value distribution in relation to aspect. Note the different scales to the left of the graphs. The four largest volumes are extreme outliers and are not shown here to improve clarity.

Morphometrically, the distribution of cells with the largest and smallest volumes on Djinn Block X depends entirely on continuity between relative depth and diameter. Since the southern and northern faces have both deep and wide cells, they exhibit significantly higher average volumes (5446.6cm^3 south and 1967.9cm^3 north) than the eastern (181.9cm^3) and western faces (500.2cm^3), though these averages have been slightly skewed by massive coalesced cells on the northern (15795.4cm^3 and 14610.8cm^3) and southern (25454.2cm^3 and 20243.3cm^3) faces. If these outliers are omitted, the northern face contains, on average, much larger cells (1131.6cm^3) than the southern face (490.9cm^3), although the discussed discrepancy

between depth and surface recession on the southern face is a factor. On the other end of the spectrum, regardless of having varied depths, small diameters on the western face dramatically reduce volume, as do the relative shallowness of eastern cells, which have a fair range of diameters. Furthermore, despite higher depths in the western cells, narrower openings result in consistently smaller volumes with only two outliers (2884.3cm³ and 1588.6cm³). The northern and southern faces were a little more spread out, but clusters of shallower and narrower cells on the north face result in lower volumes than southern cells in the minimum dataset (Figure 6.7).

Patterns in the statistical evaluation of volume more closely resemble those of diameter

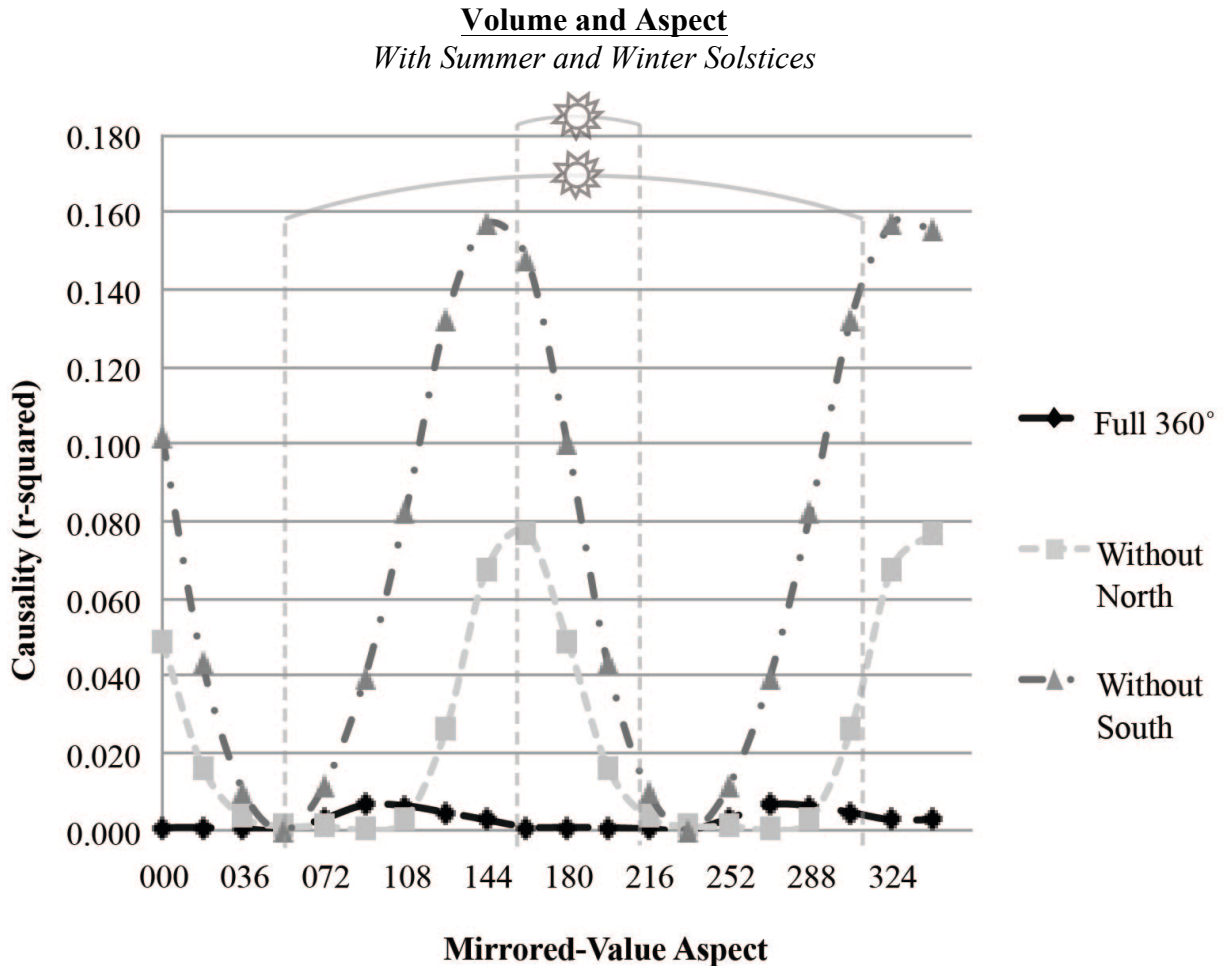


Figure 6.8 – Graph showing the volume r-squared values for the three mirrored-aspect matrices. Note the block receives significantly more direct sunlight during the summer (bottom sun) as opposed to winter (top sun).

instead of depth. Once again, the 360° data set was fairly weak with only minor increases at 090°N (due east) and 270°N (due west) but nothing substantial ($r^2 < 0.01$). The northern and southern datasets exhibit steeper changes in correlation peaking between 144°N to 162°N (south southeast) and again between 324°N and 342°N (north northwest), and, in fact, the measured aspects of both the southern (156°N) and northern (328°N) faces lie within these arcs.

The northern dataset has a much stronger correlation (top $r^2 = 0.157$ at 144°N and 324°N) than the southern dataset (top $r^2 = 0.077$ at 162°N and 342°N)(Figure 6.8). These numbers imply that up to 15.7% of all material lost (volume) is directly influenced by insolation (or aspect-dependent variables) on the northern face but only 7.7% on the southern face, which matches popular consensus regarding northern-centrism in aspect related decay (e.g. Churchill, 1982) but not field observations. The southern face appears significantly more decayed than any other face, and it is possible this deterioration is affecting the numerical analysis: many of the cells on the southern face have collapsed into non-discrete immeasurable surfaces and no longer fit tafoni parameters and, therefore, are excluded from the dataset. Nevertheless, these forms exhibit evidence of past cells (i.e. discrete cell roofs with no body or floor) and might represent an end product, or exit stage, of tafoni development and cavernous decay on Djinn X. So while statistical assessment attributes stronger aspect-dependent decay to the northern face, certain consideration must still be given to post-tafoni decay on the heavily deteriorated southern face.

6.2 Microclimate, Environment, and Aspect

The second thrust of this research assessed micrometeorological measurements, representing climatological and environmental influences, of measured tafoni cells and their relationship to aspect and overall cell morphometry. In addition to the detailed morphometric

measurements, internal and external surface temperatures, ambient air temperatures, and ambient humidities were recorded. The time of day and degree of direct sunlight were also noted per reading, though both varied throughout data collection and account for a degree of uncertainty. Although it is accepted these micrometeorological readings are static and do not represent comprehensive patterns over time, they still provided sufficient data for a basic preliminary investigation of the relationships between internal/external cell environments and aspect/cell morphometry.

6.2.1 Surface Temperature, Aspect, and Morphometry

Surface temperature was the first micrometeorological variable assessed, and presented very distinct relations to aspect. The maximum dataset exhibited a general tendency for internal cell temperatures to be cooler than external temperatures, especially on the southern face

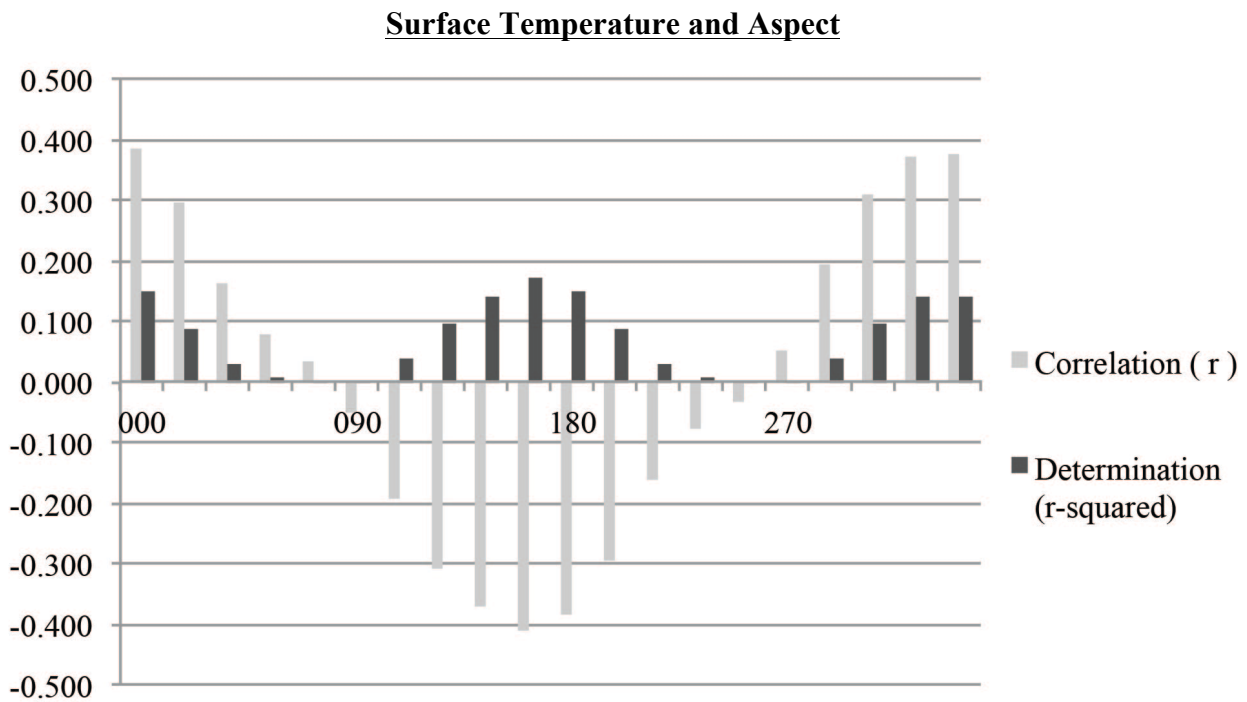


Figure 6.9 – Graph of r and r^2 values for surface temperature variation along the 20 mirrored-aspect values for Djinn Block X.

(average -1.92°C), possibly resulting from higher insolation causing evapotranspiration drawing moisture from the decayed interior and, thus, cooling the surface (Mol & Viles, 2010). Although the western and northern faces barely have temperature differences exceeding $\pm 1.50^{\circ}\text{C}$, the maximum dataset also displayed significantly greater variance between internal and external temperatures, up to 5.2°C (south), than the minimum set, which mainly remain within $\pm 0.5^{\circ}\text{C}$ difference. Moreover, the minimum dataset shows a warmer trend within the cells, especially the western face, up to $+1.45^{\circ}\text{C}$. Also, analyzed internal surface temperatures were the average of two values, roof and floor, so buildup of decayed material on the northern and western faces might have skewed the floor temperature reading.

Statistically, surface temperature had the strongest correlations to aspect among the micrometeorological variables, both positively ($r = 0.383$ at 000°N) and negatively ($r = -0.413$ at 162°N)(Figure 6.9). This suggests that as aspects near 162°N , internal surface temperatures are cooler than exterior values and when aspects continue back to $360^{\circ}/000^{\circ}$, the correlation flips and interior surface temperatures become warmer. In terms of influence, insolation and aspect-related factors have significant impact on internal and external surface temperature differences on the southern ($r^2 = 0.171$ at 162°N) and northern ($r^2 = 0.141$ at 342°N) faces as expected (aspect is already often associated with thermal heating and expansion (e.g. Ollier, 1963)). And yet, from 052°N to 090°N (east northeast) and again from 234°N to 270°N (west southwest) both influence (r^2) and correlation (r) are almost non-existent, suggesting minimal insolation influence at these aspects. This north/south dominant pattern fits popular hypotheses regarding aspect, as well as morphometric relationships (e.g. Churchill, 1982). Surface temperature displays significant correlations with both depth ($r = -0.317$) and diameter ($r = -0.387$), insinuating that as cells increase in size interior surface temperatures are more likely to be cooler than exterior surfaces,

which could be due to active capillary action within the cell walls manipulating moisture regimes (Mol & Viles, 2013). Near-surface moisture regimes have been associated with tafoni development (Mol & Viles, 2011) so it might be reasonable to stipulate that differential interior/exterior surface temperatures also contribute to cavernous decay and tafoni evolution.

6.2.2 Ambient Air Temperature, Aspect, and Morphometry

The second micrometeorologic variable, ambient air temperature, mirrored some of the patterns found with surface temperature but difference values were not as consistent and aspects with the greatest statistical significance are dissimilar. The maximum dataset showed generally cooler cells on the southern face (average difference = -0.10°C), fairly scattered values for eastern and northern faces tending to be slightly warmer, and nearly identical internal and external values on the western face. The tight consistency on the western face may have to do

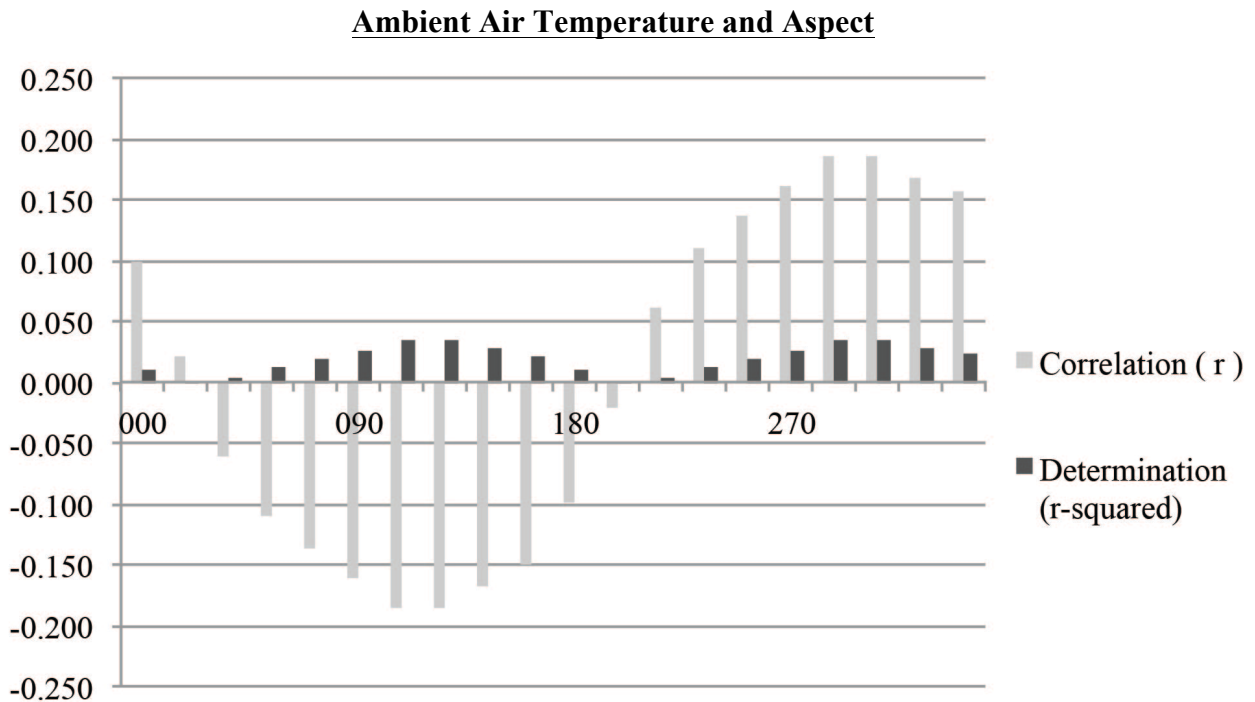


Figure 6.10 – Graph of r and r^2 values for ambient air temperature variation along the 20 mirrored-aspect values for Djinn Block X.

with prevailing wind patterns or other weather-related factors on the day of recording. There is also a much higher concentration of bird, insect, and spider nests in the cells on the western face that might suggest more consistently mild conditions. The minimum dataset exhibited a different pattern with mostly cooler cell temperatures on eastern, southern, and northern faces and a stark warm trend to the west, with only positive values. There are a few exceptions in the southern value set, but overall, the smaller cells all reveal cooler conditions, except on the western face. This western discrepancy may be the result of inconsistent times and/or recording conditions as the western face was measured over a period of two days, beginning in the afternoon (13:32-14:25) when the face was in direct sun and finished the following morning (08:19-09:07) when the face was shaded, unlike most of the other faces that were measured in one sitting. Also, high winds skewing ambient air temperature and humidity readings cut several research days short and may possibly account for a certain level of variability within the data.

Consequently, statistical analysis reflects much lower correlation values (both r and r^2) in an east/west-dominated pattern (Figure 6.10). Nearly half surface temperature, the strongest correlations between aspect and ambient air temperature are $r = -0.186$ from 108°N to 126°N (east southeast) and $r = 0.186$ from 288°N to 306°N (west northwest), mirroring the warmer interiors on western faces and cooler interiors on eastern faces. Insolation influence is even less substantial with the highest r^2 of only 0.035 at 126°N and 306°N . Morphometry also shows particularly weak correlations (depth $r = 0.158$ and diameter $r = 0.016$), which might suggest ambient air temperature is not a key component in tafoni development on Djinn Block X.

6.2.3 Ambient Humidity, Aspect, and Morphometry

The final micrometeorological variable examined in relation to aspect and morphometry was internal/external ambient humidity levels. Distributional patterns are not especially distinct for this variable, as both the minimum and maximum datasets exhibit relatively low difference values (mostly within +/-0.5% relative humidity for smaller cells and +/-1.0% for larger cells) with little variance among the aspects. Nevertheless, there are a few patterns worth discussing.

One potentially significant relationship is a minor tendency for higher internal humidity levels on the northern face in both minimum and maximum datasets. These wetter conditions could reflect the lack of direct sunlight on this face resulting in longer wetting and drying cycles within the cells, particularly the larger and deeper tafoni, corresponding with generally cooler internal temperatures on the same face (Mol & Viles, 2013). Inversely, internal cell conditions are slightly drier on the eastern and western faces in both minimum and maximum datasets,

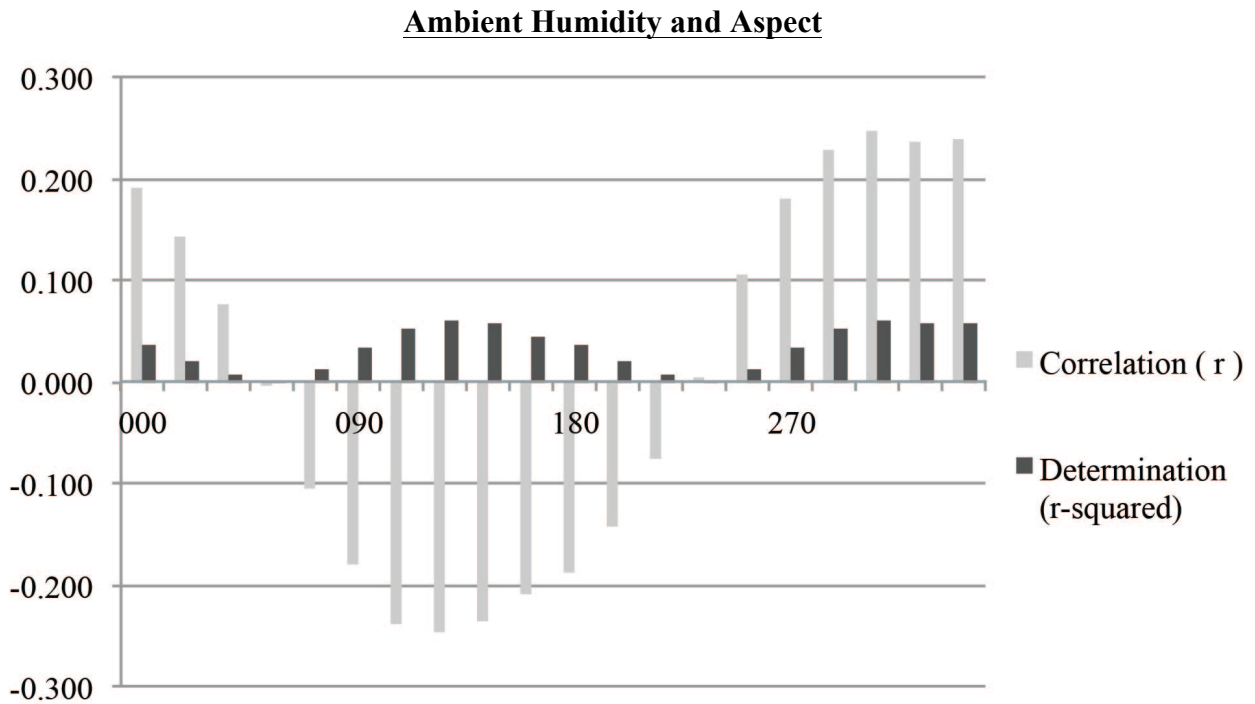


Figure 6.11 – Graph of r and r^2 values for ambient humidity variation along the 20 mirrored-aspect values for Djinn Block X.

possibly due to varied diurnal sunlight but the aspect variance is miniscule and barely noticeable.

Statistical analyses revealed clearer, but not exceptionally significant, humidity correlations with aspect (Figure 6.11). The strongest relationships are on the southeast ($r = -0.245$ and $r^2 = 0.060$ at 162°N) and northwest ($r = 0.245$ and $r^2 = 0.060$ at 306°N) faces, although correlations remain relatively higher ($r > 2.3$) for more of the northwest quadrant ($288^\circ\text{N} - 342^\circ\text{N}$) than to the southeast. The negative correlations, denoting drier interior conditions, encompass nearly the entire southern portion of Djinn X (from 072°N to 216°N) and coincide with the faces that receive the most concentrated sunlight, which may be causing more rapid and intense drying (Paradise, 2013). Morphometrically, humidity is more closely tied to diameter ($r = 0.243$) than depth ($r = 0.128$), but both have positive correlations, signifying larger cells are more likely to contain higher levels of humidity than smaller cells. The implications of this relationship to tafoni development correspond with the hypotheses presented by Paradise (2013): that the greater decay on the northern face is due in part by longer wetting and drying periods from lack of direct sunlight and, inversely, that the advanced decay on the southern face is caused by stresses from intense solar influx instigating more extreme wetting and drying cycles.

6.3 Tafoni Morphometry and Threshold Modeling

The third thrust of this research examined cell morphometry independently from aspect, although aspect influences are still discussed, culminating in a threshold-based tafoni growth model from existing cells on Djinn Block X (Figure 6.12). This component includes many of the previously discussed phenomena and decay patterns but organizes them to explain the plethora of different tafoni cell types present, which are unexpected given the relatively recent date of raw surface exposure (~2000 years). The model presented here is composed of episodic stages of

Stage Based Threshold Tafoni Genesis Model

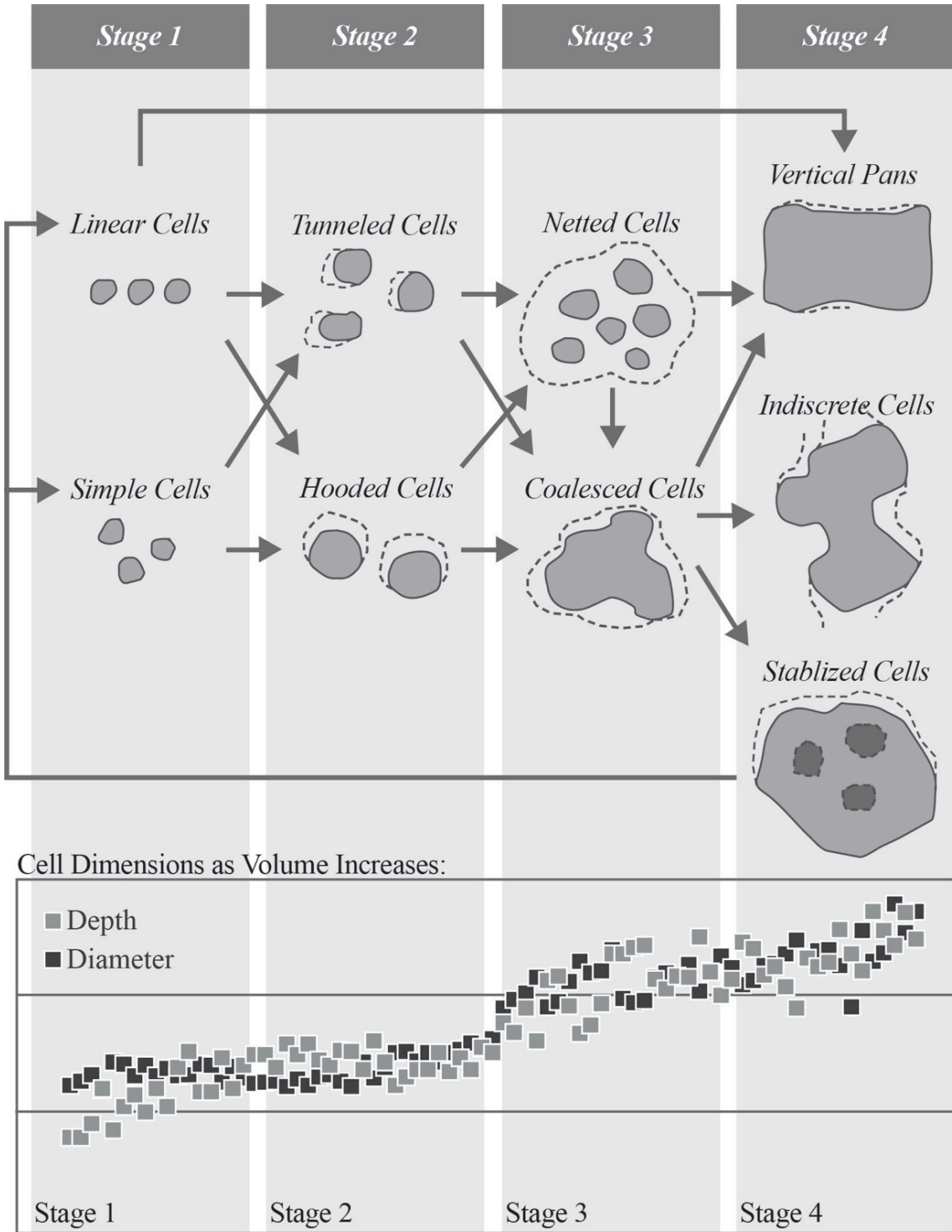


Figure 6.12 – Descriptive stage based tafoni genesis model. Note the shifts in depth and diameter as volume increases (representing the passage of time) and the cell progress into later stages of decay.

decay, as opposed to continuous decay models (e.g. Sunamura, 1996), and based on recorded cell types on Djinn Block X so the different observed cell types (i.e. stages) are described in detail, and then the supporting hypotheses and threshold theory is discussed and justified.

6.3.1 Observed Tafoni Cell Types and Descriptive Genesis Model

Based on empirical measurements of observed tafoni and threshold theory, the tafoni genesis model categorizes each cell type into four distinct stages of decay; with an optional exit stage if certain decay rate thresholds cannot be maintained. All observed cell types on Djinn Block X were organized into these stages by shape and decay patterns (ratio between depth and diameter). The order and transitions between stages were determined by assessing the relationships of measured depths and diameters of all recorded cells as volume increases. The purpose of this assessment is not to determine the exact causality of dimensional change but to identify points at which one decay rate outpaces the other and marks the advancement into the next stage of decay. Tafoni cells on Djinn Block X displayed several shifts between depth (interior) and diameter (exterior) growth rates depending on the stage of decay, suggesting the presence of threshold response between stages. Detailed descriptions of each stage of decay and the cell types of which they are comprised are provided, as well as the markers of stage progression within the model.

Stage 1: *Simple or Linear Cells*

Most commonly associated with the terms tafoni and pitting, *Simple Cells* are the most abundant cell type present on Djinn Block X and are characterized as being fairly small, discrete, and spherically shaped with width to height to depth ratios remaining around 2:2:1 (Figure 6.13).

Simple Cells aligned between two resistant bedding planes develop linearly and are given the supplementary diction of *Linear Cells* but all other cell characteristics remain analogous. Newly initiated and particularly small ($< 0.5\text{cm}^3$) cells fall within this first stage.

Simple and *Linear Cells* were recorded on every vertical surface of Djinn Block X, although with varying quantity and distribution per aspect. The less decayed surfaces (i.e. western and eastern faces) displayed significant *Simple Cell* populations while on the more heavily decayed surfaces (i.e. southern and northern faces) many of the cells have already progressed into later stages of decay. The vast majority of cells on the least decayed eastern face fall within the first stage of decay. The relative uniformity of Stage 1 cells is lost once the cell reaches a certain size ($\sim 1.7\text{cm}^3$ on Djinn X) when diameter, height, and depth begin to experience differentiated decay rates due to the myriad of physical, chemical, and biological decay processes affecting the stone and they advance into Stage 2.

Stage 1: *Simple* and *Linear Cells*

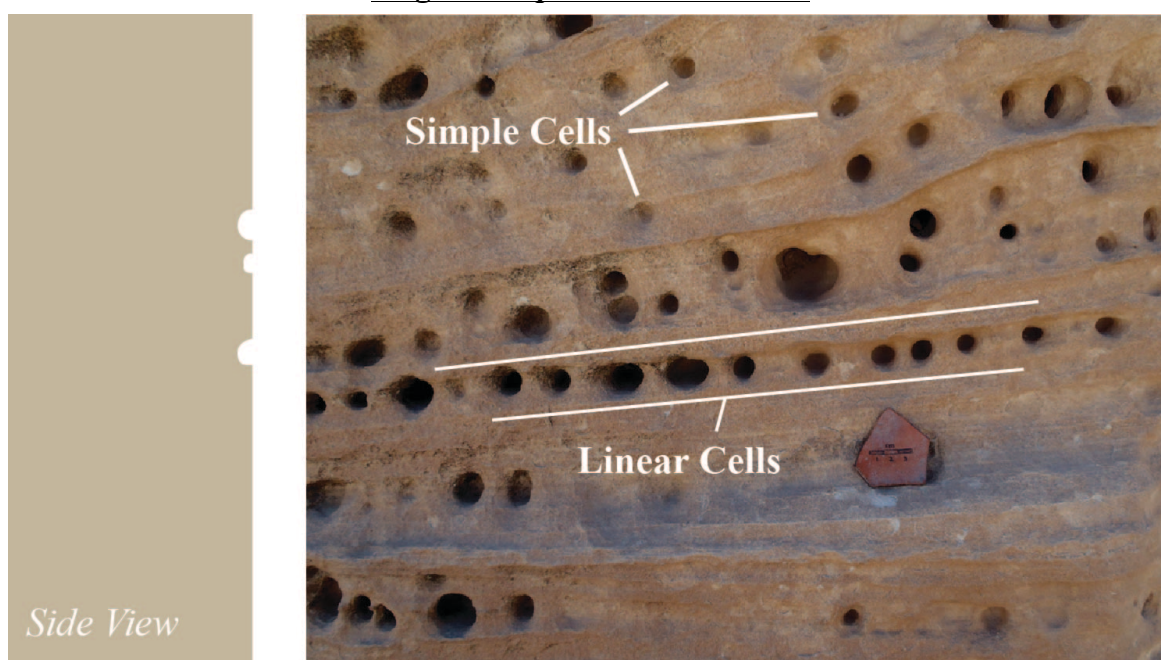


Figure 6.13 – Cross section of Stage 1 cells (left) and photograph of the western face of Djinn Block X with both Linear and Simple Cells (right). Photograph by K. Groom (2013).

Stage 2: Tunneled or Hooded Cells

While cell openings continue to decay mostly uniformly (1:1), at some point cell depth becomes more pronounced and interior decay outpaces surface decay (possibly due to minimal case hardening or core softening) advancing cells from Stage 1 into Stage 2. The distinction between *Tunneled* and *Hooded Cells* involves the direction of the greatest decay. *Tunneled Cells* are curved or angled so that the deepest point of the cell, or the cell back, is non-perpendicular to the cell opening. In the large majority of *Tunneled Cells* on Djinn X, this curvature is towards the left, despite panel aspect or cell location on the block. *Hooded Cells* are more spherical than *Tunneled Cells*, with larger interior dimensions than cell openings, creating distinctive hoods, or visors, along the upper lip of the cell opening (Figure 6.13). Many *Hooded Cells* tunnel upward slightly but the cell backs retain primarily perpendicular to the opening.

Stage 2: Tunneled and Hooded Cells

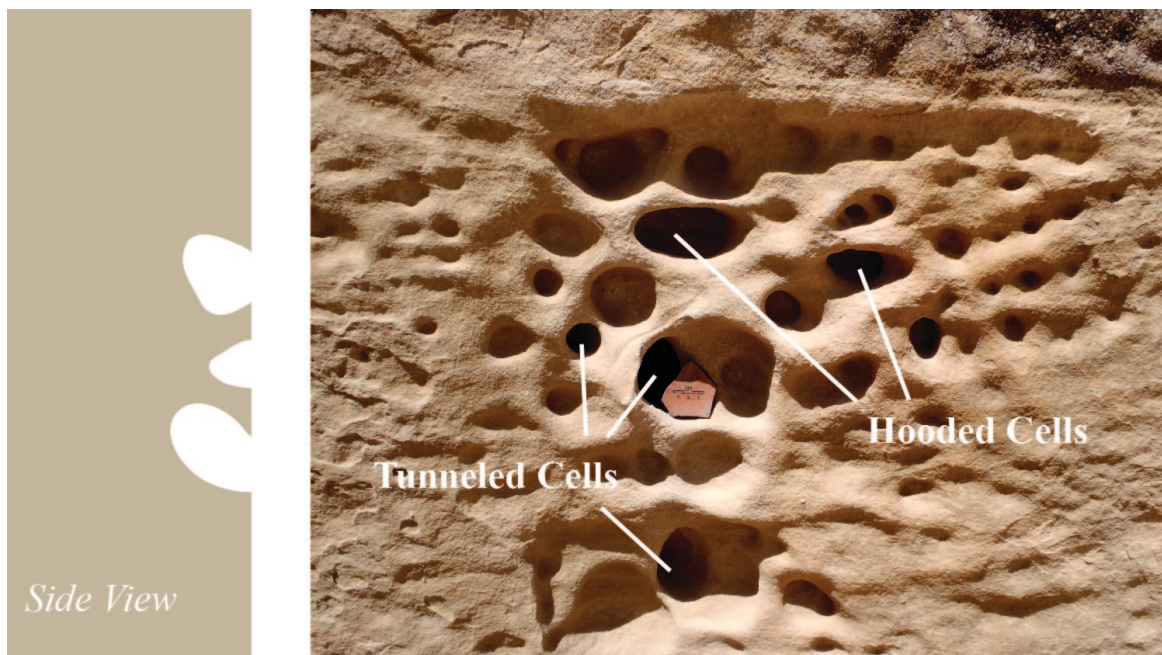


Figure 6.14 – Cross section of Stage 2 cells (left) and photograph of the eastern face of Djinn Block X with both Tunneled and Hooded Cells (right). Photograph by K. Groom (2013).

Stage 2 cells were recorded on all faces, though very few on the eastern (cells too small) and southern (decay too advanced) faces. However, numerous cells on the northern and western faces have developed tunnels and hoods and, in fact, this stage dominates western cell types. The general size of Stage 2 cells varies depending on lithological constraints/weaknesses and cell proximity/surface density. For instance, *Linear Cells* are geologically limited so it is unlikely for them to evolve into spherical *Hooded Cells*, but, if the cells are located in an internally friable stratus (possibly due to subsurface salts or moisture activity) then *Tunneled Cells* could develop, although they would still be constrained and fairly small (rare on Djinn Block X). Distributionally, isolated cells are unimpeded and have the potential to become larger (~5.4cm³ on Djinn X) before advancing to Stage 3, while closely packed cells merge into each other without requiring substantial growth.

Stage 3: *Coalesced* or *Netted Cells*

Coalesced and *Netted Cells* reference cavities composed of multiple adjacent cells that have merged into a single distinctive void. *Coalesced Cells* have irregular, often bulbous, cell openings, uneven cell backs, and display remnants of previously individual cells such as spherical pockets throughout the cell while still maintaining identifiable boundaries and the appearance of a single tafone (Figure 6.15). *Netted Cells* are a previously unrecorded tafoni phenomenon composed of a series of cell interiors that have amalgamated under the surface but the discrete cell openings have remained intact, essentially creating a large hollow cavity with the illusion of individuality (Figure 6.16). Eventually, the proverbial “net” will decay transitioning *Netted Cells* into *Coalesced Cells* without exiting Stage 3. This stage of decay also marks the evolution from single cells to joined cells that is culminated in a reversal of decay intensity: Depth begins to slow as diameter rapidly increases (i.e. more decay near the original

Stage 3: Coalesced Cells

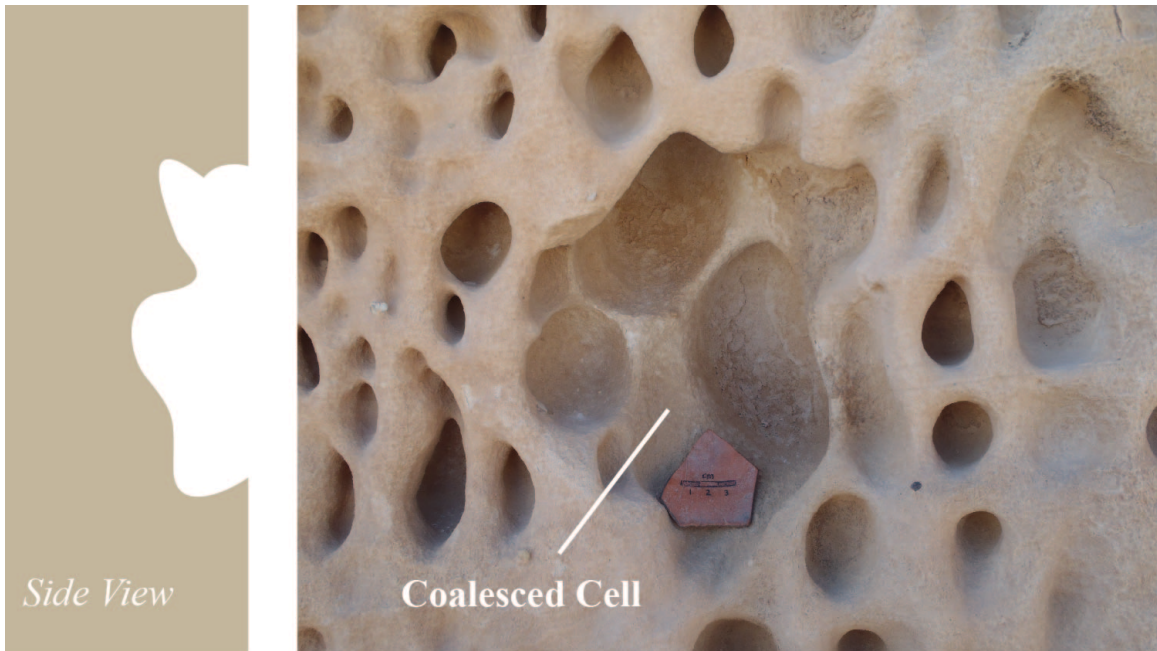


Figure 6.15 – Cross section of Stage 3 Coalesced Cells (left) and photograph a Coalesced Cell on the northern face of Djinn Block X (right). Photograph by K. Groom (2013).

Stage 3: Netted Cells



Figure 6.16 – Cross section of Stage 3 Netted Cells (left) and photograph a Netted Cell on the southern face of Djinn Block X (right). Photograph by K. Groom (2013).

surface than the interior of the cell) when two or more cells merge. In general, Stage 3 cells (both *Coalesced* and *Netted*) are deeper, and considerably wider, than single cells (Stage 1 and 2) and are, therefore, among some of the larger cells on Djinn Block X (e.g. 1441.2cm³ in Figure 6.15). *Coalesced Cells* are found on the northern, western, and southern faces but the majority are on the north and south. The largest collection of *Netted Cells* is located on the western face but with relatively smaller (~1.5 to 2.5cm) cell openings, where *Netted Cells* on the southern face have larger individual openings (~3 to 4.5cm). As long as Stage 3 cells maintain identifiably discrete cavities they have the potential to become quite large, like the immense caverns on an adjacent cliff face facing Djinn Block X, and do not advance to Stage 4.

Stage 4: *Vertical Pans* and *Indiscrete Cells*

Stage 4 cells represent the most advanced stage of decay and are separated into two categories, *Vertical Pans* and *Indiscrete Cells*, depending on lithological restraints, much like the difference between *Simple* and *Linear Cells*. Similar to the formation of horizontal pans in gnamma pits (Paradise, 2012), *Vertical Pans* are wide flat cells whose depth and diameter development have been heavily influenced by lithological restraints resulting in fairly shallow, rectangular cavities with flat backs. The limited depth of many *Vertical Pans* could reflect possible direct transitions from *Linear Cells*, bypassing Stages 2 and 3, which is supported by the overall scarcity of linear patterns in both of these stages and the close proximity of *Linear Cells* and shallow *Vertical Pans* on the western face of Djinn Block X (Figure 6.17). The only other *Vertical Pans* are located on the southern face and are actually odd combinations of *Vertical Pans* and *Indiscrete Cells*.

Stage 4: Vertical Pans and Indiscrete Cells

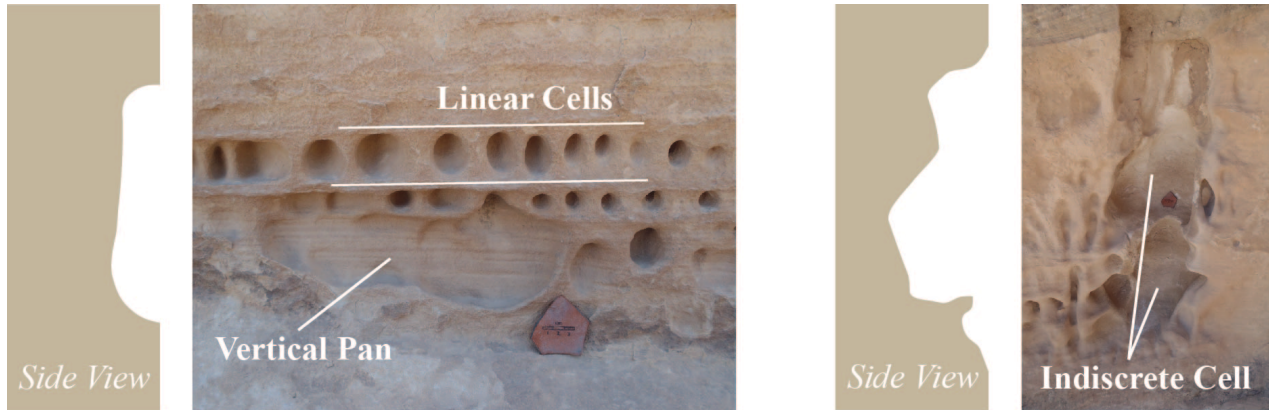


Figure 6.17 – Cross section of Stage 4 Vertical Pans and example on the western face of Djinn Block X (left) and cross section of Stage 4 Indiscrete Cells and example on the northern face of Djinn Block X (left). Photographs by K. Groom (2013).

Indiscrete Cells are large irregular cavities composed of conjoined single and coalesced cells that have decayed beyond discrete identification (i.e. no longer display clear cavity boundaries) making them difficult to measure (Figure 6.17). There are only a few such cells on Djinn X's northern face but the majority is on the heavily decayed southern face. The few *Indiscrete Cells* on the northern face show evidence of water runoff, which explains the more advanced decay, as opposed to the southern face where both forms of Stage 4 cells abound. The four large outliers (in volume) for the collected dataset fall within this stage of decay (e.g. 25454.2cm³ on the southern face). There is also potential for Stage 4 cells to either stabilize to the point that new cells can initiate on the inner walls (as seen on the northern face) and restart at Stage 1 or destabilize and deteriorate into an Exit Stage, where they no longer fit the parameters to be characterized as tafoni, as is evident on the southern face.

Exit Stage (Optional): *Post-Tafoni Voids*

Predominantly found on the severely receded southern face, *Post-Tafoni Voids* are cavities that display certain evidence of previous tafoni activity, such as curved roofs, but the rest

of the void has decayed. Most Exit Stage cells on Djinn Block X are near the base of the block and have developed features more congruent with drapery or rillen, as opposed to tafoni (Figure 6.18). The wide array of *Post-Tafoni Voids* sizes found on Djinn X might also suggest that cells in any of the four stages have the potential to deteriorate beyond tafoni distinction, thus making the Exit Stage optional and not secured linearly within the model. The concept of an Exit Stage also substantiates the presence of basic decay rate thresholds that must be met for tafoni to continue existing.

Exit Stage: Non-Tafoni Voids

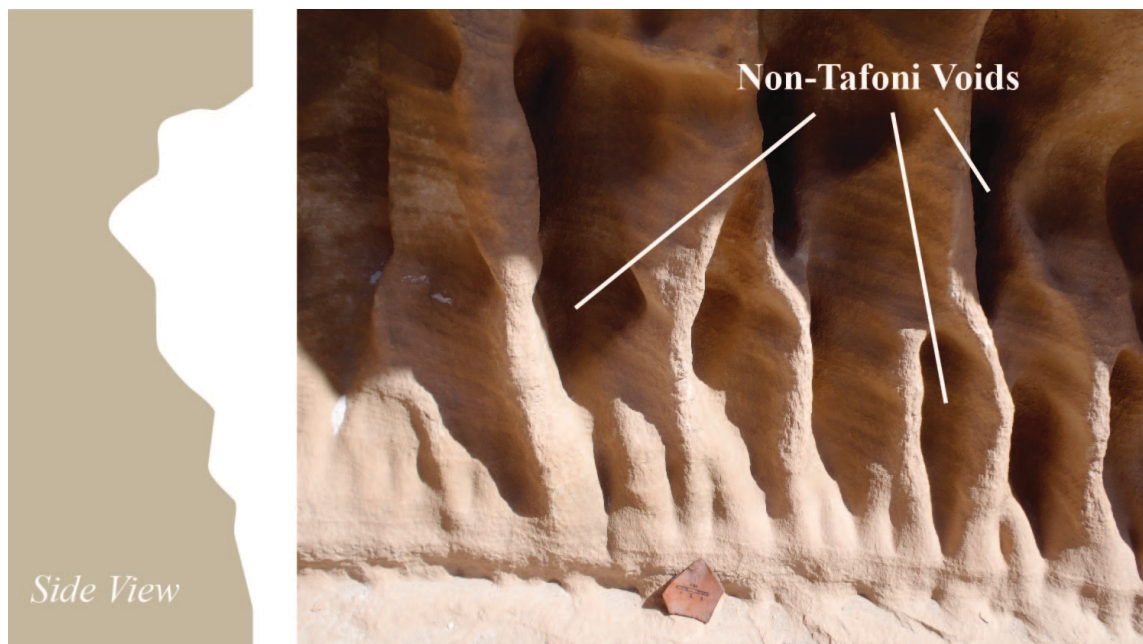


Figure 6.18 – Cross section of Exit Cells (left) and photograph of Non-Tafoni Voids on the southern face of Djinn Block X (right). Note the resemblance to stone drapery. Photograph by K. Groom (2013).

As evident on Djinn Block X, advancement from one stage to the next is not solely dependent upon size, but patterns of decay. For example, there are Exit Stage cells smaller than Stage 3 cells and there are Stage 2 cells larger than Stage 4 cells. This only means that the interior cell growth and exterior overall surface recession rates of decay differ at different stages. Ultimately, the importance of this model is to categorize tafoni cells by decay patterns and rate

thresholds as opposed to the praxis of using size as the sole surrogate for age (Figure 6.19). Essentially, a cell can remain in the same stage of evolution as long interior and exterior decay rate ratios remain consistent. For example, it would be possible for a sizeable cell to never leave Stage 1 as long as it remains spherical and simple in shape.

Cross Sections of the 5 Stages of Tafoni Evolution Model

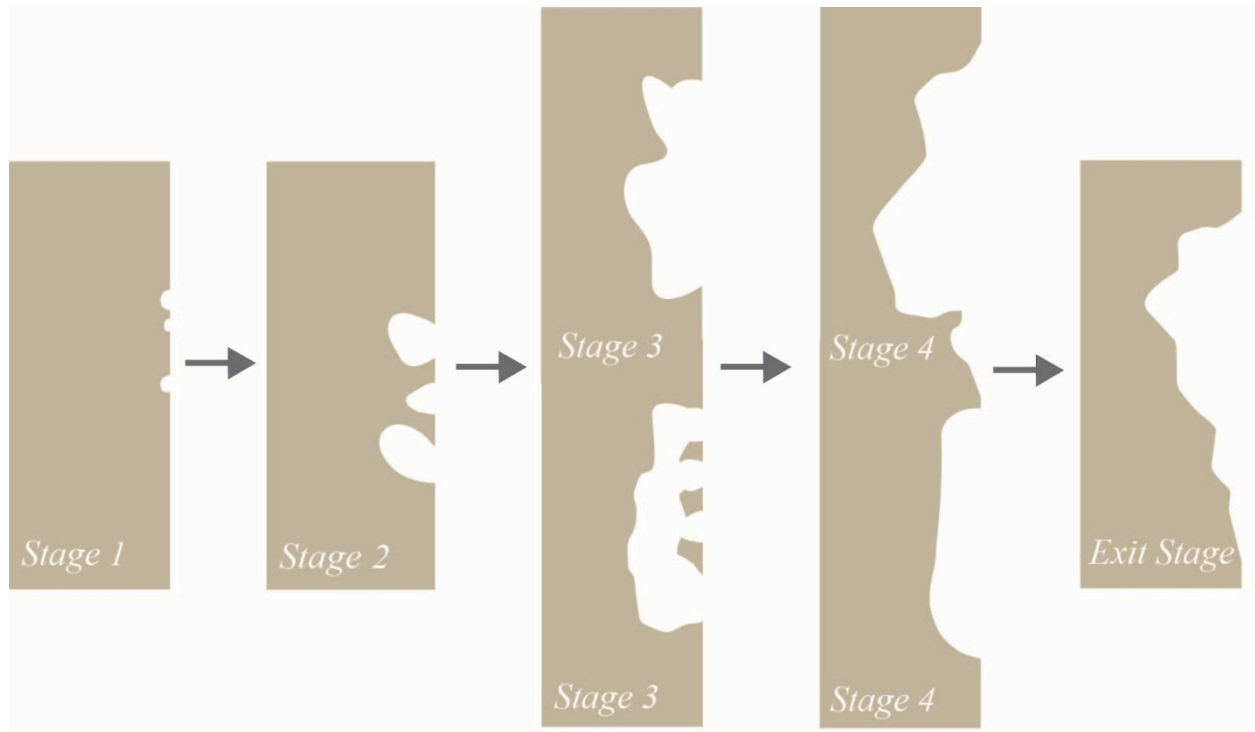


Figure 6.19 – Cross sections of the five proposed stages of tafoni evolution including Exit Stage cells.

6.3.2 Thresholds in Tafoni Development

While the application of threshold theory in rock decay research remains limited (Paradise, 1999), threshold responses are abundant in geomorphologic processes (Schumm, 1979): Dew points, slope failure (Carson, 1971), and, evident from decay patterns on Djinn Block X, tafoni evolution. There have been studies addressing thresholds in tafoni development

(although not directly), such as McBride and Picard (2000) who witnessed a change in cavity shape once the cell exceeded 20cm, but very few studies exist concerning the thresholds required for tafoni to exist at all (e.g. Achyuthan et al., 2010). Once initiated, a cell develops if the interior of the cell decays faster than the surface on which it is located, otherwise the surface decays in tandem with the cell and no shape would form, thus restricting tafoni development. This kind of rate-threshold relationship has already been accepted in the distinction between efflorescence and subflorescence of soluble salts (e.g. Rodriguez-Navarro, 1999; Huinink, 2004), so it is not unreasonable to apply similar rate and formation thresholds to tafoni progression (Figure 6.20).

The stage model presented here addresses these thresholds using the ratios between depth

Example of Possible Threshold Response in Tafoni

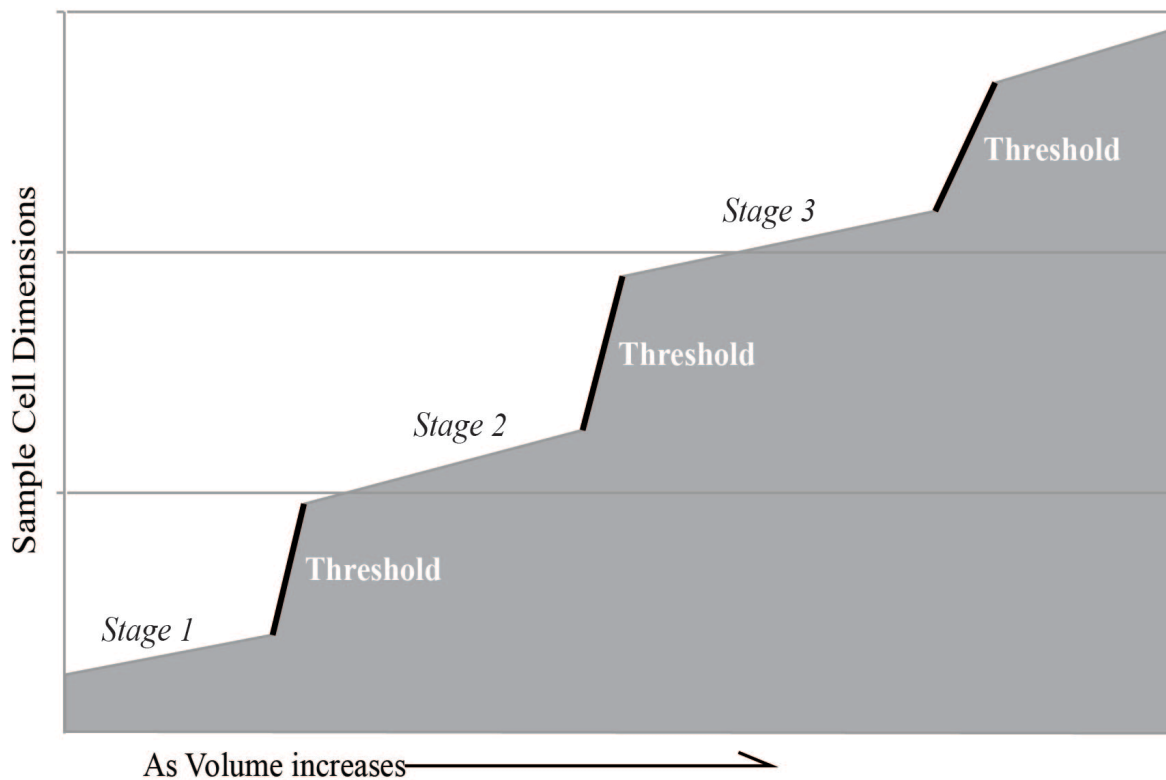


Figure 6.20 – Graph showing the exaggerated shape and steps in a threshold response system corresponding with the 5 Stage Model. Groom (2014).

and diameter as proxies for internal and external decay, respectively, driven by varying degrees of intrinsic and extrinsic influence at different stages. Certain features on Djinn Block X exhibit the two extremes of this ratio: *Netted Cells* occur when internal decay vastly outpaces external decay and *Post-Tafoni Voids* represent equal or greater external growth. The array of cell types and the subtle, but vital, distinction between each type supports the concept that there are decay thresholds that must be met for tafoni to occur, but there are also a series of other thresholds that determine when cells evolve into later stages of decay, and that cell shape and size are not random post-initiation as claimed by Pestrong (1988). Within Stage 1, both internal and external decay rate remain fairly equal, thus the uniform shapes. A cell progresses into Stage 2 when there is a shift and internal decay accelerates more than external (diameter) growth. This decay threshold could represent disparities between intrinsic and extrinsic variables in tafoni evolution. For example, a cell might meet this threshold and advance to Stage 2 if there is a breach in lithological barriers stabilizing the surface that do not exist, or even weaken, the rock deeper in the substrate, such as case hardening or core softening (Conca & Rossman, 1982; 1985). The threshold between Stages 2 and 3 is possibly the most prominent, as it represents the transition from multiple cells to a single void, dramatically increasing both depth and diameter. Less obvious, the threshold between Stages 3 and 4 are more qualitative as they represent definitive shifts more than dimensional shifts: a cell advances from Stage 3 to 4 when it either decays to the extent of its lithological restraints (*Vertical Pans*) or beyond the distinction of a singularly definable void (*Indiscrete Cells*).

In fact, the relationship between intrinsic and extrinsic influences on tafoni evolution involves several levels of threshold response. For example, intrinsic variables such as iron content (Paradise, 1999) and permeability (Somerton & Gupta, 1965) have been determined to

affect decay rates and processes within certain thresholds. Similarly, extrinsic stresses such as intense heating impact the decay of salt saturated sandstones (Somerton and Gupta, 1965) or sandstones of different mineral compositions (Somerton, 1961; Zhang et al., 2005), but only once certain temperature thresholds are met.

Even within the Disi sandstone of Djinn Block X different minerals and compositions may be influencing threshold response. Previous petrologic studies in Petra have found that higher carbonate levels, like those found in the Disi formation, increase rates of decay due to contrasting linear pro-axial expansion and contraction of calcite when heated beyond the temperature threshold of 50°C (Somerton, 1992), conditions common in Petra (Paradise 1995, 1999). In addition, the higher concentrations of iron in the Umm Ishrin, known to have intrinsic decay thresholds (Paradise, 1999), might explain the stark differences of decay between the interdigitated upper component of Djinn Block X and the highly decayed lower section.

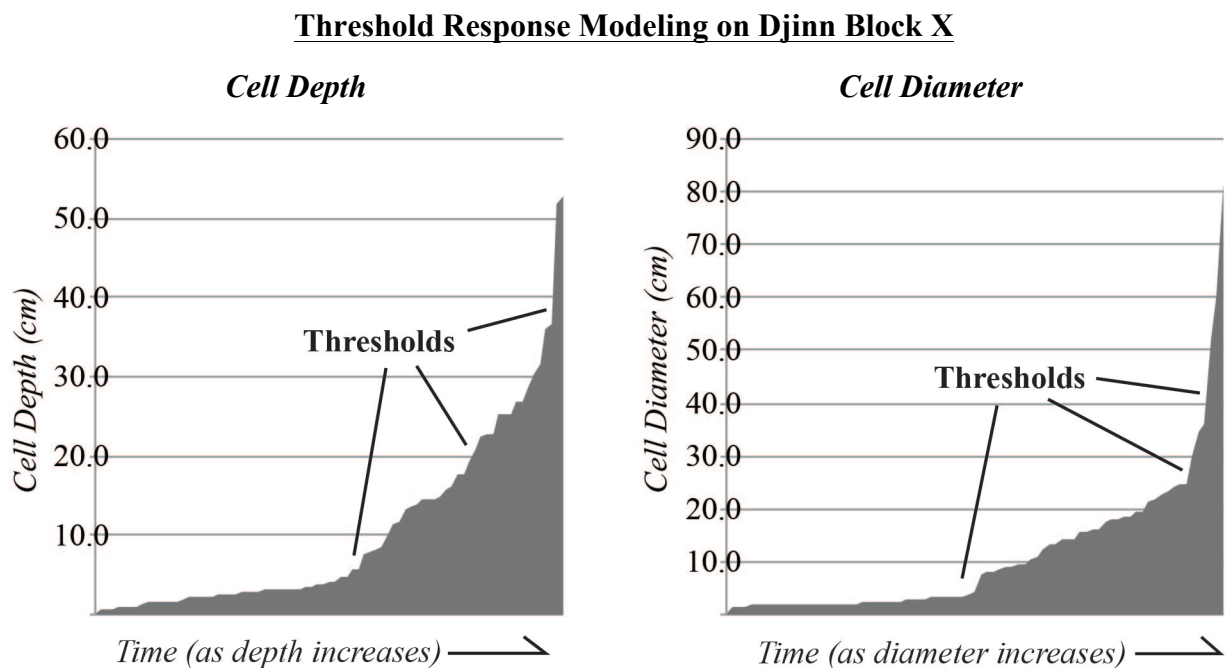


Figure 6.21 – Graphs showing evidence of threshold response (periodic jumps in size) based on empirical measurements of both depth (left) and diameter (right). Note the x-axis represents time as that dimension increases.

Even more integral to tafoni development, the analyses of depth, diameter, and volume all exhibit sudden increases in value after fairly steady growth corresponding within the stage model (Figure 6.21). Such growth spikes might suggest episodic decay events, meaning the presence of threshold response decay. These periodic jumps in dimensions are even clearer when examined logarithmically (Figure 6.22). Identifying these thresholds could radically alter tafoni age and decay rate estimations, which have to this point been based on steady rates of decay, whether they are exponentially decreasing (Sunamura, 1996), along an S-Curve (Sunamura & Aoki, 2011), or non-linear (Norwick & Dexter, 2002). More research would be needed to numerically identify these thresholds, but the evidence found on Djinn Block X supports the idea that the threshold response exists in tafoni evolution.

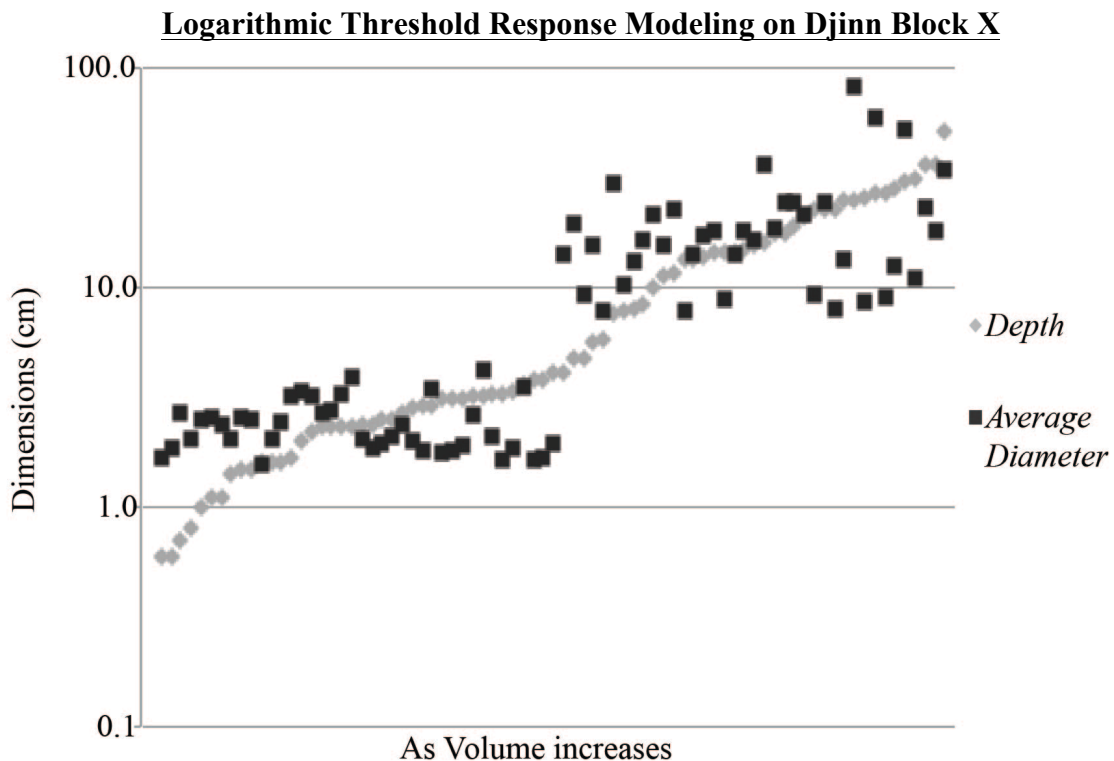


Figure 6.22 – Graph showing the logarithmic relationship between depth and diameter as volume increases (representing the passage of time). Note the large jump in diameter as depth progresses in smaller steps.

Chapter Seven – Conclusions and Implications

Cultural resource and heritage management (particularly regarding cultural stone), rock decay (weathering) research, and tafoni assessment/evolution are all interconnected and the multifaceted structure of this thesis research holds significant implications to each and the interrelationships among them (Figure 7.1). The distinctive features of cultural stone, such as established dates of exposure, largely orthographic and uniform surfaces, and known architectural elements and techniques, permit certain assumptions to be made in rock decay research that would not be possible with “natural stone”. These assumptions reduce uncertainties within geomorphologic research furthering our understanding of stone deterioration and rock decay phenomena, like tafoni development and the creation of a stage-based model of cell progression. This model then has the potential to improve evaluation techniques for dated

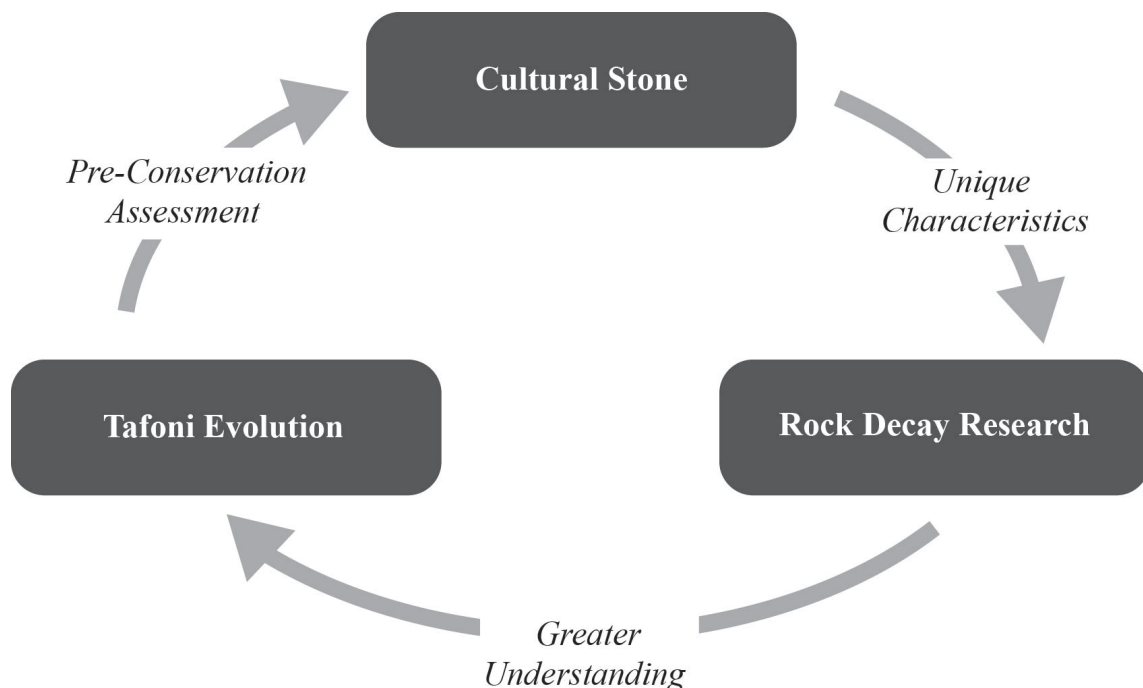


Figure 7.1 – Diagram displaying the interconnectedness and interdisciplinary implications of rock decay science, cultural heritage management, and tafoni evolution. Diagram by K. Groom (2014).

surfaces and effective pre-conservation assessment of cultural stone, thus completing the cycle. The particular characteristics of Djinn Block X (e.g. isolation, geology, dimension, and form) and the research presented here match this symbiotic cycle. Therefore, conclusions and implications consider each beneficiary (cultural resource and Heritage management, general rock decay research, and tafoni evolution and development) within the context of the three primary research thrusts: morphometry and aspect, microclimate and aspect, and independent tafoni genesis.

Aspect, as a surrogate for insolation, proved to intimately influence several elements of decay on Djinn Block X, both in terms of cell morphometry/distribution as well as cell microclimates and micrometeorologic measurements. Observational and statistical analyses of basic cell morphometry displayed significantly greater diameters (wider cells) and cell depths on the southern and northern faces, ultimately displaying the most material lost (highest volumes) is on the southern face. Despite containing over 1700 separate tafoni, the western face only displayed smaller, less advanced cells and the eastern face was nearly devoid of any substantial tafoni development. While contradicting the north-centric convention regarding aspect dependence (Churchill, 1982), these results parallel Paradise's (2013) findings of greatest surface recession on the southern aspect of Djinn Block X.

Micrometeorologic analyses also correspond with aspect, particularly regarding internal and external surface temperatures. Considerable variation among the ambient air temperature and humidity measurements made it difficult to identify any meaningful correlations but surface temperatures displayed clear relationships with cell morphometric dimensions as well as aspectual location on Djinn Block X. Morphometrically, larger cells have stronger negative correlations with differences in internal and external surface temperatures. In other words, as a

cell grows it becomes more likely that the interior cell walls will be cooler than the exterior surface on which it is located. The tendency for cooler interior surfaces is also considerably higher on the southern face than any other aspect, which could be an auto-correlation as most of the block's largest cells are found on this face. When the two factors are considered together, however, possible causalities become clearer. Paradise (2013) attributes the advanced recession of the southern face to notably higher insolation, causing more severe wetting and drying cycles, and rapid drying cycles are known to increase capillary action in sandstone causing a noticeable drop in surface temperatures (Mol & Viles, 2013). Therefore, prolonged insolation not only intensifies the drying cycle, effectively deteriorating the subsurface and promoting cavernous decay through the movement and deposition of moisture and salts (Mol & Viles, 2011), but also simultaneously decreases internal surface temperatures in the process. Ultimately, the findings of this thesis suggest insolation and other aspect dependent environmental factors have greater influence on rock decay and, consequentially pre-conservation assessments of cultural stone, than previously considered. Recognizing the distinct relationships between aspect (insolation) and decay can help heritage management agencies effectively identify monuments in higher risk of deterioration based on aspectual location and amount of prolonged insolation.

In addition, an investigation of the unusual variation among tafoni shapes, sizes, and other characteristics on Djinn Block X inspired the creation of a threshold tafoni growth model that offers an alternative context in which cavernous decay can be evaluated and assessed. Instead of trying to determine tafoni age or exact rates of decay purely based on size, which has been the primary method for years (e.g. Sunamura, 1996) and a major assumption in this research, the proposed model also involves the ratios between internal and external decay rates using empirical data and threshold theory. Although the model was generated independently

from aspect assessment, the resultant stages of decay follow similar distributional patterns as the detailed statistical analyses: The majority of cells on the least-decayed eastern face were only stage 1 and 2, western cells mainly stayed within stages 1 – 3, the northern face displayed all stages of decay but the majority fell within stages 2 – 4, and most cells on heavily decayed southern face were stage 3 or 4 with the addition of several large exit stage voids. This consistency helps validate the model's ability to visually assess tafoni deterioration without the need for detailed dimensional measurements.

In summary, the findings and repercussions presented in this research include:

- *Empirical evidence displaying aspect-dependence in tafoni development collaborating with current literature advocating for insolation as an extrinsic driving force of decay.*
- *Statistical correlations between micrometeorological conditions and cell aspect and morphometry suggesting microclimatic variables influencing cell decay.*
- *Morphometric indication of threshold response in tafoni evolution challenging dominant steady-rate weathering/tafoni research praxis and analysis.*

The multiple interrelated components of this research demonstrate the complexity of stone decay and the workings of the natural world, but it also illustrates the unending potential for future research. In the specific case of Djinn Block X, there are obvious lithological elements influencing decay that could correspond with geologic thresholds proposed by Paradise (1995), however they would require more detailed laboratory examinations to identify and obtaining petrologic sampling from Petra is a complicated procedure regulated by UNESCO and the Petra Regional Authorities. Also, diurnal and more consistent micrometeorological measurements for ambient air temperature and humidity could divulge more meaningful relationships with cell morphometry and aspectual distribution, as the measurements in this thesis were admittedly static and limited. There is also infinite potential to expand the scope of the methods to include

other monuments within Petra, such as the other djinn blocks, and even tafoni outcrops under similar arid conditions, like those found in the southwestern United States. And while the stage-based model postured here is not necessarily meant to be universal, certain stipulations can be made that such a model could be adapted to suit any climate or geologic substrate, and even allow direct comparisons of tafoni development from various locations and environmental frameworks.

Ultimately, the research presented here corroborates certain facets of accepted rock decay theory and processes, such as surface temperature affecting moisture and surface deterioration, but it also provides evidence supporting more controversial topics like insolation as a direct agent of decay and the presence of threshold response in tafoni development and evolution. With continued extensive research, it is possible for these disputed decay processes to be better comprehended and explained. So, although the extent of this thesis work is limited to Djinn Block X in Petra, Jordan, it lays the foundation for future research to further increase our understanding of tafoni evolution, rock decay thresholds, and effective cultural stone assessment worldwide.

Chapter Eight – Bibliography

- Acevedo, D., Vote, E., Laidlaw, D. H., & Joukowsky, M. S. (2001, October). Archaeological data visualization in VR: Analysis of lamp finds at the Great Temple of Petra, a case study. In *Proceedings of the conference on Visualization'01* (pp. 493-496). IEEE Computer Society.
- Achyuthan, H., Kumar, K. A., Tiwari, S. K., & Norwick, S. (2010). A reconnaissance study of tafoni development, exfoliation, and granular disintegration of natural and artificial rock surfaces in the coastal and lowland regions of tamil nadu, southern india. *Zeitschrift fur Geomorphologie*, 54(4), 491-509.
- Al-Bashaireh, K., & Hodgins, G. W. (2011). AMS ¹⁴C dating of organic inclusions of plaster and mortar from different structures at Petra-Jordan. *Journal of Archaeological Science*, 38(3), 485-491.
- Al-Jaloudy, M. A., (2006). Jordan. *Food and Agriculture Organization of the United Nations Country Pasture and Forage Resource Profiles*. www.fao.org
- Al-Okour, A., Ajlouni, A. W., & Ajlouni, A. (2013). Radiation doses due to natural radioactivity in Al Hammah Hot Springs, Jordan. *Contemporary Engineering Sciences*, 6(3), 127-134
- Al-Saad, Z., & Abdel-Halim, M. A. (2001). Laboratory evaluation of various types of mortars for the conservation of Qasr al-Bint monument, Petra–Jordan. *Engineering structures*, 23(8), 926-933.
- Al-Qudah, B. (2001). Soils of Jordan. *Soil resources of Southern and Eastern Mediterranean countries. Bari: Centre international de hautes études agronomiques méditerranéennes-Instituto Agronomico Mediterraneo di Bari (Ciheam-IAMB)*.
- Al-Weshah, R. A., & El-Khoury, F. (1999). Flood analysis and mitigation for Petra area in Jordan. *Journal of water resources planning and management*, 125(3), 170-177.
- Allen, C.D. and K.M. Groom (2013). Evaluation of Grenada’s “Carib Stones” via the Rock Art Stability Index. *Applied Geography Special Issue: Cultural Geomorphology*. 42: 165-175
- Angel, C.C. (2011). Umm Sayhoun: Culture, History and Geography. In *Archaeological Heritage Management at Petra: Drive to Development or Destruction*. Springer Press.
- Ambraseys, N. N., Douglas, J., Sarma, S. K., & Smit, P. M. (2005). Equations for the estimation of strong ground motions from shallow crustal earthquakes using data from Europe and the Middle East: horizontal peak ground acceleration and spectral acceleration. *Bulletin of Earthquake Engineering*, 3(1), 1-53.
- Andre, M. F., Hall, K. (2004). Honeycomb development on Alexander Island, glacial history of George VI Sound and palaeoclimatic implications (Two Step Cliffs/Mars Oasis, W Antarctica): *Geomorphology*, v. 65, 117-138.

- Bani-Hani, K., & Barakat, S. (2006). Analytical evaluation of repair and strengthening measures of Qasr al-Bint historical monument—Petra, Jordan. *Engineering structures*, 28(10), 1355-1366.
- Bartrum, J. A. (1936). Honeycomb Weathering of Rocks Near the Shore-Line: The New Zealand Journal of Science and Technology, v. 18, 593-600.
- Bender, F. (1975). Geology of the Arabian peninsula: Jordan. *Geological Survey Professional Paper 560-I*. United States Government Printing Office, Washington.
- Bienkowski, P., & Chlebik, B. (1991). Changing Places: Architecture and Spatial Organization of the Bedul in Petra. *Levant*, 23(1), 147-180.
- Birot, P. (1968). *The Cycle of Erosion in Different Climates*, B. T. Batsford Ltd., London, United Kingdom, 85-97.
- Blackwelder, E. (1929). Cavernous rock surfaces of the desert. *American Journal of Science*, (17), 393-399.
- Blackwelder, E. (1933). The insolation hypothesis of rock weathering. *American Journal of Science*, (152), 97-113.
- Bounni A., 1999. “Couronnement des sanctuaires du Proche-Orient hellénistique et romain: origine et développement du merlon”, *Topoi*, 9.2, 507–525.
- Boxerman, J. Z. (2005). The Evolutionary Cycle of the Tafone Weathering Pattern on Sandstone at Bean Hollow Beach. Northern California, Geological Society of America Sectional Meeting. Abstract
- Brandmeier, M., J. Kuhlemann, I. Krumrei, A. Kappler, P. W. Kubik. (2010). New challenges for tafoni research: a new approach to understand processes and weathering rates. *Earth Surface Processes and Landforms*. 36, 839-852.
- Bradley, W. C., Hutton, J. T., & Twidale, C. R. (1978). Role of salts in development of granitic tafoni, south australia. *Journal of Geology*, 86(5), 647-654.
- Browning, I. (1973). *Petra*. Noyes Press. Park Ridge, New Jersey, United States.
- Brünnow, R. E., & von Domaszewski, A. (1909). Die Provincia Arabia. Auf Grund zweier in den Jahren 1897 und 1908 unternommener Reisen und der Berichte früherer Reisender (3 volumes). Strassburg: Trübner Publishing.
- Bryan, K. (1928). Niches and other cavities in sandstone at Chaco Canyon, New Mexico. *Zeitschrift fuer Geomorphologie*, v. 3, 125-140.

Büdel, B., Weber, B., Köhl, M., Pfanz, H., Sültemeyer, D., & Wessels, D. (2004). Reshaping of sandstone surfaces by cryptoendolithic cyanobacteria: bioalkalization causes chemical weathering in arid landscapes. *Geobiology*, 2(4), 261-268.

Bull, W.B. (1991). *Geomorphic responses to climatic change*. Retrieved from <http://www.osti.gov/scitech/servlets/purl/5603696>

Bullard, J. E. (2006). Arid geomorphology. *Progress in physical geography*, 30(4), 542-552.

Burns, G. (1991). Deterioration of our cultural heritage. *Nature* 352, 658 – 660.

Butler, P. R., Mount, J.F. (1986). Corroded Cobbles in Southern Death Valley: Their Relationship to Honeycomb Weathering and Lake Shorelines: *Earth Surface Processes and Landforms*, v. 11, 377-387.

Cailleux, A., Calkin, P. (1963). Orientation of Hollows in Cavernously Weathered Boulders in Antarctica: *Biuletyn Peryglacjalny*, v. 12, 147-150.

Calkin, P., Cailleux, A., (1962). A Quantitative Study of Cavernous Weathering (Taffonis) and its Application to Glacial Chronology in Victoria Valley, Antarctica: *Zeitschrift fuer Geomorphologie*, v. 6, 317-324.

Campbell, S. W. (1999). Chemical weathering associate with tafoni at papago park, central Arizona. *Earth Surface Processes and Landforms* 24: 271-278

Carson, M. A. (1971). An application of the concept of threshold slopes to the Laramie Mountains, Wyoming, Institute of British Geographers Special Publication, 3, 31–47.

Chadwick, O. A., & Chorover, J. (2001). The chemistry of pedogenic thresholds. *Geoderma*, 100(3), 321-353.

Chatelard, G. (2010): ‘Jordan: A Refugee Haven’, *Migration Information Source*, September 2010. Available at: <http://www.migrationinformation.org>

Chorley, R. J. (1957). Climate and morphometry. *The Journal of Geology*, 65(6). 628-638.

Churchill, R. R. (1982). Aspect-induced differences in hillslope processes. *Earth Surface Processes and Landforms*, 7(2), 171-182.

Claussen, M., Kubatzki, C., Brovkin, V., Ganopolski, A., Hoelzmann, P., & Pachur, H. J. (1999). Simulation of an abrupt change in Saharan vegetation in the Mid-Holocene. *Geophysical Research Letters*, 26(14), 2037-2040.

Conca, J. L., Astor, A.M. (1987) Capillary Moisture Flow and the Origin of Cavernous Weathering in Dolerites of Bull Pass, Antarctica: *Geology*, v. 15, p. 151-154.

- Conca, J. L., & Rossman, G. R. (1982). Case hardening of sandstone. *Geology*, 10(10), 520-523.
- Conca, J. L., Rossman, G.R. (1985). Core Softening in Cavernously Weathered Tonalite: *Journal of Geology*, v. 93, 59-73.
- Cong, L., & Mitchell, B. J. (1999). Lg coda Q and its relation to the geology and tectonics of the Middle East. In *Q of the Earth: Global, Regional, and Laboratory Studies* (pp. 563-585). Birkhäuser Basel.
- Cooke, R. U. (1979). Laboratory simulation of salt weathering processes in arid environments. *Earth Surface Processes*, 4(4), 347-359.
- Cordova, C. E. (2007). *Millennial landscape change in Jordan: Geoarchaeology and cultural ecology*. University of Arizona Press.
- Crowder, J. R., & Amjad Ali, M. (1985). Weathering performance of building materials in the Middle East and UK. *Durability of building materials*, 3(2), 115-131.
- Dana, J.D. (1849). *Manual of Geology*, 1st Ed., Ivison, Blakeman, Taylor and Company, New York
- Darwin, C., (1839). *The Voyage of the Beagle*, collier & Son Company, New York.
- de Margerie, E. (1886). Géologie. *Polybiblion Revue, Bibliographique Universelle, Partie littéraire* 2, 24. 310–330.
- Delmonaco, G., Margottini, C., & Spizzichino, D. (2013). Rock-fall hazard assessment in the Siq of Petra, Jordan. In *Landslide Science and Practice* (pp. 441-449). Springer Berlin Heidelberg.
- Dixon, J. C. (2009). Aridic soils, patterned ground, and desert pavements. In *Geomorphology of desert environments* (pp. 101-122). Springer Netherlands.
- Dixon, J. C., & Thorn, C. E. (2005). Chemical weathering and landscape development in mid-latitude alpine environments. *Geomorphology*, 67(1), 127-145.
- Doehne, E. & Price, C. A. (2010). *Stone conservation: an overview of current research*. Getty Publications.
- Dorn, R. I., & Oberlander, T. M. (1982). Rock varnish. *Progress in Physical Geography*, 6(3), 317-367.
- Dorn, R.I., S.J. Gordon, C.D. Allen, N.V. Cervený, J.C. Dixon, K.M. Groom, K. Hall, E. Harrison, L. Mol, T.R. Paradise, G. Pope, P. Sumner, T.J. Thompson, & A.V. Turkington. (2013). The role of fieldwork in rock decay research: Case studies from the fringe. *Geomorphology* 200: 59-74

- Dorn, R., Whitley, D., Cerveny, N., Gordon, S., Allen, C., & Gutbrod, E. (2008). The Rock Art Stability Index: A new strategy for maximizing the sustainability of rock art. *Heritage & Society*. Left Coast Press, Inc. 37-70
- Dragovich, D. (1969). The Origin of Cavernous Surfaces (Tafoni) in Granitic Rocks of Southern South Australia: *Zeitschrift fuer Geomorphologie*, v. 13, 163-181.
- Drake, N., & Bristow, C. (2006). Shorelines in the Sahara: geomorphological evidence for an enhanced monsoon from palaeolake Megachad. *The Holocene*, 16(6), 901-911.
- Ewing, S. A., Sutter, B., Owen, J., Nishiizumi, K., Sharp, W., Cliff, S. S., ... & Amundson, R. (2006). A threshold in soil formation at Earth's arid-hyperarid transition. *Geochimica et Cosmochimica Acta*, 70(21), 5293-5322.
- Fiema, Z.T., C. Kanellopoulos, T. Waliszewski, & R. Schick (2001) The Petra Church. Amman, Jordan: *American Center for Oriental Research*.
- Fiema, Z. T. (2003). Roman Petra (AD 106–363): A Neglected Subject. *Zeitschrift des Deutschen Palästina-Vereins*, 119(1), 38-58.
- Fookes, P. G., & Collis, L. (1976). Cracking and the Middle East. *Concrete*, 10(2).
- Fookes, P. G., Pollock, D. J., & Kay, E. A. (1981). Middle East Concrete (2) Rates of deterioration. *Concrete*, 15(9).
- Franchi, R., Savelli, D., Colosi, F., Drapp, P., Gabrielli, R., Moretti, E., & Peloso, D. (2009) Petra and Beida (Jordan): two adjacent archaeological sites up to an exploitation of geomorphology-related topics for a cultural and touristic development: Mem. Descr. Carta Geol. d'It., 77-90
- French, H. M., Guglielmin, M. (2000). Cryogenic weathering of granite, Northern Victoria Land, Antarctica: Permafrost and Periglacial Processes, v. 11, 305-314.
- Fryberger, S., & Goudie, A. S. (1981). Arid geomorphology. *Progress in Physical Geography*, 5(3), 420-428.
- Gill, E. D., Segnit, E.R., McNeill, N.H. (1981). Rate of Formation of Honeycomb Weathering Features (Small Scale Tafoni) on the Otway Coast, S.E. Australia: Proceedings of the Royal Society of Victoria, v. 92, 149-154.
- Gomez-Heras, M., Wedekind, W., & Lopez-Arce, P. (2012, April). Discerning total salt contents and surface humidity on building stone with a portable moisture meter (Protimeter) in the region of Petra (Jordan). In *EGU General Assembly Conference Abstracts* (Vol. 14, 5876).
- Goudie, A. (2002). *Great warm deserts of the world: landscapes and evolution* (Vol. 1). Oxford University Press.

- Goudie, A. S., Migon, P., Allison, R. J., & Rosser, N. (2002). Sandstone geomorphology of the Al-Quwayra area of south Jordan. *Zeitschrift für Geomorphologie, NF*, 365-390.
- Goudie, A., & Seely, M. (2011). World Heritage Desert Landscapes: Potential Priorities for the Recognition of Desert Landscapes and Geomorphological Sites on the World Heritage List. *IUCN World Heritage Studies*, 9.
- Goudie, A., & Viles, H. A. (1997). *Salt weathering hazards* (p. 241). Chichester: Wiley.
- Graf, W. L. (1979). The development of montane arroyos and gullies. *Earth Surface Processes*, 4(1), 1-14.
- Grantz, A. (1976). Sandstone caves (tafoni) in the Central Santa Cruz Mountains, San Mateo County: *California Geology*, 51-54.
- Groom, K. M. (2014). Assessment and preservation of rock art: a proposal for the Thamudic petroglyphs of Wadi Rum. *Man and the Deserts: 2nd International Conference in Wadi Rum Official Report*.
- Grove, A. T. (1980). Geomorphic evolution of the Sahara and the Nile. *The Sahara and the Nile (MAJ Williams and H. Faure, Editors)*, 7-16.
- Hall, K., Thorn, C., & Sumner, P. (2012). On the persistence of 'weathering'. *Geomorphology*, 149, 1-10.
- Hammond, P. *The Crusader Fort on El-Habis at Petra: Its Survey and Interpretation*. Salt Lake City, UT: University of Utah, 1970.
- Hartmann, D. L. (1994). *Global physical climatology* (Vol. 56). Academic press.
- Heinrichs, K. (2008). Diagnosis of weathering damage on rock-cut monuments in Petra, Jordan. *Environmental Geology*, 56(3-4), 643-675.
- Huinink, H. P., Pel, L., & Kopinga, K. (2004). Simulating the growth of tafoni. *Earth Surface Processes and Landforms*, 29, 1225-1233.
- Inkpen, R. J., & Jackson, J. (2000). Contrasting weathering rates in coastal, urban and rural areas in southern Britain: preliminary investigations using gravestones. *Earth Surface Processes and Landforms*, 25(3), 229-238.
- İşcan, A. G., Kök, M. V., & Bağcı, A. S. (2006). Estimation of permeability and rock mechanical properties of limestone reservoir rocks under stress conditions by strain gauge. *Journal of Petroleum Science and Engineering*, 53(1), 13-24.

- Jaber, J. O., Mohsen, M. S., Probert, S. D., & Alees, M. (2001). Future electricity-demands and greenhouse-gas emissions in Jordan. *Applied Energy*, 69(1), 1-18.
- Jenkins, K. A., & Smith, B. J. (1990). Daytime rock surface temperature variability and its implications for mechanical rock weathering: Tenerife, Canary Islands. *Catena*, 17(4), 449-459.
- Jordanian Meteorological Division. (1971). Climatic atlas of Jordan. Amman: Ministry of Transport, Hashemite Kingdom of Jordan.
- Kejonen, A., Kielosto, S., Lahti, S.I. (1988) Cavernous Weathering Forms In Finland: *Geografiska Annaler*, v. 70A, 315-322.
- Kelletat, D. (1980). Studies on the Age of Honeycombs and Tafoni Features: *Catena*, v. 7, 317-325.
- Kennedy, A. 1925. *Petra: Its History and Monuments*. London: Country Life.
- Kerr, A., Smith, B. J., Whalley, W. B., & McGreevy, J. P. (1984). Rock temperatures from southeast Morocco and their significance for experimental rock-weathering studies. *Geology*, 12(5), 306-309.
- Krauskopf, K. B., & Bird, D. K. (1967). *Introduction to geochemistry* (Vol. 721). New York: McGraw-Hill.
- Liu, T., & Dorn, R. I. (1996). Understanding the spatial variability of environmental change in drylands with rock varnish microlaminations. *Annals of the Association of American Geographers*, 86(2), 187-212.
- Lucke, B., Schmidt, M., al-Saad, Z., Bens, O., & Hüttl, R. F. (2005). The abandonment of the Decapolis region in Northern Jordan—forced by environmental change?. *Quaternary international*, 135(1), 65-81.
- Mahmod, W. E., Watanabe, K., & Zahr-Eldeen, A. A. (2013). Analysis of groundwater flow in arid areas with limited hydrogeological data using the Grey Model: a case study of the Nubian Sandstone, Kharga Oasis, Egypt. *Hydrogeology Journal*, 21(5), 1021-1034.
- Makhlouf, I. M., & Abed, A. M. (1991). Depositional facies and environments in the Umm Ishrin Sandstone Formation, Dead Sea area, Jordan. *Sedimentary Geology*, 71(3), 177-187.
- Martin, G.J. & P.E. James. (1993) *All Possible Worlds: A History of Geographical Ideas*. Third Edition. John Wiley & Sons, Inc.
- Martini, I. P. (1978). Tafoni weathering, with examples from tuscany, italy. *Zeitschrift fur Geomorphologie*, 22(1), 44-67.

Matsukura, Y. & Matsouka, N. (1991) Rates of Tafoni Weathering on Uplifted Shore Platforms in Nojima-Zaki, Boso Peninsula, Japan: *Earth Surfaces Processes and Landforms*, v. 16, 51-56.

Matsukura, Y., Matsuoka, N., Yano, N. (1989). A Preliminary Study on Tafoni and Honeycombs in Nojima-Zaki, Boso Peninsula, Japan: Annual Report, Institute of Geoscience, University of Tsukuba, v. 25, 29-32.

McBride, E. F., & Picard, M. D. (2000). Origin of development of tafoni in tunnel spring tuff, crystal peak, utah, usa. *Earth Surface Processes and Landforms*, 25, 869-879.

McBride, E. F., & Picard, M. D. (2004). Origin of honeycomb and related weather forms in oligocene macigno sandstone, tuscan coast near livorno, italy. *Earth Surface Processes and Landforms*, 29, 713-735.

McFadden, L. D., Eppes, M. C., Gillespie, A. R., & Hallet, B. (2005). Physical weathering in arid landscapes due to diurnal variation in the direction of solar heating. *Geological Society of America Bulletin*, 117(1-2), 161-173.

McGreevy, J. P. (1985). A Preliminary Scanning Electron Microscope Study of Honeycomb Weathering Sandstone in a Coastal Environment: *Earth Surfaces Processes and Landforms*, v. 10, 509-518.

Mellor, A., Short, J., Kirkby, S.J. (1997). Tafoni in the El Chorro Area, Andalucia, Southern Spain: *Earth Surfaces Processes and Landforms*, v. 22, 817-833.

Migon, P. (2009). Sandstone Geomorphology of south-west Jordan, Middle East, and its relation to Danxia Landform of China: First International Symposium on Danxia Landform. Danxiashan Guangdong, China

Migoñ, P., Goudie, A., Allison, R., & Rosser, N. (2005). The origin and evolution of footslope ramps in the sandstone desert environment of south-west Jordan. *Journal of arid environments*, 60(2), 303-320.

Mol, L., In Review. Investigations into the relationship between changes in internal moisture regimes and surface weathering in cavernous sandstone weathering features (Golden Gate Highlands National Park, South Africa). *Earth Surface Processes and Landforms*.

Mol, L., & Viles, H. A. (2010). Geoelectric investigations into sandstone moisture regimes: Implications for rock weathering and the deterioration of san rock art in the golden gate reserve, south africa. *Geomorphology*, 118, 280-287.

Mol, L., & Viles, H. A. (2011). The role of rock surface hardness and internal moisture in tafoni development in sandstone. *Earth Surface Processes and Landforms*, 37, 301-314.

- Mol, L. & H. Viles. (2013) Exposing drying patterns: using electrical resistivity tomography to monitor capillary rise in sandstone under varying drying conditions. *Environmental Earth Science*, 86, 1647-1659
- Mottershead, D., Gorbushina, A., Lucas, G., Wright, J. (2003). The Influence of Marine Salts, Aspect and Microbes in the Weathering of Sandstone in Two Historic Structures: Building and Environment, v. 38, 1193-1204.
- Mottershead, D. N., Pye, K. (1994). Tafoni on Coastal Slopes, South Devon, U.K.: Earth Surfaces Processes and Landforms, v. 19, 543-563.
- Mottershead, D. N. (1997). A morphological study of greenschist weathering on dated coastal structures, South Devon, UK. *Earth Surface Processes and Landforms*, 22(5), 491-506.
- Muhs, D. R. (1984). Intrinsic thresholds in soil systems. *Physical Geography*, 5(2), 99-110.
- Mustoe, G. E. (1971). Biochemical origin of coastal weathering features in the chuckanut formation of northwest washington. *Western Washington State College*, 1-85.
- Mustoe, G. E. (1983). Cavernous weathering in the capitol reef desert, utah. *Earth Surface Processes and Landforms*, 8, 517-526.
- Mustoe, G. E. (1982). Origin of honeycomb weathering.pdf: *GSA Bulletin*, v. 93,108-115.
- Nairn, A. E. M., & Alsharhan, A. S. (1997). *Sedimentary basins and petroleum geology of the Middle East*. Access Online via Elsevier.
- Nicholas, R.M., Dixon, J.C., 1986. Sandstone scarp retreat in the Land of Standing Rocks, Canyonlands National Park, Utah. *Z. Geomorphol.* 30, 167–187.
- Norwick, S. A., & Dexter, L. R. (2002). Rates of development of tafoni in the moekopi and kaibab formations in meteor crater and on the colorado plateau, northeastern arizona. *Earth Surface Processes and Landforms*, 27, 11-27.
- Ollier, C. D. (1963). Insolation weathering; examples from central Australia. *American Journal of Science*, 261(4), 376-381.
- Ortloff, C. R. (2005). The water supply and distribution system of the Nabataean City of Petra (Jordan), 300 BC–AD 300. *Cambridge Archaeological Journal*, 15(01), 93-109.
- Osborn, G., & Duford, J. M. (1981). Geomorphological processes in the inselberg region of south-western Jordan. *Palestine Exploration Quarterly*, 113(1), 1-17.
- Paradise, T. R. (1995). Sandstone weathering thresholds in Petra, Jordan. *Physical Geography*, 16(3), 205-222.

- Paradise, T. R. (1998). Limestone weathering and rate variability, Great Temple of Amman, Jordan. *Physical Geography*, 19(2), 133-146.
- Paradise, T. R. (1999). Analysis of sandstone weathering of the Roman theater in Petra, Jordan. *Annals of the Department of Antiquities of Jordan*, 43, 353-368.
- Paradise, T.R. (1999). National Atlas of Jordan (*Unpublished*).
- Paradise, T. R. (2002). Sandstone weathering and aspect in Petra, Jordan. *Zeitschrift fur Geomorphologie*, 46, 1-17
- Paradise, T. R. (2005). Weathering of sandstone architecture in Petra, Jordan: influences and rates. A. Turkington (Ed.), GSA Special 390: Stone decay in the architectural environment. 39–49
- Paradise, T. R. (2010). Sandstone chamber humidity and tourism in Petra, Jordan. *Journal of Architectural Conservation*, 16, 63-79
- Paradise, T. R. (2012). The great flood of Petra: evidence for a 4th-5th century catastrophic flood. *Annual of the Jordan Department of Antiquities*, 56(1). 143-158.
- Paradise, T. R. (2013). Assessment of tafoni distribution and environmental factors on a sandstone djinn block above Petra, Jordan. *Applied Geography*, 42. 176-185
- Paradise, T. R. (2013). Tafoni and other rock basins. In: J.F. Shroder (ed.) Treatise on Geomorphology, volume 4, Elsevier Inc., San Diego, USA, 111-126.
- Parsons, A. J., & Abrahams, A. D. (1994). *Geomorphology of desert environments* (pp. 3-12). Springer Netherlands.
- Patton, M. Q. (2005). *Qualitative Research in Encyclopedia of Statistics in Behavioral Science*. John Wiley & Sons, Ltd. Published Online.
- Pestrong, R. (1988). Tafoni weathering of old structures along the northern california coast, usa. *Engineering Geology of Ancient Works, Monuments and Historical Sites, Marinos & Koukis*, 1049-1053.
- Petra National Trust (PNT). (2012). Annual visitors to petra from 1985-2012. <http://petranationaltrust.org/ui>
- Phillips, J. D. (2006). Evolutionary geomorphology: thresholds and nonlinearity in landform response to environmental change. *Hydrology and Earth System Sciences Discussions*, 3(2), 365-394.

- Pope, G. A., Dorn, R. I., & Dixon, J. C. (1995). A new conceptual model for understanding geographical variations in weathering. *Annals of the Association of American Geographers*, 85(1), 38-64.
- Pope, G. A., Meierding, T. C., & Paradise, T. R. (2002). Geomorphology's role in the study of weathering on cultural stone. *Geomorphology*, 47, 211-225.
- Prebble, M. M. (1967). Cavernous Weathering in the Taylor Dry Valley, Victoria Land, Antarctica: *Nature*, v. 216, 1194-1195.
- Price, D. G. (1995). Weathering and weathering processes. *Quarterly Journal of Engineering Geology and Hydrogeology*, 28(3), 243-252.
- Pye, K., Mottershead, D.N. (1995). Honeycomb Weathering of Carboniferous sandstone in a Sea Wall at Weston-super-Mare, UK: *Quarterly Journal of Engineering Geology*, v. 28, 333-347.
- Ramrez, O. A., Ward, F. A., Al-Tabini, R., & Phillips, R. (2009). Efficient water conservation in agriculture for growing urban water demands in Jordan. *Water Policy*, 13(1), 102.
- Reiche, P. (1962). A survey of weathering processes and products (No. 3). University of New Mexico Press.
- Rodriguez-Navarro, C. (1998). Evidence of Honeycomb Weathering on Mars: *Geophysical Research Letters*, v. 25, 3249-3252.
- Rodriguez-Navarro, C., Doehne, E., & Sebastian, E. (1999). Origins of honeycomb weathering: the role of salts and wind. *GSA Bulletin*, 111(8), 1250-1255.
- Russell, K. W. (1980). The earthquake of May 19, AD 363. *Bulletin of the American Schools of Oriental Research*, (238), 47-64.
- Russell, K. W. (1993). Ethnohistory of the Bedul Bedouin of Petra. *Annals of the Department of Antiquities of Jordan* 37: 15-35.
- Sancho, C., Benito, G. (1990). Factors Controlling Tafoni Weathering in the Ebro Basin (NE Spain): *Zeitschrift fur Geomorphologie*, v. 34, 165-177.
- Schumm, S. A. (1973). Geomorphic thresholds and complex response of drainage systems. *Fluvial geomorphology*, 6, 69-85.
- Schumm, S. A. (1979). Geomorphic thresholds: the concept and its applications. *Transactions of the Institute of British Geographers*, 485-515.
- Schumm, S. A., & Khan, H. R. (1972). Experimental study of channel patterns. *Geological Society of America Bulletin*, 83(6), 1755-1770.

- Seber, D., Vallvé, M., Sandvol, E., Steer, D., & Barazangi, M. (1997). Middle East tectonics; applications of geographic information systems (GIS). *GSA Today*, 7(2), 1-6.
- Selby, M. J. (1979). Salt Weathering of Landforms and an Antarctic Example: New Zealand Geography Conference, 30-35.
- Simms, S. R., & Russell, K. W. (1997). Tur Imdai rockshelter: Archaeology of recent pastoralists in Jordan. *Journal of field archaeology*, 24(4), 459-472.
- Smith, B. J. (1978). The origin and geomorphic implications of cliff foot recesses and tafoni on limestone hamadas in the northwest sahara. *Zeitschrift fuer Geomorphologie*, v. 22, 21-43.
- Smith, B. J. (2009) Weathering Processes and Forms in Parsons, A. J., & Abrahams, A. D. (eds) *Geomorphology of desert environments 2nd Edition* (pp. 69-70). Springer Netherlands.
- Smith, B. J. (1988). Weathering of superficial limestone debris in a hot desert environment. *Geomorphology*, 1(4), 355-367.
- Smith, B. J., Gomez-Heras, M., & McCabe, S. (2008). Understanding the decay of stone-built cultural heritage. *Progress in Physical Geography*, 32(4), 439-461.
- Smith, B. J., & McGreevy, J. P. (1983). A simulation study of salt weathering in hot deserts. *Geografiska Annaler. Series A. Physical Geography*, 127-133.
- Smith, B. J., Turkington, A. V., & Curran, J. M. (2005). Urban stone decay: The great weathering experiment?. *Special Papers-Geological Society of America*, 390, 1.
- Smith, B., Whalley, B., & Magee, R. (1992). Assessment of building stone decay: a geomorphological approach. In *Stone cleaning and the nature, soiling and decay mechanisms of stone: proceedings of the international conference held in Edinburgh, UK, 14-16 April 1992*: 249-257.
- Somerton, W. H. (1961, January). Thermo-Mechanical Behavior Of Porous Rocks. In *SPE California Regional Meeting*. Society of Petroleum Engineers.
- Somerton, W. H. (1992). *Thermal properties and temperature-related behavior of rock/fluid systems* (Vol. 37). Elsevier.
- Somerton, W. H., & Gupta, V. S. (1965). Role of fluxing agents in thermal alteration of sandstones. *Journal of Petroleum Technology*, 17(05), 585-588.
- Song, Y. Q., Ryu, S., & Sen, P. N. (2000). Determining multiple length scales in rocks. *Nature*, 406(6792), 178-181.
- Staley, J. T., Adams, J. B., & Palmer, F. E. (1992). Desert varnish: a biological perspective. *Soil biochemistry*, 7, 173-195.

- Sunamura, T. (1996). A physical model for the rate of coastal tafoni development. *The Journal of Geology*, 104(6), 741-748.
- Sunamura, T., & Aoki, H. (2011). Application of an S-shaped curve model to the temporal development of tafoni of salt-weathering origin. *Earth Surface Processes and Landforms*, 36(12), 1624-1631.
- Suzuki, T. & Hachinohe, S. (1995). Weathering Rates in Bedrock Forming Marine Terraces in Boso Peninsula, Japan: Transactions, Japanese Geomorphological Union, v. 16, 93-113.
- Taylor, J. (2007). *Petra and the Lost Kingdom of the Nabateans*. Amman, Jordan: Al-'Uzza Books by arrangement with I.B. Tauris & Co Ltd.
- Tholbecq, L. (2007). Nabataean monumental Architecture. In *The World of the Nabataeans: International Conference 'The World of the Herods and the Nabataeans', London, British Museum 17-19 April 2001*, (1)103-144. Steiner Verlag Stuttgart.
- Thomas, D. S. (Ed.). (2011). *Arid zone geomorphology: process, form and change in drylands*. John Wiley & Sons, Ltd. West Sussex, UK
- Thornbush, M. J., & Viles, H. A. (2008). Photographic monitoring of soiling and decay of roadside walls in central Oxford, England. *Environmental Geology*, 56(3-4), 777-787.
- Tooth, S. (2007). Arid geomorphology: investigating past, present and future changes. *Progress in Physical Geography*.
- Tschang, H. (1974). Geomorphological observations on the tafoni forms of hong kong. *The Chung Chi Journal*, 32-54.
- Turkington, A. V., Phillips, J.D. (2004). Cavernous Weathering, Dynamical Instability and Self-Organization: *Earth Surface Processes and Landforms*, v. 29, 665-675.
- Twidale, C. R., & Sved, G. (1978). Minor granite landforms associated with the release of compressive stress. *Australian Geographical Studies*, 16(2), 161-174.
- Twenhaile, A. S. (1992). Chapter 2 - Chemical and Salt Weathering, *Geomorphology of Rock Coasts*, Oxford, U.K., Oxford University Press, 31-58.
- Viles, H. A. (2002). Implications of future climate change for stone deterioration. *Geological Society, London, Special Publications*, 205(1), 407-418.
- Viles, H. A., Goudie, A.S. (2004). Biofilms and Case Hardening on Sandstones from Al-Quwayra, Jordan: *Earth Surfaces Process and Landforms*, v. 29, 1473-1485.

- Viles, H., Goudie, A., Grab, S., & Lalley, J. (2011). The use of the Schmidt Hammer and Equotip for rock hardness assessment in geomorphology and heritage science: a comparative analysis. *Earth Surface Processes and Landforms*, 36(3), 320-333.
- Warke, P. A. (2007). Complex weathering in drylands: Implications of 'stress' history for rock debris breakdown and sediment release. *Geomorphology*, 85(1), 30-48.
- Warke, P. A., & Smith, B. J. (1998). Effects of direct and indirect heating on the validity of rock weathering simulation studies and durability tests. *Geomorphology*, 22(3), 347-357.
- Warke, P. A., Smith, B. J., & Magee, R. W. (1996). Thermal response characteristics of stone: implications for weathering of soiled surfaces in urban environments. *Earth Surface Processes and Landforms*, 21(3), 295-306.
- Webb, R. H., Leake, S. A., & Malloy, R. A. (2013). Geologic, Hydrologic, and Urban Hazards for Design in Desert Environments. *Design with the Desert: Conservation and Sustainable Development*, 91.
- Wedekind, W., & Ruedrich, J. (2006). Salt-weathering, conservation techniques and strategies to protect the rock cut facades in Petra/Jordan. *Heritage, weathering and conservation*. Taylor & Francis/Balkema, Leiden, 261-268.
- Weiss, T., Siegesmund, S., Kirchner, D., & Sippel, J. (2004). Insolation weathering and hygric dilatation: two competitive factors in stone degradation. *Environmental Geology*, 46(3-4), 402-413.
- Wellman, H.W., Wilson A.T. (1965). Salt weathering, a neglected geological erosive agent in coastal and arid environments: *Nature*, 205, 1097-1098.
- Wilhelmy, H. (1964). Cavernous rock surfaces (tafoni) in semiarid and arid climates, Pakistan Geographical Review, 19, 8-13.
- Williams, R. B. G., & Robinson, D. A. (2000). Effects of aspect on weathering: anomalous behaviour of sandstone gravestones in southeast England. *Earth Surface Processes and Landforms*, 25(2), 135-144.
- Winkler, E. M. (1979). Role of salts in development of granitic tafoni, South Australia: *Journal of Geology*, v. 88, 119-120.
- Young, A. R. M. (1987). Salt as an Agent in the Development of Cavernous Weathering: *Geology*, v. 15, 962-966.
- Young, R. W., Young, A., & Wray, R. (1992). *Sandstone landforms*. Berlin: Springer.
- Zhang, Y., Zhang, X., & Zhao, Y. S. (2005). Process of sandstone thermal cracking. *Chinese Journal of Geophysics*, 48(3), 722-726.

Appendices

A: Photographs

B: Tables

C: Graphs

D: Field Matrices

Appendix A – Photographs

A.1: Interdigitation on one of the djinn blocks in the Siq. Photograph by K. Groom (2013).



A.2: Tour horse at the base of one of the tombs before the Siq. Photograph by K. Groom (2013).



A.3: Iron banding in the sandstone in the Siq. Photograph by K. Groom (2013).



A.4: Tour horse cart in the Siq. Photograph by K. Groom (2013).



A.5: Drapery formations in the Siq. Photograph by K. Groom (2013).



A.6: Treasury (al-Khazneh) at the end of the Siq. Photograph by K. Groom (2013).



A.7: Bedouin camel guide in front of Treasury (al-Khazneh). Photograph by K. Groom (2013).



A.8: Camels in front of a shop in the Upper Siq. Photograph by K. Groom (2013).



A.9: Great Temple in the main valley. Photograph by K. Groom (2013).



A.10: Petra Church across from the Great Temple. Photograph by K. Groom (2013).



A.11: Several tombs in the main valley of Petra. Photograph by K. Groom (2013).



A.12: Royal Tombs in the main valley. Photograph by K. Groom (2013).



A.13: Djinn Block X from a distance. Photograph by K. Groom (2013).



A.14: Tafoni at the base of the western face on Djinn Block X. Photograph by K. Groom (2013).



A.15: Bedouin goatherd of the side of a mountain across from Djinn Block X. Photograph by K. Groom (2013).



A.16: Jabel Haroun from Djinn Block X. Photograph by K. Groom (2013).



A.17: Bird nest in a western tafone on Djinn Block X. Photograph by K. Groom (2013).



A.18: Odd composites at the Umm Ishrin and Disi contact on Djinn Block X. Photograph by K. Groom (2013).



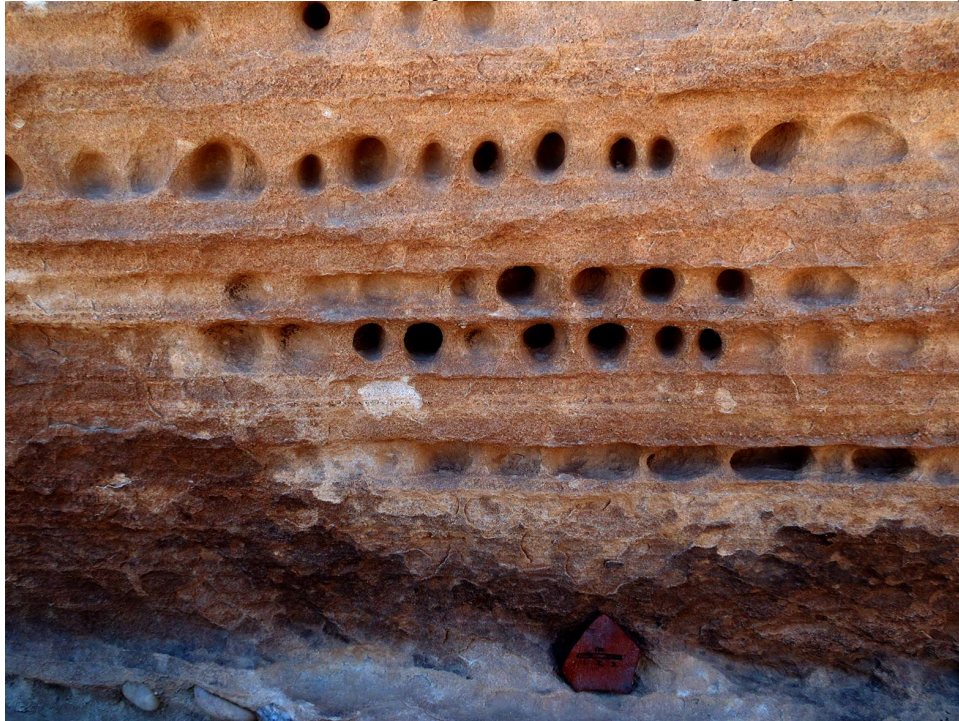
A.19: Extreme climate conditions during fieldwork. Photograph by K. Groom (2013).



A.20: Carved grooves on the top of Djinn Block X. Photograph by K. Groom (2013).



A.21: Linear tafoni on the western face on Djinn Block X. Photograph by K. Groom (2013).



A.22: Horsemen leaving Petra in Wadi Mousa. Photograph by K. Groom (2013).



A.23: Tom Paradise (consented) flat ledge directly south of Djinn Block X. Photograph by K. Groom (2013).



A.24: Quarry walls directly west of Djinn Block X. Photograph by K. Groom (2013).



A.25: Djinn Block X from the edge of the ledge to the south. Photograph by K. Groom (2013).



A.26: Large vertical pan on the southern face of Djinn Block X. Photograph by K. Groom (2013).



A.27: My arm in a netted cell on the southern face of Djinn Block X. Photograph by K. Groom (2013).



A.28: Very deep tafone on the western face on Djinn Block X. Photograph by K. Groom (2013).



A.29: Large tafone on the northern face with a hole leading to the eastern face of Djinn Block X. Photograph by K. Groom (2013).



A.30: My arm reaching through that hole from north to east. Photograph by K. Groom (2013).



A.31: Tafoni cells at the contact on the eastern face of Djinn Block X. Photograph by K. Groom (2013).



A.32: Fire damage on the eastern face of Djinn Block X. Photograph by K. Groom (2013).



A.33: Bug nest on the western face of Djinn Block X. Photograph by K. Groom (2013).



A.34: Large spall preparing to detach on the eastern face of Djinn Block X. Photograph by K. Groom (2013).



A.35: Main valley as seen from atop al-Habis. Photograph by K. Groom (2013).



A.36: Western part of the main valley from atop al-Habis. Photograph by K. Groom (2013).



A.37: Hewn pit behind al-Habis. Photograph by K. Groom (2013).



A.38: Royal Tombs from the path to al-Deir. Photograph by K. Groom (2013).



A.39: Tom Paradise (consent to publish) and Waimel al-Bedoul (consent to publish) at the Great Temple. Photograph by K. Groom (2013).



A.40: Me, Waimel al-Bedoul (consent to publish), and Peter von Groote (consent to publish) at the Great Temple. Photograph by T. Paradise (2013).



A.41: Peter von Groote (consent to publish) on a donkey up to al-Deir. Photograph by K. Groom (2013).



A.42: Restaurant benches in front of al-Deir. Photograph by K. Groom (2013).



Appendix B – Tables

B.1 – Mirrored Aspect Values for Djinn Block X:

| Mirror Values for 000° to 162° | | | | | | | | | | |
|--------------------------------|-----|-----|-----|-----|-----|-----|-----|-----|-----|-----|
| | 000 | 018 | 036 | 054 | 072 | 090 | 108 | 126 | 144 | 162 |
| 000 | 180 | 162 | 144 | 126 | 108 | 090 | 072 | 054 | 036 | 018 |
| 018 | 162 | 180 | 162 | 144 | 126 | 108 | 090 | 072 | 054 | 036 |
| 036 | 144 | 162 | 180 | 162 | 144 | 126 | 108 | 090 | 072 | 054 |
| 054 | 126 | 144 | 162 | 180 | 162 | 144 | 126 | 108 | 090 | 072 |
| 072 | 108 | 126 | 144 | 162 | 180 | 162 | 144 | 126 | 108 | 090 |
| 090 | 090 | 108 | 126 | 144 | 162 | 180 | 162 | 144 | 126 | 108 |
| 108 | 072 | 090 | 108 | 126 | 144 | 162 | 180 | 162 | 144 | 126 |
| 126 | 054 | 072 | 090 | 108 | 126 | 144 | 162 | 180 | 162 | 144 |
| 144 | 036 | 054 | 072 | 090 | 108 | 126 | 144 | 162 | 180 | 162 |
| 162 | 018 | 036 | 054 | 072 | 090 | 108 | 126 | 144 | 162 | 180 |
| 180 | 000 | 018 | 036 | 054 | 072 | 090 | 108 | 126 | 144 | 162 |
| 198 | 018 | 000 | 018 | 036 | 054 | 072 | 090 | 108 | 126 | 144 |
| 216 | 036 | 018 | 000 | 018 | 036 | 054 | 072 | 090 | 108 | 126 |
| 234 | 054 | 036 | 018 | 000 | 018 | 036 | 054 | 072 | 090 | 108 |
| 252 | 072 | 054 | 036 | 018 | 000 | 018 | 036 | 054 | 072 | 090 |
| 270 | 090 | 072 | 054 | 036 | 018 | 000 | 018 | 036 | 054 | 072 |
| 288 | 108 | 090 | 072 | 054 | 036 | 018 | 000 | 018 | 036 | 054 |
| 306 | 126 | 108 | 090 | 072 | 054 | 036 | 018 | 000 | 018 | 036 |
| 324 | 144 | 126 | 108 | 090 | 072 | 054 | 036 | 018 | 000 | 018 |
| 342 | 162 | 144 | 126 | 108 | 090 | 072 | 054 | 036 | 018 | 000 |
| Faces on Djinn Block X | | | | | | | | | | |
| 328 | 148 | 130 | 112 | 094 | 076 | 058 | 040 | 022 | 004 | 014 |
| 226 | 046 | 028 | 010 | 008 | 026 | 044 | 062 | 080 | 098 | 116 |
| 156 | 024 | 042 | 060 | 078 | 096 | 114 | 132 | 150 | 168 | 174 |
| 082 | 098 | 116 | 134 | 152 | 170 | 172 | 154 | 136 | 118 | 100 |

| Mirror Values for 180° to 342° | | | | | | | | | |
|--------------------------------|-----|-----|-----|-----|-----|-----|-----|-----|-----|
| 180 | 198 | 216 | 234 | 252 | 270 | 288 | 306 | 324 | 342 |
| 000 | 018 | 036 | 054 | 072 | 090 | 108 | 126 | 144 | 162 |
| 018 | 000 | 018 | 036 | 054 | 072 | 090 | 108 | 126 | 144 |
| 036 | 018 | 000 | 018 | 036 | 054 | 072 | 090 | 108 | 126 |
| 054 | 036 | 018 | 000 | 018 | 036 | 054 | 072 | 090 | 108 |
| 072 | 054 | 036 | 018 | 000 | 018 | 036 | 054 | 072 | 090 |
| 090 | 072 | 054 | 036 | 018 | 000 | 018 | 036 | 054 | 072 |
| 108 | 090 | 072 | 054 | 036 | 018 | 000 | 018 | 036 | 054 |
| 126 | 108 | 090 | 072 | 054 | 036 | 018 | 000 | 018 | 036 |

| | | | | | | | | | |
|------------------------|-----|-----|-----|-----|-----|-----|-----|-----|-----|
| 144 | 126 | 108 | 090 | 072 | 054 | 036 | 018 | 000 | 018 |
| 162 | 144 | 126 | 108 | 090 | 072 | 054 | 036 | 018 | 000 |
| 180 | 162 | 144 | 126 | 108 | 090 | 072 | 054 | 036 | 018 |
| 162 | 180 | 162 | 144 | 126 | 108 | 090 | 072 | 054 | 036 |
| 144 | 162 | 180 | 162 | 144 | 126 | 108 | 090 | 072 | 054 |
| 126 | 144 | 162 | 180 | 162 | 144 | 126 | 108 | 090 | 072 |
| 108 | 126 | 144 | 162 | 180 | 162 | 144 | 126 | 108 | 090 |
| 090 | 108 | 126 | 144 | 162 | 180 | 162 | 144 | 126 | 108 |
| 072 | 090 | 108 | 126 | 144 | 162 | 180 | 162 | 144 | 126 |
| 054 | 072 | 090 | 108 | 126 | 144 | 162 | 180 | 162 | 144 |
| 036 | 054 | 072 | 090 | 108 | 126 | 144 | 162 | 180 | 162 |
| 018 | 036 | 054 | 072 | 090 | 108 | 126 | 144 | 162 | 180 |
| Faces on Djinn Block X | | | | | | | | | |
| 032 | 050 | 068 | 086 | 104 | 122 | 140 | 158 | 176 | 166 |
| 134 | 152 | 170 | 172 | 154 | 136 | 118 | 100 | 082 | 064 |
| 156 | 138 | 120 | 102 | 084 | 066 | 048 | 030 | 012 | 006 |
| 082 | 064 | 046 | 028 | 010 | 008 | 026 | 044 | 062 | 080 |

B.2 – Statistic values for aspect vs. morphometry:

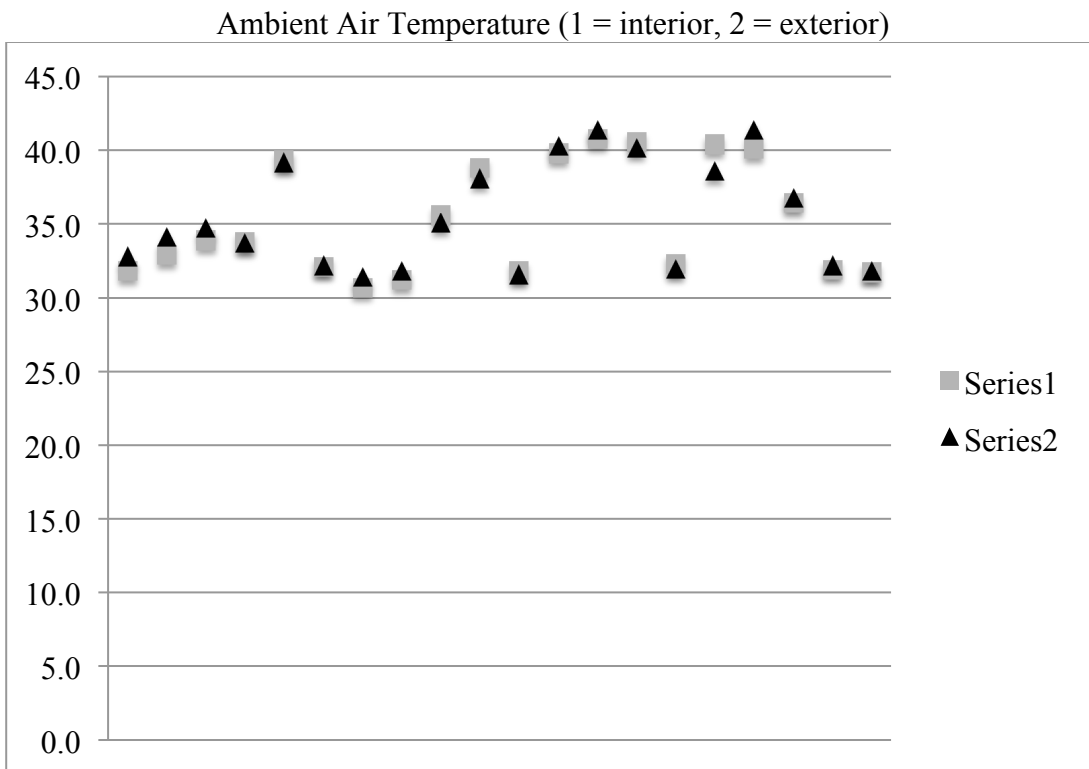
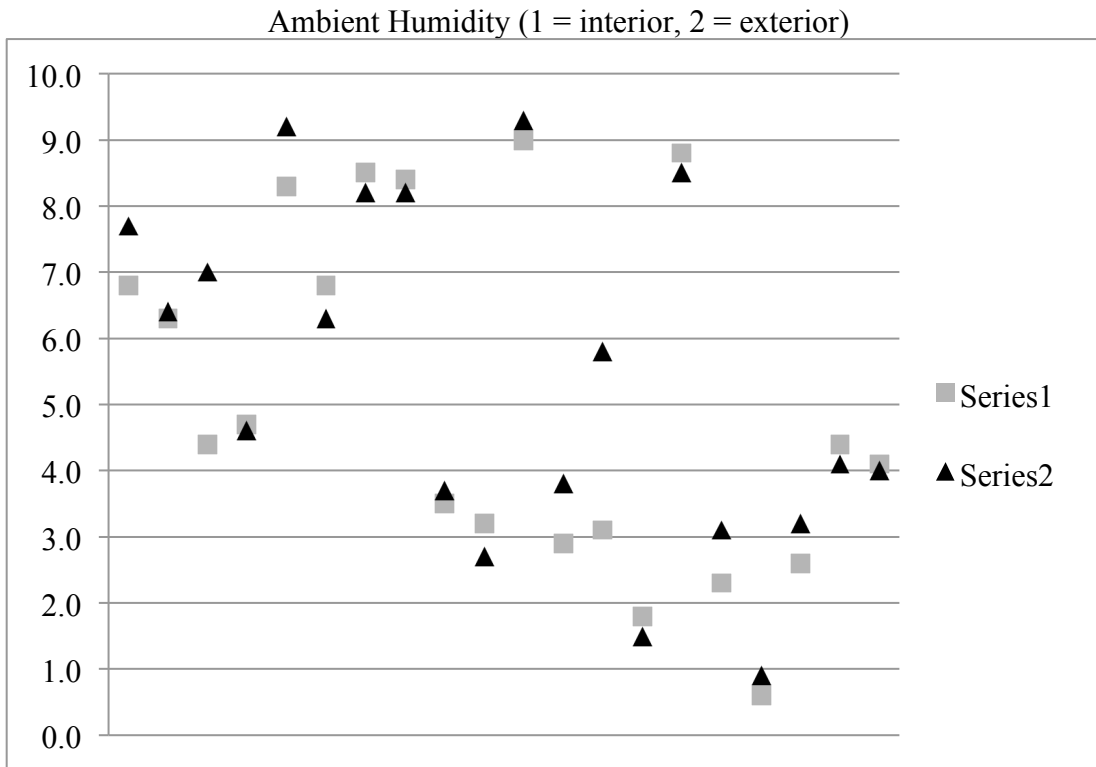
| Mirror Values | 360 Degrees - R ² | | | W/o North - R ² | | | W/o South - R ² | | |
|---------------|------------------------------|-------|-------|----------------------------|-------|-------|----------------------------|-------|-------|
| | Vol. | Depth | Diam. | Vol. | Depth | Diam. | Vol. | Depth | Diam. |
| 000 | 0.001 | 0.007 | 0.001 | 0.049 | 0.083 | 0.041 | 0.102 | 0.008 | 0.080 |
| 018 | 0.001 | 0.001 | 0.002 | 0.016 | 0.121 | 0.009 | 0.043 | 0.002 | 0.042 |
| 036 | 0.000 | 0.016 | 0.002 | 0.003 | 0.123 | 0.000 | 0.010 | 0.022 | 0.016 |
| 054 | 0.000 | 0.043 | 0.001 | 0.001 | 0.120 | 0.000 | 0.000 | 0.051 | 0.002 |
| 072 | 0.003 | 0.077 | 0.001 | 0.001 | 0.120 | 0.000 | 0.012 | 0.088 | 0.002 |
| 090 | 0.007 | 0.100 | 0.002 | 0.000 | 0.116 | 0.001 | 0.039 | 0.115 | 0.014 |
| 108 | 0.006 | 0.102 | 0.003 | 0.003 | 0.096 | 0.009 | 0.082 | 0.130 | 0.040 |
| 126 | 0.005 | 0.078 | 0.003 | 0.026 | 0.046 | 0.039 | 0.132 | 0.122 | 0.075 |
| 144 | 0.003 | 0.049 | 0.002 | 0.067 | 0.001 | 0.078 | 0.157 | 0.087 | 0.099 |
| 162 | 0.001 | 0.026 | 0.001 | 0.077 | 0.020 | 0.078 | 0.148 | 0.047 | 0.103 |
| 180 | 0.001 | 0.007 | 0.001 | 0.049 | 0.083 | 0.041 | 0.100 | 0.008 | 0.079 |
| 198 | 0.001 | 0.001 | 0.002 | 0.016 | 0.121 | 0.009 | 0.043 | 0.002 | 0.042 |
| 216 | 0.000 | 0.016 | 0.002 | 0.003 | 0.123 | 0.000 | 0.010 | 0.022 | 0.016 |
| 234 | 0.000 | 0.043 | 0.001 | 0.001 | 0.120 | 0.000 | 0.000 | 0.051 | 0.002 |
| 252 | 0.003 | 0.077 | 0.001 | 0.001 | 0.120 | 0.000 | 0.012 | 0.088 | 0.002 |
| 270 | 0.007 | 0.100 | 0.002 | 0.000 | 0.116 | 0.001 | 0.039 | 0.115 | 0.014 |
| 288 | 0.006 | 0.102 | 0.003 | 0.003 | 0.096 | 0.009 | 0.082 | 0.130 | 0.040 |
| 306 | 0.005 | 0.078 | 0.003 | 0.026 | 0.046 | 0.039 | 0.132 | 0.122 | 0.075 |
| 324 | 0.003 | 0.049 | 0.002 | 0.067 | 0.001 | 0.078 | 0.157 | 0.087 | 0.099 |
| 342 | 0.003 | 0.039 | 0.002 | 0.077 | 0.005 | 0.086 | 0.155 | 0.066 | 0.101 |

B.3 – Statistic values for aspect vs. micrometeorology:

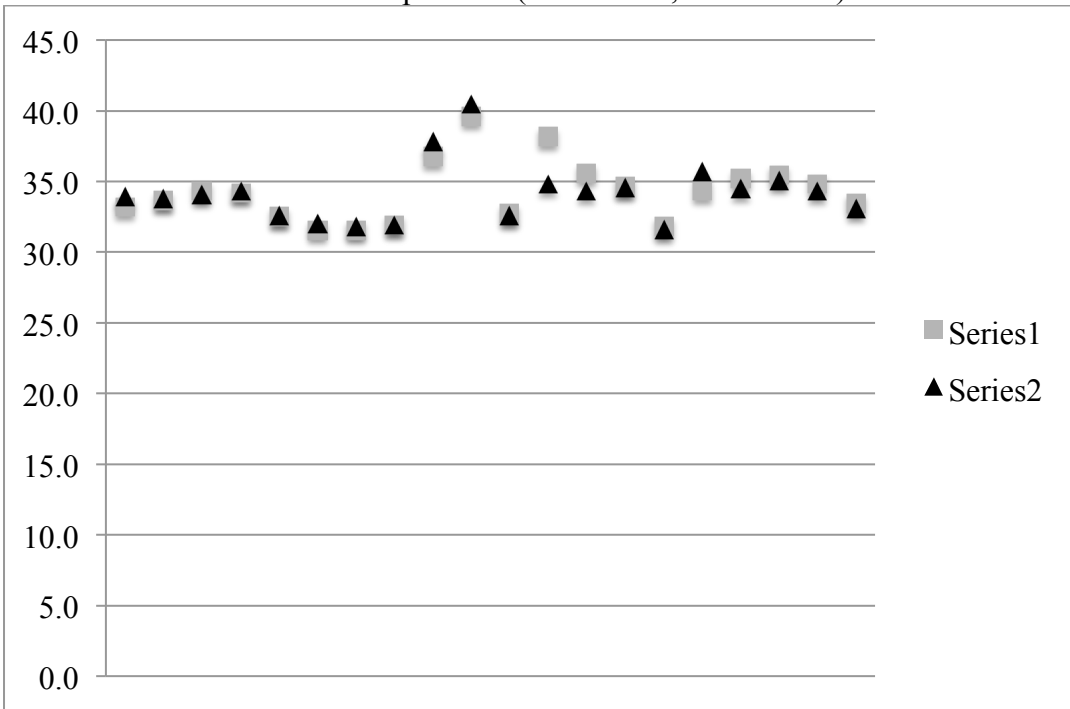
| Mirrored Values | Micrometeorology - R | | | Micrometeorology - R2 | | |
|-----------------|----------------------|---------------|------------------|-----------------------|---------------|------------------|
| | Surface Temp. | Ambient Temp. | Ambient Humidity | Surface Temp. | Ambient Temp. | Ambient Humidity |
| 000 | 0.383 | 0.098 | 0.191 | 0.147 | 0.010 | 0.036 |
| 018 | 0.295 | 0.020 | 0.143 | 0.087 | 0.000 | 0.021 |
| 036 | 0.164 | -0.061 | 0.075 | 0.027 | 0.004 | 0.006 |
| 054 | 0.076 | -0.110 | -0.005 | 0.006 | 0.012 | 0.000 |
| 072 | 0.031 | -0.137 | -0.106 | 0.001 | 0.019 | 0.011 |
| 090 | -0.051 | -0.161 | -0.180 | 0.003 | 0.026 | 0.032 |
| 108 | -0.192 | -0.186 | -0.238 | 0.037 | 0.034 | 0.052 |
| 126 | -0.308 | -0.186 | -0.245 | 0.095 | 0.035 | 0.060 |
| 144 | -0.372 | -0.169 | -0.237 | 0.138 | 0.028 | 0.056 |
| 162 | -0.413 | -0.149 | -0.208 | 0.171 | 0.022 | 0.043 |
| 180 | -0.386 | -0.098 | -0.187 | 0.149 | 0.010 | 0.035 |
| 198 | -0.295 | -0.020 | -0.143 | 0.087 | 0.000 | 0.021 |
| 216 | -0.164 | 0.061 | -0.075 | 0.027 | 0.004 | 0.006 |
| 234 | -0.076 | 0.110 | 0.005 | 0.006 | 0.012 | 0.000 |
| 252 | -0.031 | 0.137 | 0.106 | 0.001 | 0.019 | 0.011 |
| 270 | 0.051 | 0.161 | 0.180 | 0.003 | 0.026 | 0.032 |
| 288 | 0.192 | 0.186 | 0.228 | 0.037 | 0.034 | 0.052 |
| 306 | 0.308 | 0.186 | 0.245 | 0.095 | 0.035 | 0.060 |
| 324 | 0.372 | 0.169 | 0.237 | 0.138 | 0.028 | 0.056 |
| 342 | 0.375 | 0.156 | 0.238 | 0.141 | 0.024 | 0.057 |

Appendix C – Graphs

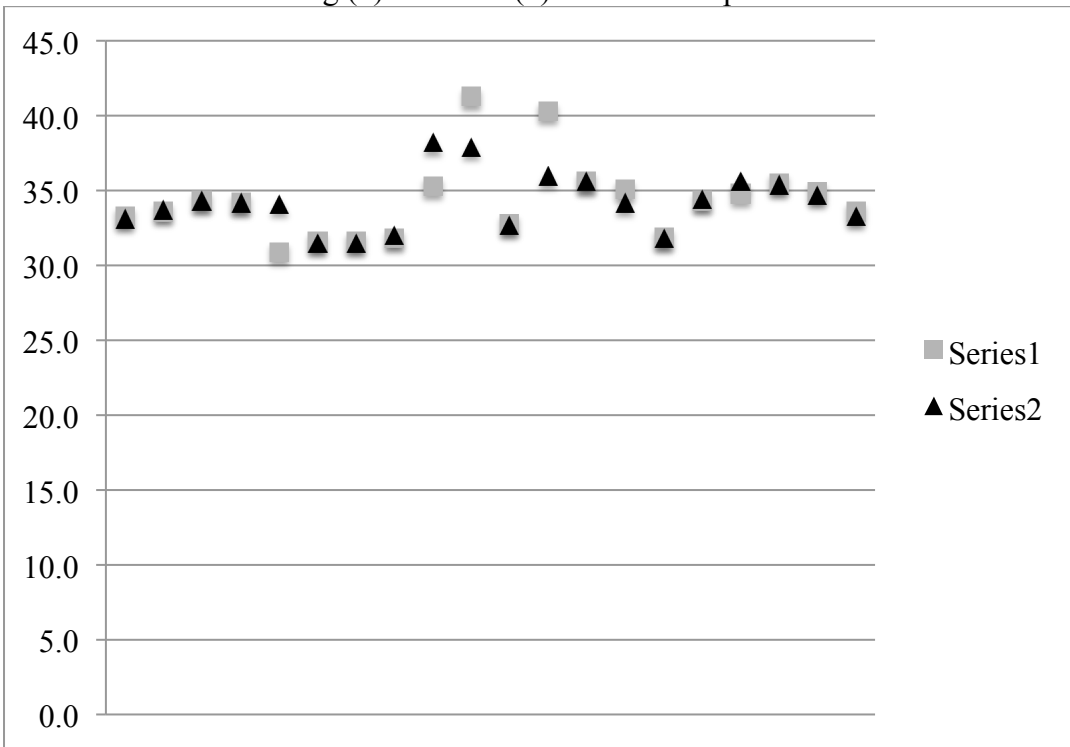
C.1 – Internal and external microclimatic readings per aspect: EAST



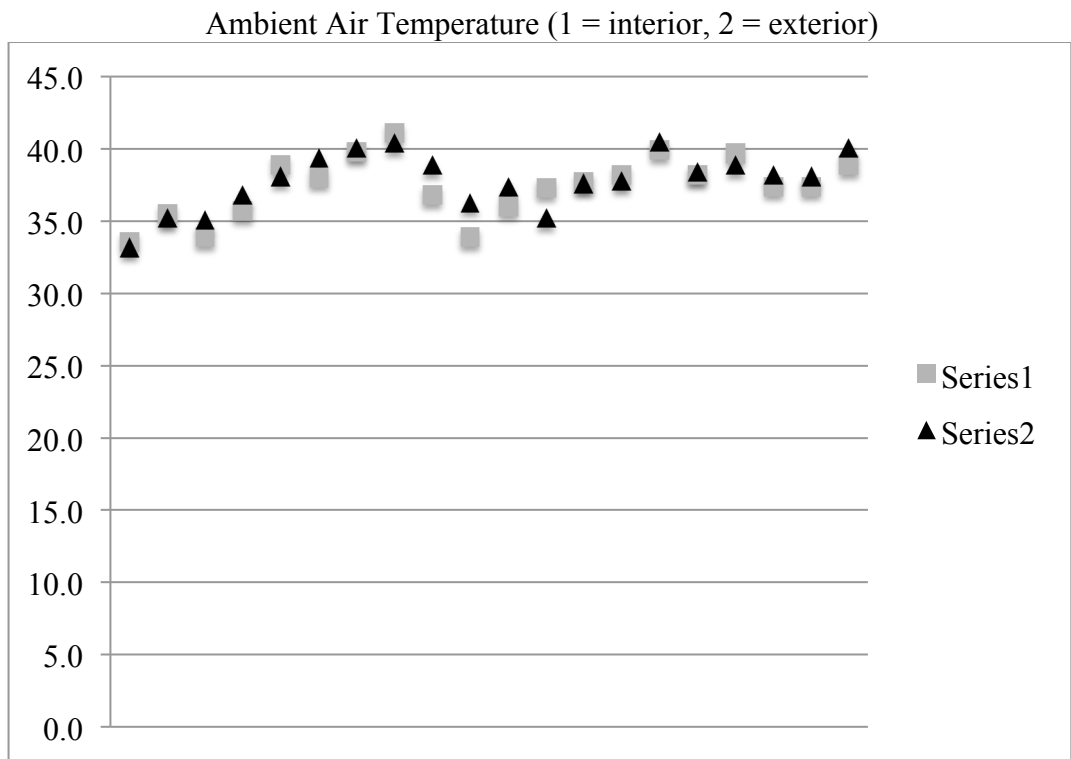
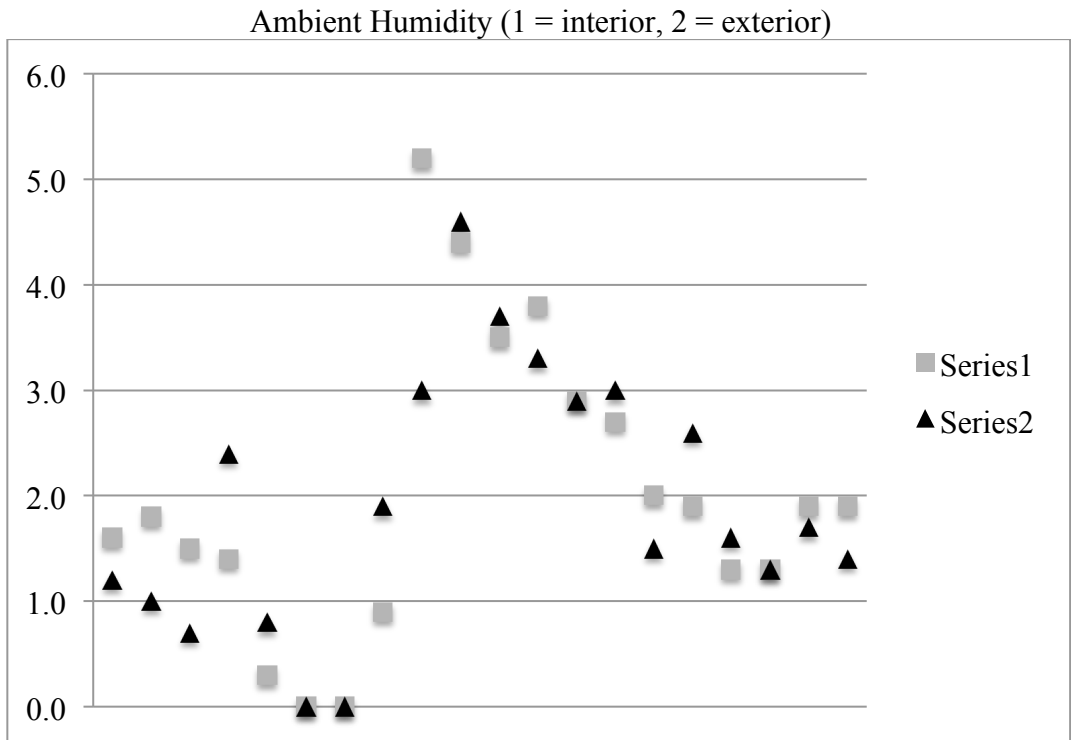
Surface Temperature (1 = interior, 2 = exterior)



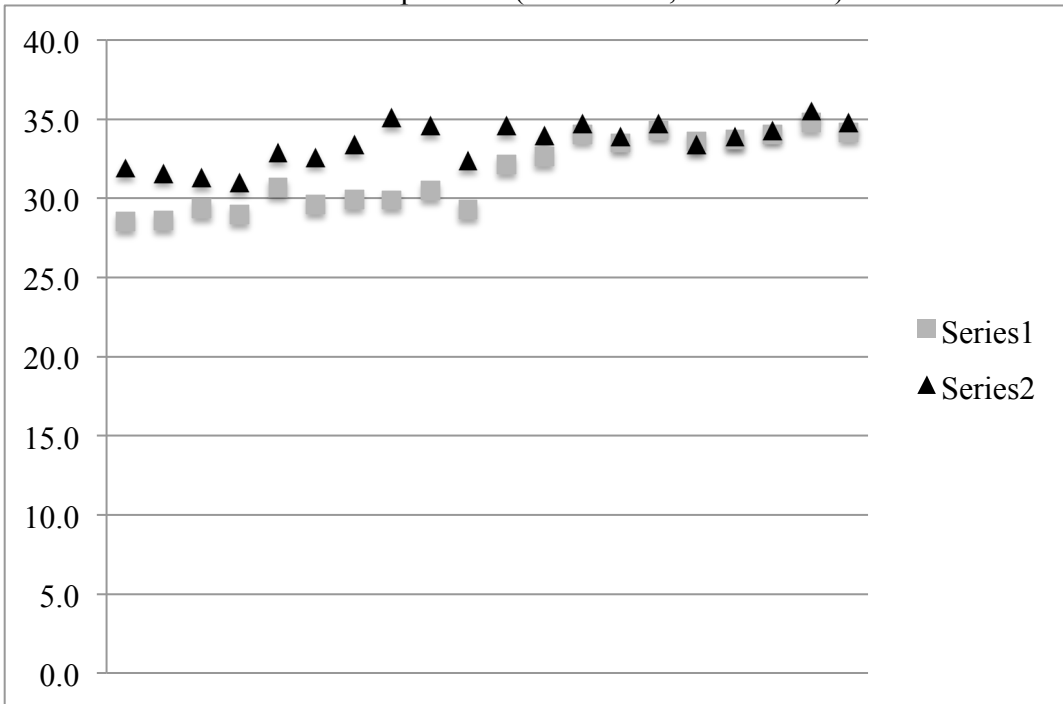
Ceiling (1) vs. Floor (2) Surface Temperatures



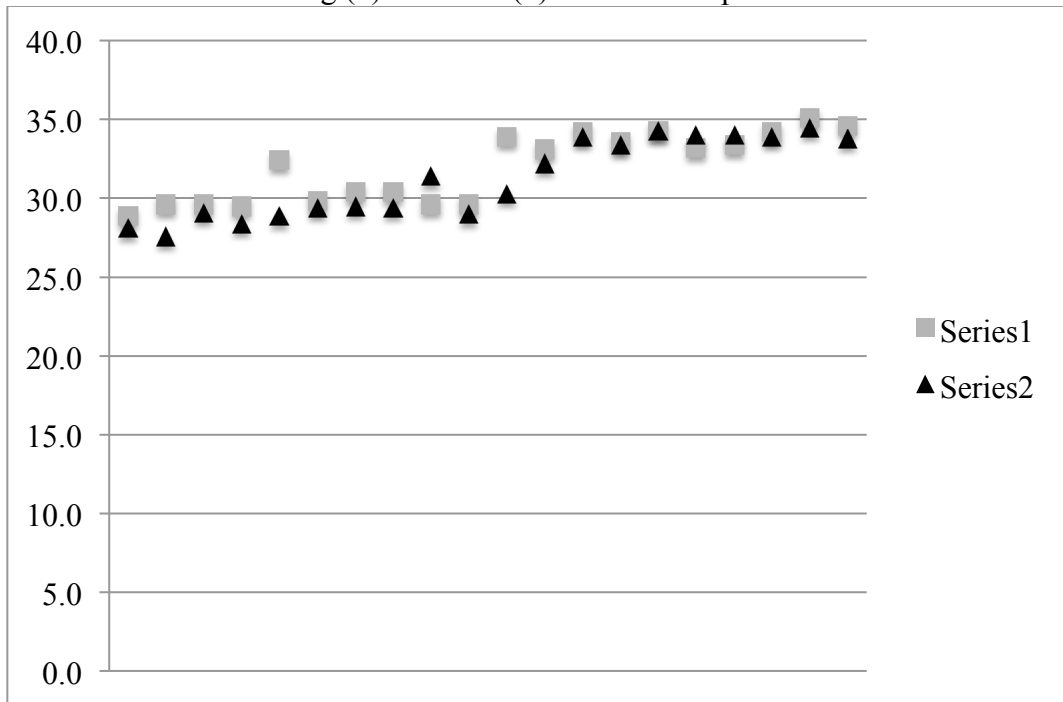
C.2 – Internal and external microclimatic readings per aspect: South



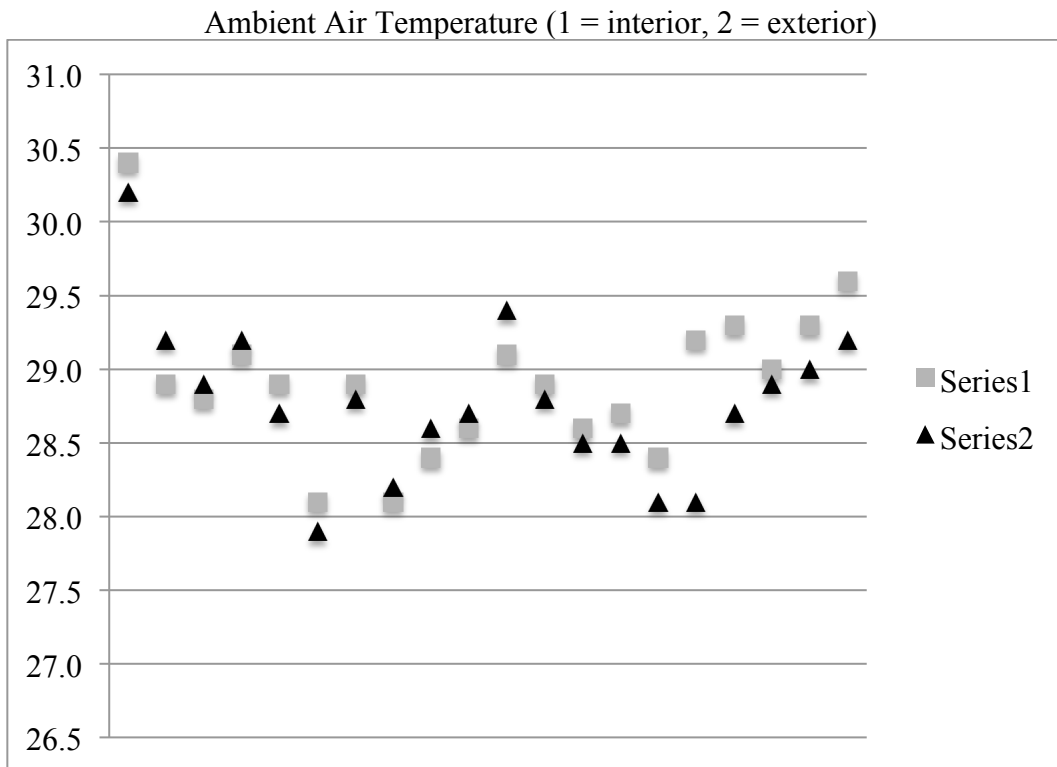
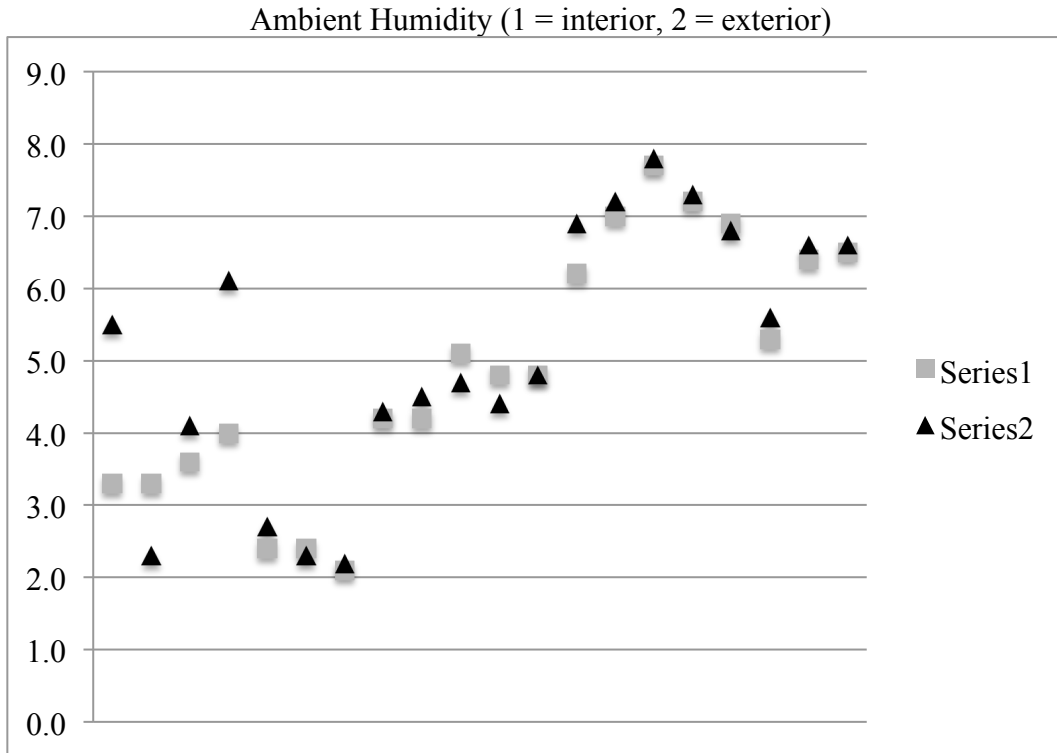
Surface Temperature (1 = interior, 2 = exterior)



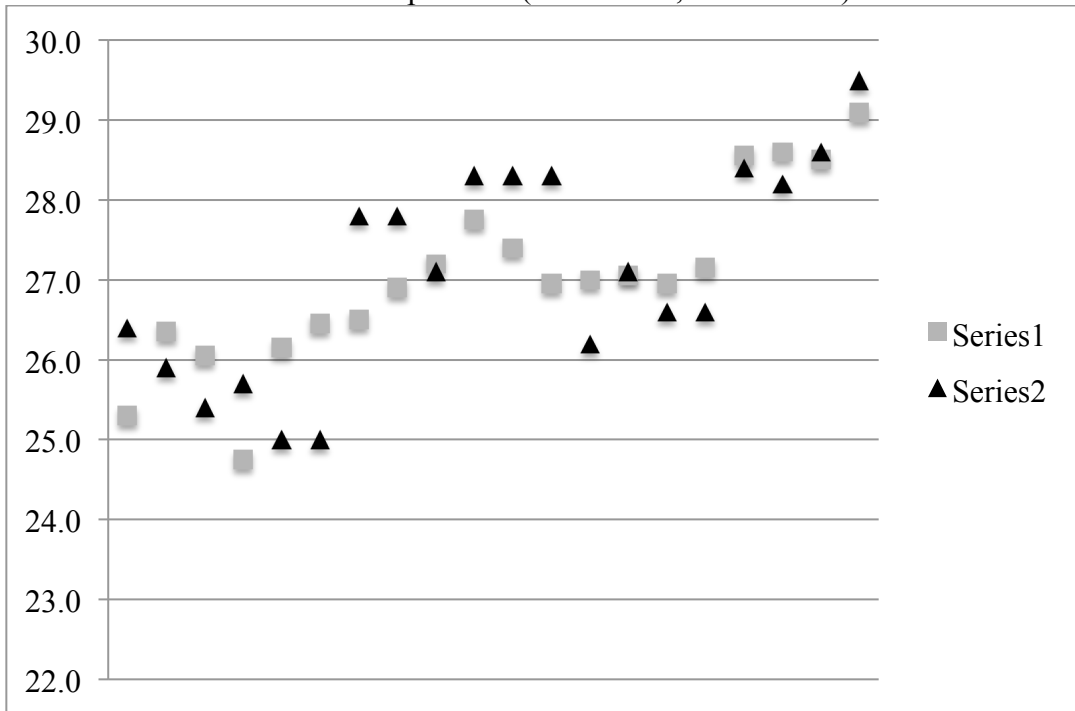
Ceiling (1) vs. Floor (2) Surface Temperatures



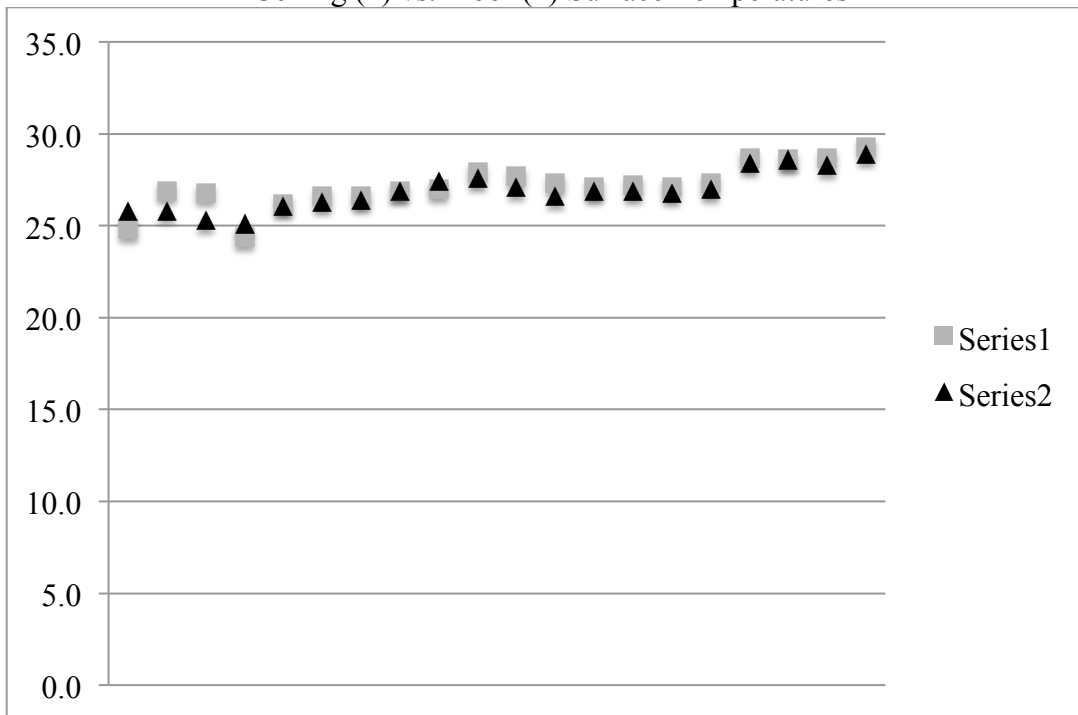
C.3 – Internal and external microclimatic readings per aspect: West



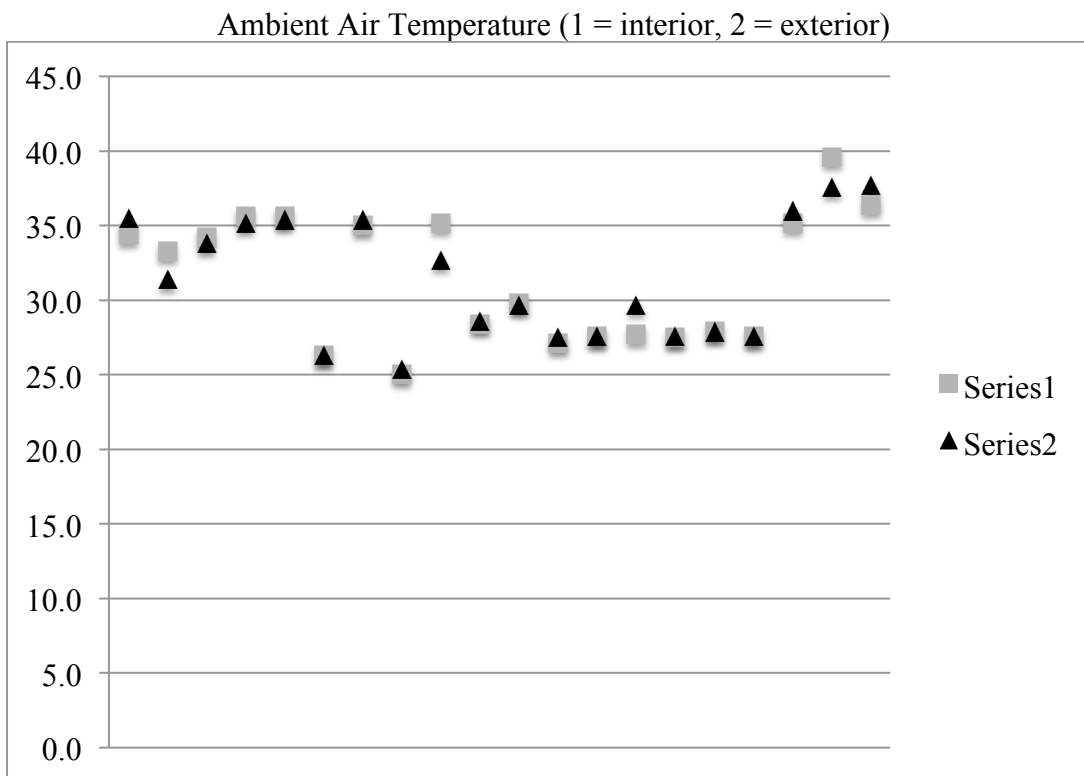
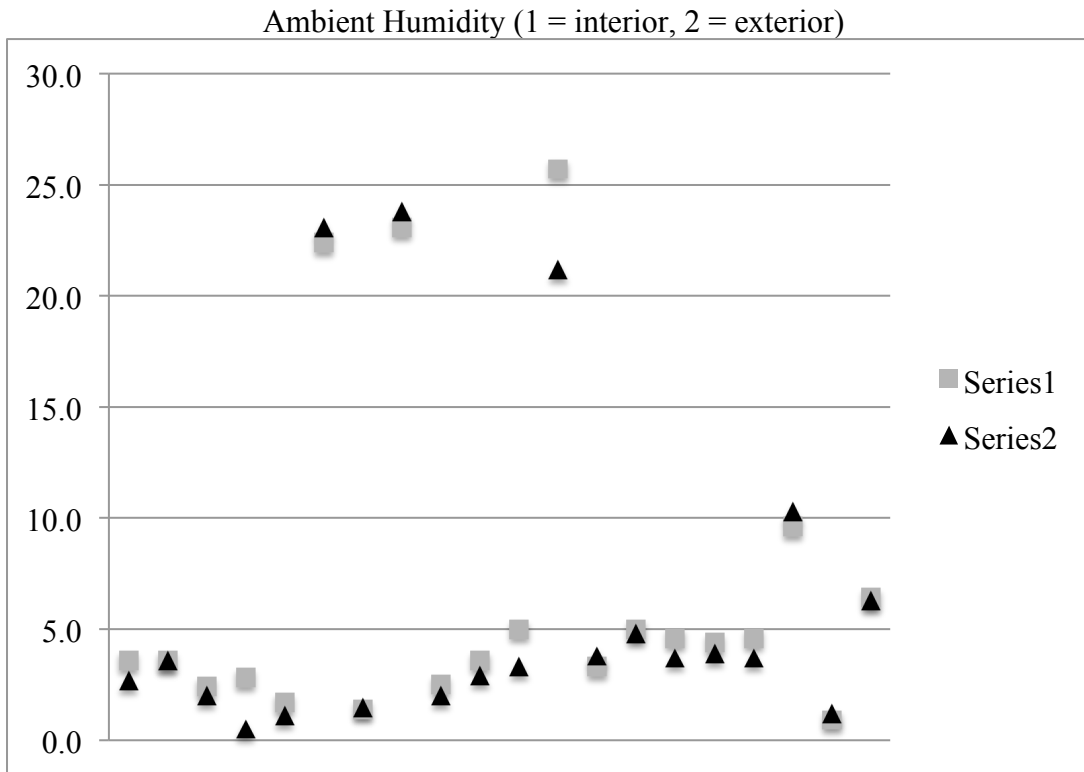
Surface Temperature (1 = interior, 2 = exterior)



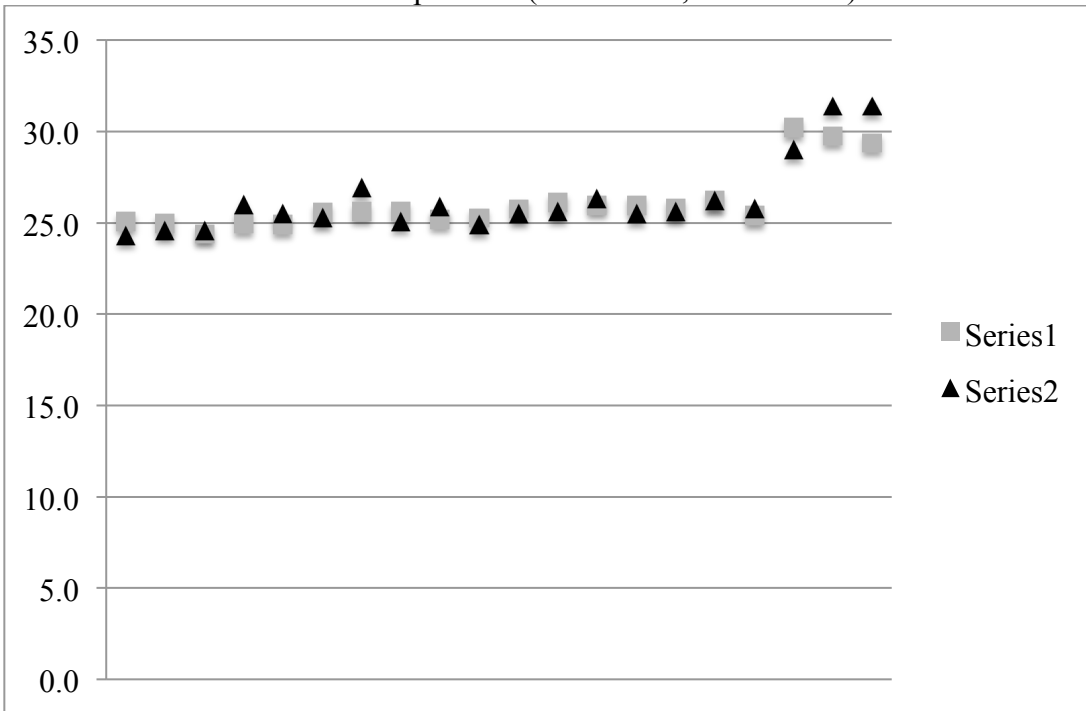
Ceiling (1) vs. Floor (2) Surface Temperatures



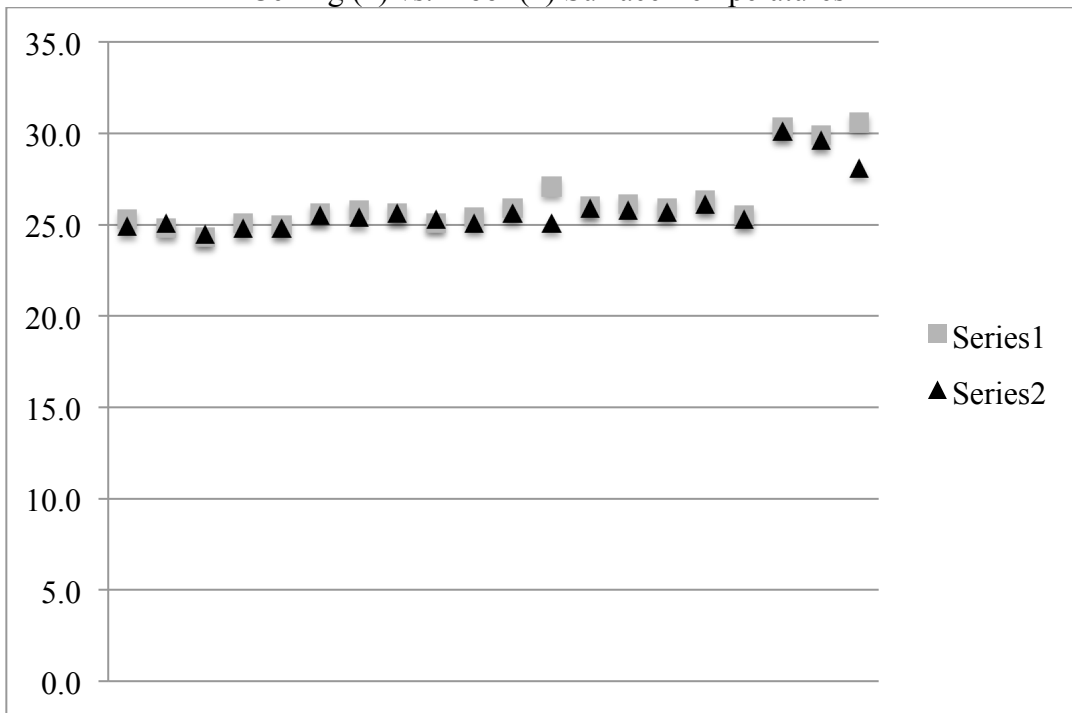
C.4 – Internal and external microclimatic readings per aspect: North



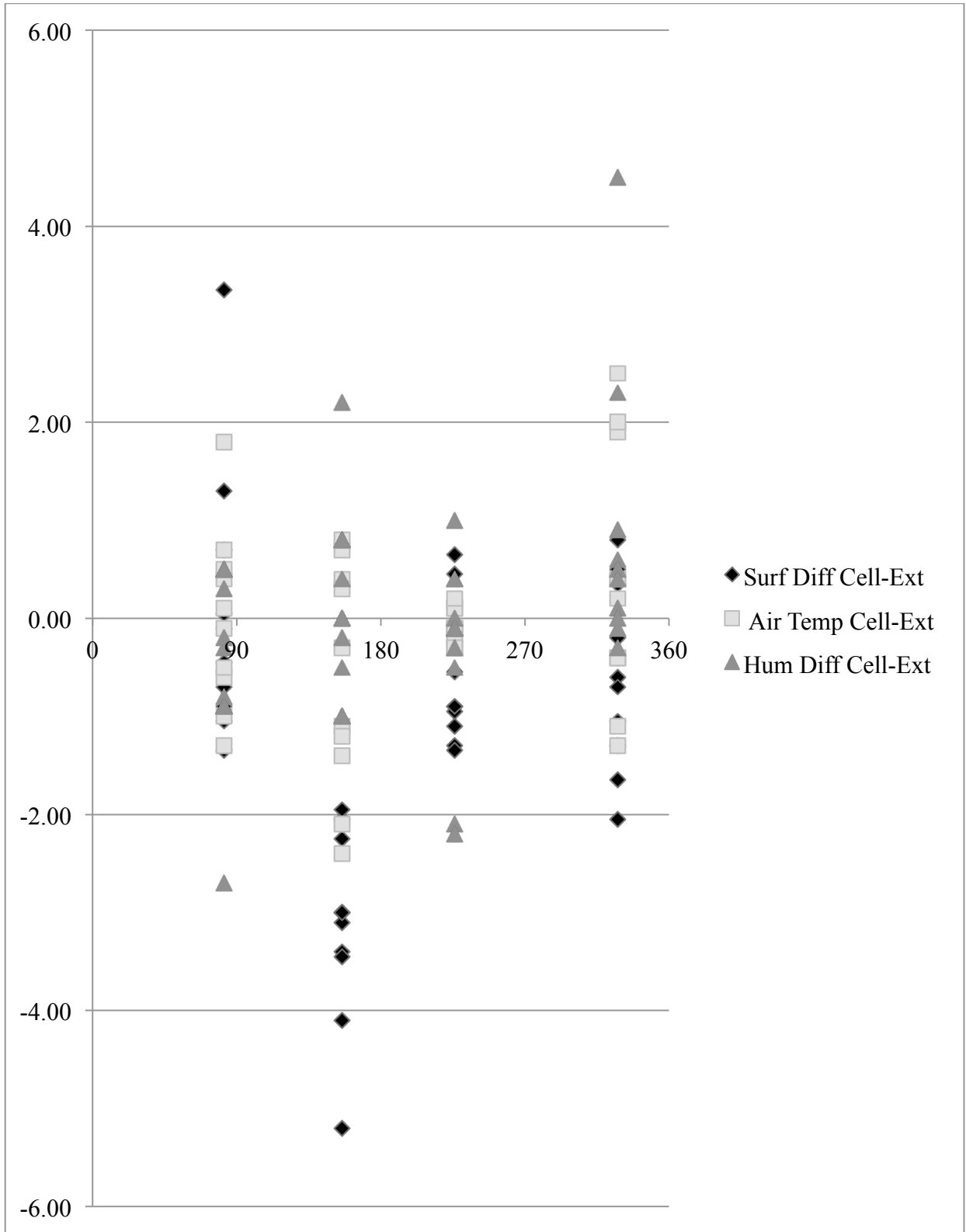
Surface Temperature (1 = interior, 2 = exterior)



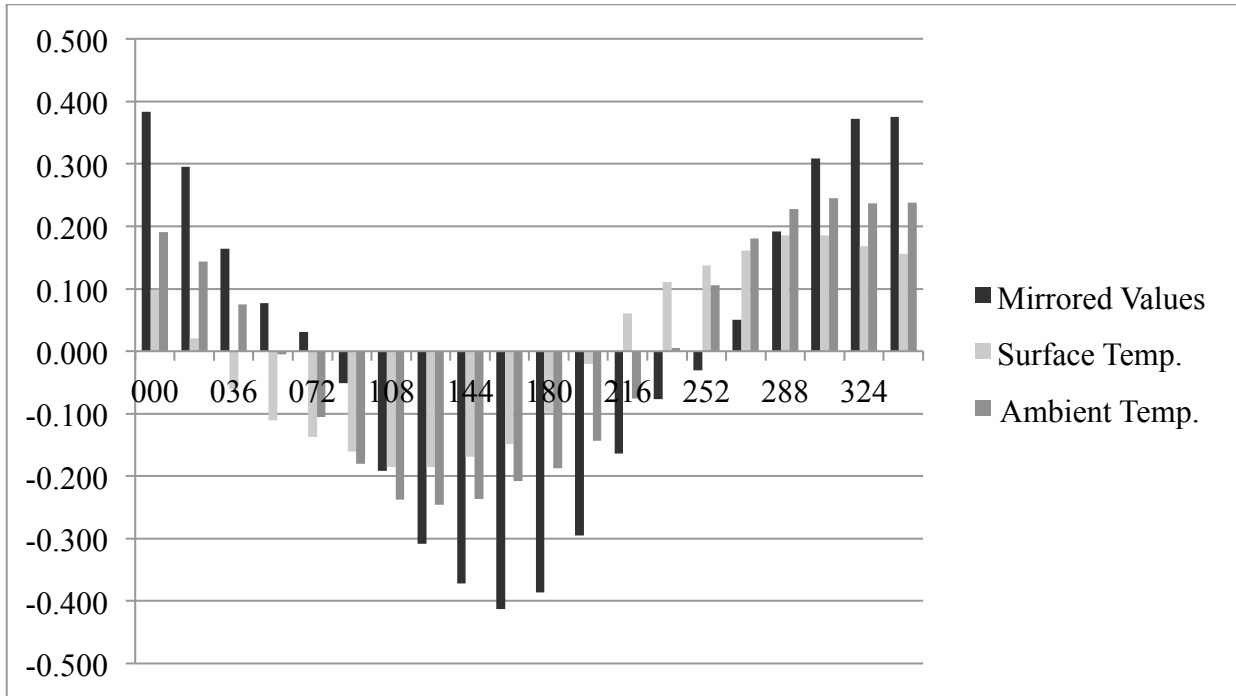
Ceiling (1) vs. Floor (2) Surface Temperatures



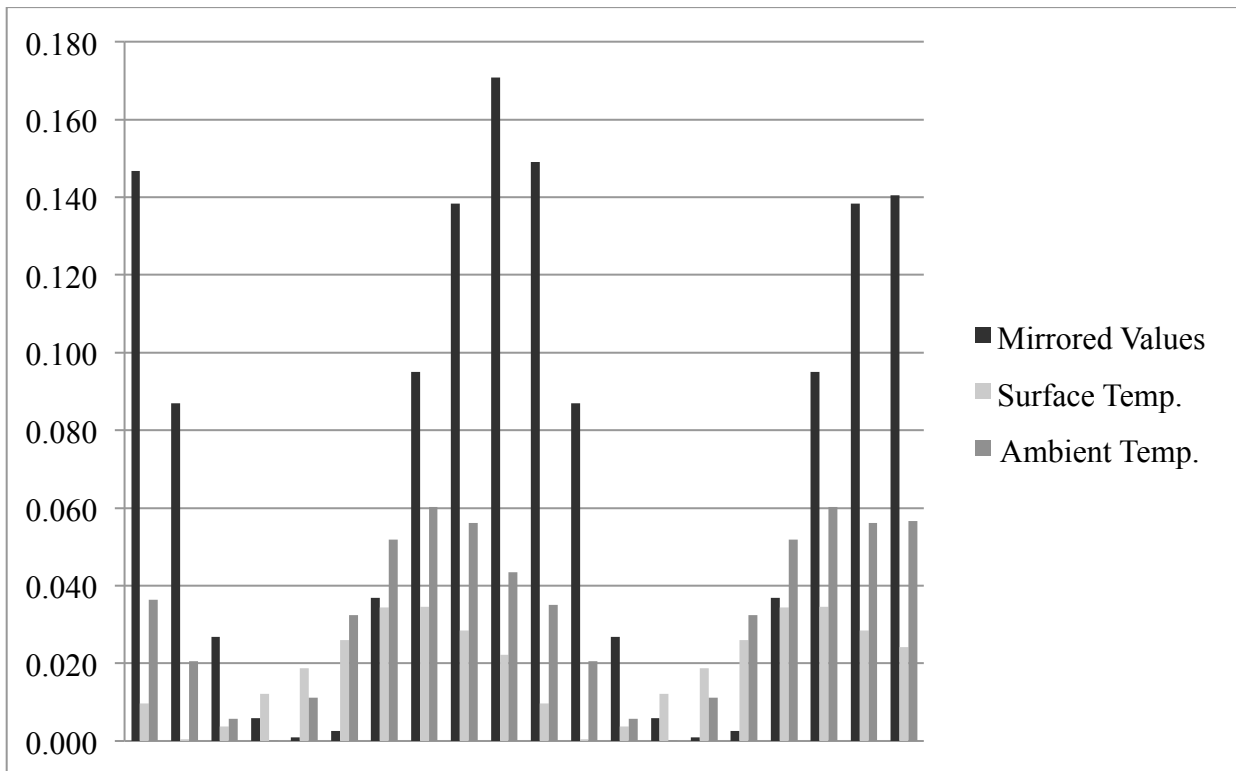
C.5 – Distribution of Micrometeorological measurements:



C.6: Micrometeorological correlations in relation to each other:



C.6: Micrometeorological coefficients of determination in relation to each other:



Appendix D – Field Matrices

D.1: Front of sheet 1:

| Panel Aspect | Cell Panel | Cell Quad | Cell Type | Hood | Cell Dimensions in mm (if > 2 mm) | | | | Inner Cell in mm (if different/hooded) | | | | | | | | | |
|--------------|------------|-----------|-----------|------|-----------------------------------|-----------|------------|------------|--|-------|-----------|------------|------------|------------|-------|--|--|------|
| | | | | | Depth | Long Axis | Short Axis | Vert. Axis | Horz. Axis | Circ. | Long Axis | Short Axis | Vert. Axis | Horz. Axis | Circ. | | | |
| | 8 | 3 | D-0 | N | 3.5 | 4.4 | 2.1 | 4.4 | 3.2 | | | | | | | | | |
| | | | I-C | N | 3.2 | 7.4 | 3.4 | 6.4 | 5.9 | | | | | | | | | |
| | | | D-C | N | 4.2 | 3.4 | 3.0 | 3.0 | 3.4 | | | | | | | | | |
| | | | D-0 | Y | 4.7 | 5.8 | 3.3 | 3.6 | 5.6 | | | | | | | | | |
| | | | D-C | N | 3.2 | 3.7 | 2.3 | 2.4 | 3.6 | | | | | | | | | |
| | | | D-0 | Y | 4.6 | 4.9 | 2.9 | 3.2 | 4.4 | | | | | | | | | |
| | | | D-C | N | 3.5 | 3.0 | 2.0 | 2.5 | 2.3 | | | | | | | | | |
| | | | D-C | N | 2.7 | 4.7 | 2.6 | 2.6 | 4.7 | | | | | | | | | |
| | | | D-C | N | 3.1 | 3.9 | 2.9 | 3.4 | 3.7 | | | | | | | | | |
| | | | I-D | N | 4.7 | 4.1 | 2.4 | 4.1 | 2.4 | | | | | | | | | |
| | | | I-D | N | 5.7 | 5.9 | 5.0 | 5.9 | 5.0 | | | | | | | | | |
| | | | D-C | N | 2.3 | 3.4 | 2.1 | 3.4 | 2.1 | | | | | | | | | |
| | | | D-C | N | 2.1 | 3.4 | 2.3 | 3.4 | 2.3 | | | | | | | | | |
| | | | I-C | Y | 18.5 | 16.4 | 8.6 | 16.4 | 13.1 | | | 26.3 | 11.2 | 11.2 | 26.3 | | | |
| | | | I-D | N | 3.1 | 6.7 | 1.8 | 6.7 | 2.4 | | | | | | | | | |
| | | | I-C | N | 7.1 | 14.6 | 4.0 | 14.6 | 4.8 | | | | | | | | | |
| | | | I-C | Y | 9.3 | 14.4 | 6.5 | 14.4 | 7.4 | | | 11.3 | 10.5 | 11.3 | 10.5 | | | 10.8 |
| | | | I-D | N | 5.3 | 11.4 | 4.0 | 11.4 | 4.0 | | | | | | | | | |
| | | | I-B | N | 2.8 | 7.0 | 4.5 | 5.6 | 4.5 | | | | | | | | | |
| | | | D-C | N | 6.0 | 8.4 | 6.1 | 8.4 | 6.1 | | | | | | | | | |
| | | | D-C | N | 1.8 | 4.9 | 2.3 | 4.9 | 2.3 | | | | | | | | | |
| | | | I-B | N | 18.8 | 12.6 | 7.4 | 12.6 | 7.4 | | | | | | | | | |
| | | | D-0 | N | 4.4 | 5.6 | 2.8 | 5.6 | 2.8 | | | | | | | | | |
| | | | D-A | N | 3.8 | 5.6 | 4.3 | 5.4 | 4.3 | | | | | | | | | |
| | | | I-C | N | 16.1 | 54.4 | 14.3 | 20.1 | 54.4 | | | | | | | | | |

D.3: Front of sheet 2:

| Panel Aspect | Cell Panel | Cell Quad | Cell Type | Hood | Cell Dimensions in mm (if > 2 mm) | | | | Inner Cell in mm (if different/hooded) | | | | | | | | |
|--------------|------------|-----------|-----------|------|-----------------------------------|-----------|------------|------------|--|-------|-----------|------------|------------|------------|-------|--|--|
| | | | | | Depth | Long Axis | Short Axis | Vert. Axis | Horz. Axis | Circ. | Long Axis | Short Axis | Vert. Axis | Horz. Axis | Circ. | | |
| | Z | V | D-O | N | 4.2 | 9.5 | 3.7 | 3.7 | 9.3 | | | | | | | | |
| | | | D-C | N | 5.3 | 3.8 | 2.5 | 3.1 | 3.0 | | | | | | | | |
| | | | D-C | N | 5.1 | 4.4 | 2.0 | 2.3 | 3.9 | | | | | | | | |
| | | | D-C | N | 2.2 | 5.1 | 2.9 | 5.4 | 2.9 | | | | | | | | |
| | | | D-C | N | 2.0 | 3.4 | 2.1 | 3.4 | 2.1 | | | | | | | | |
| | | | D-C | N | 1.8 | 2.2 | 2.1 | 2.2 | 2.1 | | | | | | | | |
| | Z | L-B | D-C | Y | 52.8 | 27.3 | 11.4 | 27.3 | 11.4 | | | 52.0 | 39.4 | 39.4 | 52.0 | | |
| | | | D-O | Y | 36.0 | 29.4 | 17.2 | 28.1 | 17.8 | | | 30.0 | 24.1 | 30.0 | 24.1 | | |
| | | | I-C | Y | 22.7 | 30.4 | 20.2 | 20.2 | 27.1 | | | 28.7 | 31.5 | 31.5 | 28.7 | | |
| | | | I-C | N | 20.8 | 30.5 | 8.4 | 30.5 | 16.3 | | | | | | | | |
| | | | D-C | Y | 25.2 | 15.6 | 11.0 | 11.0 | 15.6 | | | 18.6 | 17.3 | 17.3 | 18.6 | | |
| | | | I-C | N | 11.7 | 29.6 | 16.2 | 27.9 | 16.6 | | | | | | | | |
| | | | I-C | N | 19.2 | 39.2 | 10.3 | 15.9 | 32.8 | | | | | | | | |
| | | | D-C | Y | 12.9 | 11.4 | 10.2 | 11.4 | 10.2 | | | 11.0 | 6.5 | 11.0 | 6.5 | | |
| | | | D-C | N | 14.9 | 15.0 | 9.6 | 9.6 | 19.0 | | | | | | | | |
| | Z | L-S | D-C | N | 8.3 | 8.8 | 7.2 | 8.7 | 8.8 | | | | | | | | |
| | | | D-C | N | 3.3 | 2.4 | 1.8 | 2.4 | 1.8 | | | | | | | | |
| | | | D-C | N | 3.8 | 2.6 | 1.9 | 2.6 | 1.9 | | | | | | | | |
| | | | D-C | Y | 3.7 | 2.8 | 2.0 | 2.8 | 2.0 | | | too small | | | | | |
| | | | D-C | Y | 2.4 | 2.4 | 1.7 | 2.4 | 1.7 | | | too small | | | | | |
| | | | D-C | N | 2.5 | 2.1 | 1.8 | 2.1 | 1.8 | | | | | | | | |
| | | | D-C | Y | 4.1 | 2.3 | 1.6 | 2.3 | 1.6 | | | too small | | | | | |
| | | | D-C | N | 2.5 | 2.2 | 2.0 | 2.2 | 2.0 | | | | | | | | |
| | | | D-C | Y | 2.8 | 2.3 | 1.7 | 2.3 | 1.7 | | | too small | | | | | |
| | | | D-C | Y | 3.8 | 2.9 | 1.6 | 2.9 | 1.6 | | | too small | | | | | |
| | | | D-C | Y | 2.7 | 2.4 | 2.4 | 2.4 | 2.4 | | | too small | | | | | |
| | Z | V | D-C | N | 5.1 | 7.9 | 2.7 | 7.8 | 2.7 | | | | | | | | |
| | Z | L-B | D-C | Y | 36.5 | 23.8 | 12.6 | 14.0 | 21.7 | | | 48.7 | 19.8 | 15.8 | 98.7 | | |
| | | | D-P | N | 5.6 | 19.2 | 11.9 | 14.2 | 17.3 | | | | | | | | |
| | | | D-P | N | 7.7 | 39.6 | 19.9 | 19.9 | 39.6 | | | | | | | | |
| | | | D-O | N | 6.1 | 2.4 | 3.2 | 3.2 | 7.1 | | | | | | | | |
| | | | D-O | Y | 7.2 | 7.4 | 4.4 | 4.4 | 7.4 | | | | | | | | |
| | | | I-C | Y | 14.5 | 11.5 | 6.2 | 11.5 | 6.2 | | | 13.2 | 10.2 | 10.2 | 13.2 | | |
| | | | D-C | Y | 11.8 | 9.9 | 7.6 | 9.6 | 7.6 | | | 10.9 | 6.6 | 10.9 | 6.6 | | |

D.4: Back of sheet 2:

| Est. Volume (mm ³) Min/Max | Microclimates in °C and % humidity | | | | | Cont. T Surf. | Cont. T Air | Cont. Hum | Time (24:00) | Comments and Notes |
|---|------------------------------------|-------|------|------|-----|------------------|----------------|--------------|-----------------|--------------------|
| | Rqof | Floor | Cell | Hum | Hum | | | | | |
| | 24.1 | 24.3 | 28.9 | 10.0 | | 24.0 | 27.2 | 10.3 | 8:02 | |
| | 24.0 | 24.3 | 32.0 | 8.7 | | 23.9 | 31.4 | 7.7 | 8:05 | |
| | 24.6 | 24.7 | 32.7 | 6.3 | | 24.1 | 32.3 | 3.6 | 8:07 | |
| | 24.9 | 25.1 | 31.4 | 7.9 | | 24.1 | 31.3 | 7.8 | 8:10 | |
| | 25.1 | 25.1 | 32.5 | 6.1 | | 25.0 | 32.1 | 6.9 | 8:12 | |
| | 25.2 | 25.0 | 34.4 | 4.8 | | 25.0 | 32.7 | 5.8 | 8:13 | |
| | 25.3 | 24.9 | 34.4 | 3.6 | | 24.3 | 35.5 | 2.7 | 8:19 | |
| | 24.8 | 25.1 | 33.3 | 3.6 | | 24.6 | 31.4 | 3.6 | 8:22 | |
| | 24.3 | 24.5 | 34.2 | 2.4 | | 24.6 | 33.8 | 2.0 | 8:25 | |
| | 25.1 | 24.8 | 35.6 | 2.8 | | 26.0 | 35.2 | 0.5 | 8:27 | |
| | 25.0 | 24.9 | 35.6 | 1.7 | | 25.8 | 35.4 | 1.1 | 8:30 | |
| | 25.8 | 25.4 | 35.0 | 1.4 | | 26.9 | 35.4 | 1.5 | 8:33 | |
| | 25.7 | 25.3 | 35.2 | 2.5 | | 25.9 | 34.7 | 2.0 | 8:35 | |
| | 25.1 | 25.3 | 32.5 | 1.8 | | 25.5 | 32.7 | 1.8 | 8:39 | |
| | 25.3 | 25.1 | 29.8 | 4.4 | | 25.6 | 30.1 | 2.6 | 8:40 | |
| | 25.6 | 25.6 | 32.9 | 2.6 | | 25.4 | 31.8 | 2.3 | 8:42 | |
| | 25.4 | 25.1 | 28.4 | 3.6 | | 24.9 | 28.6 | 2.9 | 8:45 | |
| | 25.4 | 25.0 | 30.2 | 2.2 | | 24.7 | 27.3 | 1.5 | 8:47 | |
| | 25.8 | 25.8 | 29.3 | 3.9 | | 25.1 | 28.1 | 2.4 | 8:50 | |
| | 25.9 | 25.6 | 29.8 | 5.0 | | 25.5 | 29.7 | 3.3 | 8:52 | |
| | 26.0 | 25.9 | 27.6 | 3.3 | | 26.3 | 27.6 | 3.8 | 8:55 | |
| | 26.1 | 25.8 | 27.7 | 5.0 | | 26.0 | 27.5 | 4.8 | 8:57 | |
| | 25.9 | 25.7 | 27.5 | 4.6 | | 25.6 | 27.6 | 3.7 | 8:59 | |
| | 26.3 | 26.1 | 27.9 | 4.4 | | 26.2 | 27.9 | 3.9 | 9:02 | |
| | 26.1 | 25.9 | 27.9 | 4.5 | | 26.1 | 27.8 | 4.9 | 9:04 | |
| | 25.5 | 25.3 | 27.6 | 4.6 | | 25.8 | 27.6 | 3.7 | 9:07 | |
| | 24.1 | 25.3 | 28.0 | 3.0 | | 25.7 | 28.0 | 3.0 | 9:07 | |
| | 24.8 | 25.8 | 30.4 | 3.3 | | 26.4 | 30.2 | 5.5 | 9:21 | |
| | 26.9 | 25.8 | 28.9 | 3.3 | | 25.7 | 29.2 | 2.3 | 9:24 | |
| | 26.8 | 25.3 | 28.8 | 3.6 | | 25.4 | 28.9 | 4.1 | 9:26 | |
| | 26.4 | 26.0 | 28.2 | 4.3 | | 25.9 | 28.0 | 4.8 | 9:27 | |
| | 26.3 | 25.8 | 28.4 | 4.5 | | 25.5 | 28.3 | 4.6 | 9:30 | |
| | 24.4 | 25.1 | 29.1 | 4.0 | | 20.7 | 29.2 | 6.1 | 9:32 | |
| | 26.0 | 25.8 | 27.7 | 3.1 | | 26.6 | 27.8 | 4.0 | 9:36 | |

D.5: Front of sheet 3:

| Panel Aspect | Cell Panel | Cell Quad | Cell Type | Hood | Cell Dimensions in mm (if > 2 mm) | | | | Inner Cell in mm (if different/hooded) | | | | | | |
|--------------|------------|-----------|-----------|------|-----------------------------------|-----------|------------|------------|--|-------|-----------|------------------------------|-----------------------|------------------|-------|
| | | | | | Depth | Long Axis | Short Axis | Vert. Axis | Horz. Axis | Circ. | Long Axis | Short Axis | Vert. Axis | Horz. Axis | Circ. |
| | 3 | L-B | D-C | Y | 10.3 | 8.5 | 5.9 | 6.8 | 7.1 | - | 11.9 | 8.2 | 11.9 | 8.2 | - |
| | | ↓ | D-C | N | 5.4 | 7.6 | 4.8 | 4.8 | 7.6 | - | | | | | |
| | 3 | L-S | D-C | N | 5.0 | 7.7 | 3.6 | 3.6 | 7.7 | - | | | | | |
| | | ↓ | D-C | N | 1.6 | 2.4 | 1.7 | 2.4 | 1.7 | - | | | | | |
| | | ↓ | D-C | N | 3.0 | 2.4 | 1.8 | 2.4 | 1.8 | - | | | | | |
| | | ↓ | D-C | Y | 2.9 | 2.4 | 1.7 | 2.4 | 1.7 | - | | | | | |
| | | ↓ | D-C | Y | 3.6 | 3.0 | 2.5 | 3.0 | 2.5 | - | | too small | turned up | turned left | |
| | | ↓ | D-C | Y | 3.1 | 2.4 | 1.6 | 2.4 | 1.6 | - | | too small | turned left | turned left | |
| | | ↓ | D-C | N | 3.0 | 2.6 | 2.0 | 2.6 | 2.0 | - | | | | | |
| | | ↓ | D-C | Y | 4.2 | 1.9 | 1.7 | 1.9 | 1.7 | - | | WAY | too small - turned up | turned up | |
| | | ↓ | D-C | Y | 3.7 | 2.1 | 2.0 | 2.0 | 2.1 | - | | | | | |
| | | ↓ | D-C | Y | 3.2 | 2.4 | 2.0 | 2.4 | 2.0 | - | | | | | |
| | | ↓ | D-C | N | 2.4 | 1.9 | 1.8 | 1.9 | 1.8 | - | | | | | |
| | 4 | L-B | I-C | Y | 22.4 | 13.3 | 5.6 | 12.8 | 5.6 | - | 24.7 | 21.1 | 21.1 | 24.7 | |
| | | ↓ | I-C | Y | 17.9 | 9.2 | 5.9 | 5.9 | 9.2 | - | 17.6 | 8.9 | 8.9 | 17.6 | |
| | | ↓ | I-C | Y | 28.4 | 15.4 | 7.0 | 13.2 | 14.1 | - | 34.8 | 19.2 | 19.2 | 34.8 | |
| | | ↓ | D-O | N | 8.6 | 11.6 | 5.2 | 5.2 | 11.6 | - | | | | | |
| | | ↓ | D-C | Y | 22.7 | 9.0 | 7.5 | 7.6 | 7.6 | - | 16.7 | 13.2 | 13.2 | 16.7 | |
| | | ↓ | D-O | N | 5.2 | 10.5 | 5.9 | 5.9 | 10.5 | - | | | | | |
| | | ↓ | D-C | Y | 13.9 | 7.2 | 5.2 | 5.2 | 7.2 | - | 11.9 | 7.0 | 7.0 | 11.9 | |
| | | ↓ | I-C | Y | 28.4 | 9.2 | 7.9 | 7.9 | 9.2 | - | | | | | |
| | | ↓ | I-C | Y | 26.9 | 10.9 | 7.0 | 10.9 | 7.6 | - | | | | | |
| | | ↓ | I-C | Y | 31.5 | 15.6 | 6.7 | 13.4 | 8.1 | - | | | | | |
| | 4 | L-S | D-C | Y | 3.0 | 2.5 | 2.2 | 2.2 | 2.5 | - | | | | | |
| | | ↓ | D-C | N | 1.6 | 1.6 | 1.5 | 1.5 | 1.6 | - | | | | | |
| | | ↓ | D-C | Y | 4.2 | 2.2 | 1.7 | 1.7 | 2.2 | - | | too small - turned left | turned left | turned left | |
| | | ↓ | D-C | Y | 2.9 | 1.9 | 1.7 | 1.7 | 1.7 | - | | too small - turned up + left | turned up + left | turned up + left | |
| | | ↓ | D-C | Y | 3.3 | 1.8 | 1.5 | 1.8 | 1.5 | - | | too small - turned up + left | turned up + left | turned up + left | |
| | | ↓ | D-C | Y | 3.1 | 1.8 | 1.7 | 1.8 | 1.7 | - | | too small - turned up | turned up | turned up | |
| | | ↓ | D-C | N | 3.1 | 2.1 | 1.5 | 2.1 | 1.5 | - | | | | | |
| | | ↓ | D-C | N | 3.4 | 1.9 | 1.8 | 1.7 | 1.8 | - | | | | | |
| | | ↓ | D-C | Y | 3.8 | 1.8 | 1.6 | 1.8 | 1.6 | - | | too small - turned up | turned up | turned up | |
| | | ↓ | D-C | N | 3.8 | 1.8 | 1.5 | 1.8 | 1.5 | - | | | | | |

Panel 2
Panel 1

D.6: Back of sheet 3:

| Est. Volume (mm ³) | Microclimates in °C and % humidity | | | Cont. T | | Cont. Hum | Time (24:00) | Comments and Notes |
|--------------------------------|------------------------------------|-------|------|---------|-------|-----------|--------------|--------------------|
| | Roof | Floor | Cell | Hum | Surf. | | | |
| Min/Max | | | | | | | | |
| | 25.7 | 26.0 | 28.7 | 4.9 | 26.3 | 28.8 | 9:40 | |
| | 26.3 | 26.1 | 29.7 | 2.7 | 24.9 | 27.2 | 9:42 | |
| | 26.3 | 25.9 | 28.8 | 2.6 | 26.1 | 28.7 | 9:44 | |
| | 26.2 | 26.1 | 28.9 | 2.4 | 25.0 | 28.7 | 9:46 | |
| | 26.3 | 25.7 | 28.4 | 2.8 | 25.5 | 28.4 | 9:49 | |
| | 26.7 | 26.4 | 28.6 | 2.4 | 26.1 | 28.4 | 9:50 | |
| | 26.6 | 26.3 | 28.5 | 2.5 | 25.8 | 28.3 | 9:52 | |
| | 26.7 | 26.4 | 29.1 | 3.3 | 28.8 | 28.9 | 9:54 | |
| | 26.9 | 26.5 | 28.4 | 1.9 | 26.1 | 28.3 | 9:56 | |
| | 26.8 | 26.6 | 28.3 | 1.5 | 26.4 | 28.3 | 9:59 | |
| | 26.9 | 26.7 | 28.8 | 0.9 | 26.6 | 28.6 | 10:00 | |
| | 27.0 | 26.8 | 28.9 | 1.4 | 26.5 | 28.8 | 10:02 | |
| | 26.6 | 26.3 | 28.1 | 2.4 | 25.9 | 28.4 | 10:05 | |
| | 26.6 | 26.4 | 28.9 | 2.1 | 27.8 | 28.8 | 10:12 | |
| | 26.9 | 26.8 | 28.6 | 2.8 | 26.9 | 28.7 | 10:15 | |
| | 26.9 | 26.9 | 29.1 | 4.2 | 27.8 | 28.2 | 10:17 | |
| | 27.3 | 26.6 | 29.1 | 3.5 | 27.1 | 28.8 | 10:20 | |
| | 27.0 | 27.4 | 28.4 | 4.2 | 27.1 | 28.6 | 10:24 | |
| | 27.4 | 27.2 | 28.2 | 4.4 | 26.7 | 28.4 | 10:27 | |
| | 26.9 | 27.1 | 28.7 | 4.3 | 27.4 | 28.2 | 10:30 | turned left |
| | 27.9 | 27.6 | 28.6 | 5.1 | 28.3 | 28.7 | 10:32 | can't reach inside |
| | 27.7 | 27.1 | 29.1 | 4.8 | 29.3 | 29.4 | 10:35 | can't reach inside |
| | 27.3 | 26.6 | 28.9 | 4.8 | 28.3 | 28.8 | 10:37 | can't reach inside |
| | 26.9 | 27.0 | 28.7 | 5.8 | 26.8 | 28.4 | 10:45 | turned up + left |
| | 27.1 | 26.9 | 28.6 | 6.9 | 26.2 | 28.5 | 10:47 | |
| | 26.9 | 26.8 | 28.3 | 7.4 | 26.3 | 28.4 | 10:51 | turned left |
| | 27.2 | 26.9 | 28.7 | 7.0 | 27.1 | 28.5 | 10:54 | |
| | 27.1 | 26.8 | 28.4 | 7.7 | 26.6 | 28.1 | 10:56 | |
| | 27.3 | 27.0 | 29.2 | 7.2 | 26.6 | 28.1 | 11:00 | |
| | 26.7 | 28.4 | 29.3 | 6.9 | 28.4 | 28.7 | 11:02 | |
| | 28.6 | 28.6 | 29.0 | 5.3 | 29.2 | 28.9 | 11:05 | |
| | 28.7 | 29.3 | 29.3 | 6.4 | 28.6 | 29.0 | 11:08 | |
| | 29.3 | 28.9 | 29.6 | 6.5 | 29.5 | 29.2 | 11:11 | |

D.7: Front of sheet 4:

| Panel Aspect | Cell Panel | Cell Quad | Cell Type | Hood | Cell Dimensions in mm (if > 2 mm) | | | | Inner Cell in mm (if different/hooded) | | | | | | | |
|--------------|------------|-----------|-----------|------|-----------------------------------|-----------|------------|------------|--|-------|-----------|------------|------------|------------|-------|---|
| | | | | | Depth | Long Axis | Short Axis | Vert. Axis | Horz. Axis | Circ. | Long Axis | Short Axis | Vert. Axis | Horz. Axis | Circ. | |
| | 5 | L-B | D-O | N | 13.6 | 20.5 | 7.9 | 20.5 | 7.9 | - | - | - | - | - | | |
| | | | I-C | N | 17.7 | 35.2 | 17.2 | 35.2 | 17.2 | - | - | - | - | - | | |
| | | | I-C | N | 10.0 | 32.0 | 11.4 | 32.0 | 11.4 | - | - | - | - | - | | |
| | | | I-C | Y | 15.8 | 22.2 | 9.2 | 22.2 | 9.2 | - | - | 23.2 | 18.7 | 23.2 | 19.7 | - |
| | | | I-C | N | 30.2 | 75.8 | 40.1 | 75.8 | 40.1 | - | - | - | - | - | - | - |
| | | | I-C | N | 25.2 | 134.2 | 25.3 | 134.2 | 25.3 | - | - | - | - | - | - | - |
| | | | I-C | N | 13.8 | 25.0 | 11.2 | 25.0 | 11.2 | - | - | - | - | - | - | - |
| | | | I-C | Y | 17.6 | 26.9 | 10.2 | 26.9 | 10.2 | - | - | 28.5 | 11.4 | 28.5 | 11.4 | - |
| | | | D-O | N | 14.8 | 24.1 | 12.2 | 24.1 | 12.2 | - | - | - | - | - | - | - |
| | | | D-O | N | 14.6 | 21.4 | 9.6 | 21.4 | 9.6 | - | - | - | - | - | - | - |
| | | | D-O | N | 3.1 | 2.2 | 1.6 | 2.2 | 1.6 | - | - | - | - | - | - | - |
| | | | D-C | N | 3.2 | 3.4 | 1.9 | 3.4 | 1.9 | - | - | - | - | - | - | - |
| | | | D-O | N | 2.3 | 3.7 | 1.7 | 3.7 | 1.7 | - | - | - | - | - | - | - |
| | | | D-O | N | 2.2 | 4.1 | 2.3 | 4.1 | 2.3 | - | - | - | - | - | - | - |
| | | | D-C | N | 1.6 | 2.8 | 2.1 | 2.8 | 2.1 | - | - | - | - | - | - | - |
| | | | D-C | N | 2.3 | 4.9 | 2.9 | 4.9 | 2.9 | - | - | - | - | - | - | - |
| | | | D-O | N | 2.9 | 5.3 | 1.6 | 5.3 | 1.6 | - | - | - | - | - | - | - |
| | | | D-O | N | 2.3 | 4.8 | 1.7 | 4.8 | 1.7 | - | - | - | - | - | - | - |
| | | | D-C | N | 3.6 | 3.7 | 3.3 | 3.3 | 3.7 | - | - | - | - | - | - | - |
| | | | D-C | N | 3.2 | 4.4 | 4.1 | 4.4 | 4.1 | - | - | - | - | - | - | - |
| | | | D-C | N | 10.5 | 31.9 | 14.7 | 31.9 | 14.7 | - | - | - | - | - | - | - |
| | 6 | I-A | I-B | N | 14.4 | 29.5 | 7.9 | 29.5 | 7.9 | - | - | 28.0 | - | - | - | - |
| | | | D-O | N | 4.7 | 30.4 | 8.6 | 30.4 | 8.6 | - | - | 30.4 | - | - | - | - |
| | | | D-O | N | 4.4 | 8.2 | 5.1 | 8.2 | 5.1 | - | - | - | - | - | - | - |
| | | | D-C | N | 4.3 | 7.1 | 6.8 | 6.8 | 7.1 | - | - | - | - | - | - | - |
| | | | I-C | N | 3.2 | 14.8 | 5.3 | 14.8 | 5.3 | - | - | - | - | - | - | - |
| | | | I-C | N | 11.3 | 22.7 | 12.1 | 22.7 | 12.1 | - | - | - | - | - | - | - |
| | | | D-C | N | 4.9 | 10.7 | 7.6 | 10.7 | 7.6 | - | - | - | - | - | - | - |
| | | | D-O | N | 3.6 | 7.2 | 3.9 | 7.2 | 3.9 | - | - | - | - | - | - | - |
| | | | I-C | N | 8.1 | 18.4 | 8.0 | 18.4 | 8.0 | - | - | - | - | - | - | - |
| | | | D-O | N | 1.7 | 6.7 | 1.8 | 6.7 | 1.8 | - | - | - | - | - | - | - |
| | | | I-C | N | 3.3 | 7.0 | 2.1 | 7.0 | 2.1 | - | - | - | - | - | - | - |
| | | | D-C | N | 2.2 | 3.7 | 1.9 | 3.7 | 1.9 | - | - | - | - | - | - | - |
| | | | D-C | N | 3.0 | 4.1 | 1.6 | 4.1 | 1.6 | - | - | - | - | - | - | - |

D.8: Back of sheet 4:

| Est. Volume (mm ³) Min/Max | Microclimates in °C and % humidity | | | Cont. T | | Cont. Hum | Time (24:00) | Comments and Notes |
|---|------------------------------------|-------|------|---------|-------|-----------|--------------|-------------------------------|
| | Roof | Floor | Cell | Hum | Surf. | | | |
| | 28.9 | 28.1 | 33.6 | 1.6 | 31.9 | 33.2 | 11:30 | |
| | 29.6 | 27.6 | 35.5 | 1.8 | 31.6 | 35.2 | 11:33 | |
| | 29.6 | 29.1 | 33.9 | 1.5 | 31.3 | 35.1 | 11:35 | |
| | 29.5 | 28.4 | 36.7 | 1.4 | 31.0 | 36.7 | 11:39 | |
| | 32.4 | 28.9 | 38.7 | 0.5 | 32.7 | 38.1 | 11:42 | Roof only Pen |
| | 29.8 | 29.4 | 38.0 | 0.0 | 32.6 | 37.4 | 11:46 | |
| | 30.4 | 29.5 | 39.8 | 0.0 | 33.4 | 40.8 | 11:48 | |
| | 30.4 | 29.4 | 41.1 | 0.9 | 35.1 | 40.4 | 11:53 | |
| | 29.6 | 31.4 | 36.8 | 5.2 | 34.6 | 38.9 | 11:59 | |
| | 29.6 | 29.0 | 33.9 | 4.4 | 32.4 | 36.3 | 12:04 | |
| | 33.9 | 30.3 | 36.0 | 3.5 | 34.6 | 37.4 | 12:12 | |
| | 33.1 | 32.3 | 37.5 | 3.8 | 34.0 | 35.2 | 12:15 | |
| | 34.2 | 33.9 | 37.7 | 2.9 | 34.7 | 37.6 | 12:17 | |
| | 33.6 | 33.4 | 38.2 | 2.7 | 33.9 | 37.8 | 12:19 | |
| | 34.3 | 34.3 | 39.9 | 2.0 | 34.7 | 40.5 | 12:21 | |
| | 33.2 | 34.0 | 38.2 | 1.9 | 33.4 | 38.4 | 12:23 | |
| | 33.4 | 34.0 | 39.7 | 1.3 | 33.7 | 38.7 | 12:26 | |
| | 34.2 | 33.9 | 37.4 | 1.3 | 34.3 | 38.2 | 12:28 | |
| | 35.1 | 34.5 | 37.4 | 1.9 | 35.5 | 38.1 | 12:31 | |
| | 34.6 | 33.8 | 38.9 | 1.9 | 34.8 | 40.1 | 12:32 | |
| | 37.3 | 35.0 | 40.1 | 1.5 | 37.2 | 41.0 | 12:37 | |
| | 35.3 | 38.2 | 35.6 | 3.5 | 37.8 | 35.1 | 12:42 | at content w/ Broken roof |
| | 41.3 | 37.9 | 38.8 | 3.2 | 40.5 | 38.1 | 12:45 | |
| | 43.5 | 39.1 | 40.8 | 2.5 | 41.4 | 40.6 | 12:47 | roof only 1.5cm thick-Exposed |
| | 41.4 | 39.3 | 38.1 | 4.1 | 38.6 | 38.8 | 13:27 | |
| | 38.0 | 36.7 | 36.8 | 3.4 | 37.4 | 37.2 | 13:28 | |
| | 40.3 | 36.0 | 39.8 | 2.9 | 34.8 | 40.3 | 13:30 | |
| | 35.6 | 35.0 | 40.8 | 3.1 | 34.3 | 41.4 | 13:34 | All along content |
| | 35.0 | 34.8 | 35.9 | 2.9 | 34.6 | 39.1 | 13:36 | |
| | 35.1 | 34.2 | 40.6 | 1.8 | 34.6 | 40.2 | 13:39 | |
| | 34.9 | 35.3 | 43.2 | 0.8 | 35.0 | 41.1 | 13:42 | |
| | 35.2 | 34.9 | 44.4 | 0.2 | 34.4 | 43.0 | 13:45 | |
| | 34.1 | 34.8 | 41.2 | 1.3 | 34.8 | 40.8 | 13:47 | |
| | 34.4 | 34.8 | 40.2 | 1.1 | 34.8 | 39.8 | 13:50 | |

D.10: Back of sheet 5:

| Est. Volume (mm ³) Min/Max | Microclimates in °C and % humidity | | | Cont. T | | Cont. Hum | Time (24:00) | Comments and Notes |
|---|------------------------------------|-------|------|---------|------|-----------|--------------|-------------------------------------|
| | Roof | Floor | Cell | Surf. | Air | | | |
| | 34.3 | 34.4 | 40.4 | 2.3 | 35.7 | 31.6 | 13:52 | roof broken |
| | 34.8 | 35.6 | 40.1 | 0.6 | 34.5 | 41.4 | 13:54 | Roof broken on contact |
| | 35.5 | 35.9 | 36.9 | 2.6 | 35.1 | 36.8 | 13:57 | Wear base |
| | 34.4 | 34.3 | 35.7 | 2.9 | 33.9 | 35.7 | 14:00 | |
| | 34.8 | 34.4 | 33.5 | 3.0 | 34.5 | 33.2 | 14:02 | |
| | 34.9 | 34.7 | 31.9 | 4.4 | 34.3 | 32.2 | 14:04 | |
| | 33.6 | 33.3 | 31.7 | 4.1 | 33.1 | 31.8 | 14:06 | |
| | 33.9 | 33.4 | 39.8 | 0.4 | 33.9 | 39.4 | 14:15 | |
| | 29.9 | 29.6 | 39.6 | 0.9 | 31.4 | 37.6 | 14:20 | Broken through to other corner (Pg) |
| | 29.8 | 28.4 | 37.6 | 1.3 | 29.3 | 37.1 | 14:23 | |
| | 31.1 | 30.9 | 39.1 | 0.5 | 30.4 | 39.1 | 14:25 | |
| | 31.0 | 30.6 | 40.9 | 0.0 | 30.2 | 39.5 | 14:29 | |
| | 29.6 | 30.9 | 33.1 | 2.3 | 31.6 | 34.1 | 14:31 | |
| | 25.9 | 25.6 | 30.2 | 17.4 | 25.4 | 32.1 | 8:23 | |
| | 25.5 | 25.2 | 29.6 | 18.2 | 25.1 | 29.1 | 8:25 | |
| | 25.8 | 25.7 | 27.9 | 20.4 | 25.6 | 27.4 | 8:27 | |
| | 25.6 | 25.6 | 26.4 | 21.9 | 24.8 | 26.3 | 8:30 | |
| | 25.8 | 25.5 | 26.3 | 22.4 | 25.3 | 26.3 | 8:31 | |
| | 25.8 | 25.4 | 26.4 | 23.3 | 25.1 | 26.3 | 8:32 | |
| | 25.6 | 25.6 | 25.0 | 23.1 | 25.1 | 25.4 | 8:35 | |
| | 25.7 | 25.6 | 25.9 | 23.4 | 25.1 | 26.2 | 8:36 | |
| | 25.6 | 25.6 | 26.0 | 22.9 | 25.3 | 25.9 | 8:39 | |
| | 25.8 | 25.5 | 27.1 | 21.8 | 25.9 | 27.2 | 8:42 | |
| | 25.8 | 25.6 | 28.2 | 20.8 | 25.2 | 28.1 | 8:45 | |
| | 26.0 | 25.9 | 27.1 | 21.2 | 26.1 | 27.1 | 8:47 | |
| | 25.9 | 25.6 | 26.5 | 21.1 | 25.9 | 27.0 | 8:50 | Broken back wall to bigger cell |
| | 27.1 | 25.1 | 27.1 | 22.7 | 25.6 | 27.5 | 8:55 | |
| | 26.1 | 26.0 | 27.4 | 21.3 | 25.5 | 27.1 | 8:52 | time swap |

D.11: Front of sheet 6:

| Panel Aspect | Cell Panel | Cell Quad | Cell Type | Hood | Cell Dimensions in mm (if > 2 mm) | | | | Inner Cell in mm (if different/hooded) | | | | | | |
|--------------|------------|-----------|-----------|------|-----------------------------------|-----------|------------|------------|--|-------|-----------|------------|------------|------------|-------|
| | | | | | Depth | Long Axis | Short Axis | Vert. Axis | Horz. Axis | Circ. | Long Axis | Short Axis | Vert. Axis | Horz. Axis | Circ. |
| | 8 | 1 | D-O | N | 5.8 | 10.3 | 6.2 | 6.0 | 8.5 | 26.7 | | | | | |
| | 8 | 1 | D-C | N | 5.0 | 4.8 | 4.2 | 4.8 | 4.5 | 16.2 | | | | | |
| | 8 | 1 | D-C | N | 1.8 | 2.3 | 1.7 | 2.0 | 2.3 | 5.5 | | | | | |
| | 8 | 1 | 1-S | N | 1.7 | 7.2 | 2.0 | 2.8 | 7.2 | 8.3 | | | | | |
| | 8 | 1 | D-C | N | 1.6 | 1.9 | 1.8 | 1.9 | 1.8 | 6.0 | | | | | |
| | 8 | 1 | D-O | N | 1.9 | 7.0 | 3.4 | 4.5 | 6.7 | 18.0 | | | | | |
| | 8 | 1 | D-O | Y | 5.8 | 11.2 | 5.2 | 5.2 | 11.2 | 26.1 | 9.0 | 5.8 | 9.0 | 21.7 | |
| | 8 | 1 | 1-C | N | 2.2 | 5.0 | 2.7 | 3.0 | 4.4 | 13.0 | | | | | |
| | 8 | 1 | D-C | N | 1.6 | 2.0 | 1.4 | 1.4 | 2.0 | 5.2 | | | | | |
| | 8 | 1 | D-C | Y | 1.9 | 2.8 | 2.7 | 2.7 | 2.8 | 6.9 | 2.4 | 2.2 | 2.4 | 6.3 | |
| | 8 | 1 | D-C | N | 3.0 | 6.5 | 5.7 | 5.7 | 6.5 | 8.2 | | | | | |
| | 8 | 1 | D-C | N | 3.2 | 5.5 | 3.4 | 4.2 | 5.3 | 3.4 | | | | | |
| | 8 | 1 | D-O | Y | 5.0 | 8.7 | 4.9 | 4.9 | 8.7 | 6.4 | 6.0 | 3.6 | 6.0 | 4.9 | |
| | 8 | 1 | D-C | Y | 2.6 | 4.5 | 2.7 | 4.5 | 2.7 | 10.0 | 4.0 | 3.5 | 4.0 | 3.5 | 10.9 |
| | 8 | 1 | D-C | N | 1.7 | 5.0 | 3.4 | 3.4 | 4.8 | 11.9 | | | | | |
| | 8 | 1 | D-C | Y | 4.4 | 3.5 | 3.4 | 3.4 | 3.5 | 10.5 | 3.6 | 3.5 | 3.6 | 10.4 | |
| | 8 | 1 | D-C | N | 1.7 | 3.1 | 2.7 | 3.7 | 3.1 | 9.2 | | | | | |
| | 8 | 1 | D-C | Y | 13.4 | 9.5 | 7.0 | 8.2 | 6.8 | 23.7 | 8.6 | 8.6 | 5.3 | 31.2 | |
| | 8 | 1 | D-C | N | 2.1 | 6.4 | 4.7 | 6.4 | 4.7 | 19.3 | | | | | |
| | 8 | 1 | D-C | Y | 3.0 | 4.2 | 2.7 | 4.2 | 2.8 | 11.2 | 3.8 | 3.8 | 3.8 | 3.8 | 8.9 |
| | 8 | 1 | D-C | N | 1.5 | 3.8 | 2.7 | 2.7 | 3.8 | 10.2 | | | | | |
| | 8 | 1 | D-C | N | 1.1 | 5.2 | 4.0 | 5.2 | 4.0 | 10.4 | | | | | |
| | 8 | 1 | D-C | N | 1.9 | 5.8 | 3.4 | 5.8 | 3.4 | 13.2 | | | | | |
| | 8 | 1 | D-C | N | 2.5 | 7.9 | 7.4 | 7.9 | 7.4 | 21.8 | | | | | |
| | 8 | 1 | D-O | N | 3.3 | 12.6 | 8.0 | 12.2 | 7.3 | 35.1 | | | | | |
| | 8 | 1 | D-O | W | 4.8 | 9.6 | 5.9 | 9.6 | 5.9 | 23.1 | | | | | |
| | 8 | 1 | D-C | N | 1.5 | 3.1 | 2.0 | 2.0 | 3.0 | 9.9 | | | | | |
| | 8 | 1 | D-C | N | 2.2 | 6.4 | 5.0 | 5.5 | 5.8 | 17.2 | | | | | |
| | 8 | 1 | D-C | N | 1.0 | 2.6 | 2.4 | 2.6 | 2.4 | 7.3 | | | | | |
| | 8 | 2 | D-O | N | 2.8 | 3.3 | 3.4 | 5.0 | 3.6 | 11.8 | | | | | |
| | 8 | 2 | 1-S | N | .7 | 2.8 | 2.6 | 2.6 | 2.8 | 7.3 | | | | | |
| | 8 | 2 | 1-S | N | 1.4 | 5.4 | 2.5 | 3.5 | 5.0 | 12.0 | | | | | |
| | 8 | 2 | 1-S | N | 1.4 | 7.4 | 4.0 | 4.1 | 7.4 | 16.8 | | | | | |
| | 8 | 2 | D-C | N | 1.6 | 2.0 | | | | | | | | | |

D.12: Back of sheet 6:

| Est. Volume (mm ³) | Microclimates in °C and % humidity | | | Cont. T Surf. | Cont. T Air | Cont. Hum | Time (24:00) | Comments and Notes |
|--------------------------------|------------------------------------|------|-------|---------------|-------------|-----------|--------------|-------------------------|
| | Hor/Vert | Roof | Floor | | | | | |
| | | 33.3 | 33.1 | 31.8 | 32.8 | 7.7 | 10:27 | |
| | | 31.7 | 32.0 | 31.6 | 32.8 | 6.8 | 10:36 | |
| | | 33.6 | 33.7 | 32.9 | 33.8 | 6.4 | 10:40 | |
| | | 34.3 | 34.5 | 32.7 | 34.6 | 5.7 | 10:44 | |
| | | 34.7 | 34.7 | 33.9 | 34.7 | 7.0 | 10:48 | |
| | | 33.1 | 33.3 | 31.7 | 32.9 | 5.9 | 10:52 | |
| | | 31.8 | 31.9 | 32.2 | 31.7 | 6.9 | 11:01 | |
| | | 33.5 | 33.6 | 33.9 | 33.8 | 5.5 | 11:05 | |
| | | 34.7 | 34.2 | 33.8 | 34.3 | 4.6 | 11:08 | |
| | | 33.1 | 33.9 | 30.1 | 33.4 | 6.3 | 11:16 | |
| | | 32.3 | 32.6 | 31.3 | 32.5 | 6.1 | 11:20 | |
| | | 32.6 | 32.1 | 31.5 | 32.8 | 6.1 | 11:23 | |
| | | 32.8 | 32.6 | 32.5 | 33.0 | 5.6 | 11:28 | |
| | | 32.9 | 32.6 | 31.3 | 32.8 | 6.4 | 11:33 | |
| | | 32.8 | 32.8 | 32.0 | 32.9 | 6.0 | 11:36 | |
| | | 32.2 | 32.1 | 32.1 | 32.1 | 6.3 | 11:42 | |
| | | 32.3 | 32.4 | 32.8 | 32.6 | 7.1 | 11:46 | |
| | | 31.6 | 31.5 | 32.1 | 32.0 | 6.3 | 11:49 | Cell angled to the left |
| | | 31.9 | 31.6 | 30.7 | 32.1 | 7.1 | 11:56 | |
| | | 32.6 | 32.3 | 32.0 | 32.4 | 6.5 | 12:00 | |
| | | 32.1 | 31.9 | 31.4 | 32.0 | 6.2 | 12:02 | |
| | | 31.9 | 31.9 | 31.8 | 32.2 | 7.0 | 12:06 | |
| | | 32.1 | 31.9 | 33.2 | 32.3 | 5.9 | 12:09 | |
| | | 32.1 | 31.8 | 32.4 | 31.9 | 5.3 | 12:12 | |
| | | 31.6 | 31.3 | 30.8 | 31.7 | 7.8 | 12:18 | |
| | | 31.3 | 31.1 | 31.4 | 31.4 | 7.4 | 12:22 | Cell angled to the left |
| | | 31.6 | 31.5 | 30.7 | 31.8 | 8.2 | 12:27 | |
| | | 31.9 | 31.7 | 30.4 | 31.9 | 8.9 | 12:31 | |
| | | 31.8 | 32.0 | 31.2 | 31.9 | 8.2 | 12:34 | |
| | | 33.1 | 32.8 | 31.6 | 32.6 | 9.3 | 13:27 | |
| | | 32.8 | 32.7 | 31.8 | 32.6 | 9.3 | 13:29 | |
| | | 32.1 | 31.4 | 30.1 | 31.3 | 12.5 | 13:32 | |
| | | 31.6 | 31.4 | 30.2 | 31.6 | 12.8 | 13:35 | |

D.13: Front of sheet 7:

| Panel Aspect | Cell Panel | Cell Quad | Cell Type | Hood | Cell Dimensions in mm (if > 2 mm) | | | | Circ. | Inner Cell in mm (if different/hooded) | | | | | | | | | | |
|--------------|------------|-----------|-----------|------|-----------------------------------|-----------|------------|------------|-------|--|-----------|------------|------------|------------|-------|--|--|--|--|--|
| | | | | | Depth | Long Axis | Short Axis | Vert. Axis | | Horz. Axis | Long Axis | Short Axis | Vert. Axis | Horz. Axis | Circ. | | | | | |
| | 6 | L-A | I-B | N | 8.4 | 26.2 | 6.3 | 6.3 | 26.2 | - | | | | | | | | | | |
| | | | I-B | N | 7.8 | 15.1 | 5.6 | 5.6 | 15.1 | - | | | | | | | | | | |
| | | | D-C | N | 1.5 | 3.1 | 2.0 | 3.1 | 2.0 | - | | | | | | | | | | |
| | | | D-0 | N | 1.6 | 3.7 | 1.8 | 1.8 | 3.7 | - | | | | | | | | | | |
| | | | D-0 | N | 1.5 | 3.4 | 2.2 | 2.2 | 3.4 | - | | | | | | | | | | |
| | | | D-0 | N | 1.1 | 3.3 | 1.8 | 1.8 | 3.3 | - | | | | | | | | | | |
| | | | D-0 | N | 1.1 | 2.9 | 1.8 | 2.9 | 1.8 | - | | | | | | | | | | |
| | | | D-0 | N | 1.1 | 3.3 | 3.3 | 6.9 | 3.3 | - | | | | | | | | | | |
| | 7 | L-A | D-C | N | 2.3 | 6.8 | 3.3 | 3.3 | 6.8 | - | | | | | | | | | | |
| | | | I-C | Y | 51.7 | 41.9 | 30.0 | 30.0 | 35.9 | - | 35.6 | 34.2 | 34.2 | 35.6 | - | | | | | |
| | | | D-0 | N | 14.3 | 13.7 | 5.6 | 13.7 | 5.6 | - | | | | | | | | | | |
| | | | D-C | N | 3.7 | 5.3 | 3.6 | 5.3 | 3.6 | - | | | | | | | | | | |
| | | | D-0 | N | 4.2 | 15.4 | 3.9 | 15.4 | 3.9 | - | | | | | | | | | | |
| | | | D-C | N | 4.2 | 6.5 | 5.4 | 6.5 | 5.4 | - | | | | | | | | | | |
| | | | D-C | N | 3.8 | 5.3 | 4.9 | 4.9 | 5.3 | - | | | | | | | | | | |
| | | | I-D | N | 5.5 | 7.1 | 2.9 | 7.1 | 2.9 | - | | | | | | | | | | |
| | | | D-0 | N | 3.2 | 4.8 | 3.2 | 4.8 | 3.2 | - | | | | | | | | | | |
| | | | D-C | N | 2.2 | 4.9 | 2.3 | 4.9 | 2.3 | - | | | | | | | | | | |
| | | | I-C | N | 2.0 | 5.1 | 1.2 | 5.1 | 1.9 | - | | | | | | | | | | |
| | | | I-B | N | 4.1 | 7.1 | 5.4 | 5.4 | 7.1 | - | | | | | | | | | | |
| | | | D-0 | N | 1.7 | 4.2 | 2.2 | 4.2 | 2.2 | - | | | | | | | | | | |
| | | | I-C | N | 3.2 | 7.2 | 1.9 | 7.2 | 3.1 | - | | | | | | | | | | |
| | | | I-C | N | 3.2 | 5.3 | 1.8 | 5.3 | 1.8 | - | | | | | | | | | | |
| | | | D-0 | N | 3.0 | 8.3 | 2.1 | 8.3 | 2.1 | - | | | | | | | | | | |
| | | | D-0 | N | 3.6 | 6.6 | 3.4 | 6.6 | 3.4 | - | | | | | | | | | | |
| | | | D-0 | N | 4.5 | 11.1 | 2.4 | 11.1 | 2.4 | - | | | | | | | | | | |
| | | | D-0 | Y | 8.2 | 11.3 | 4.4 | 11.3 | 4.4 | - | 11.6 | 5.1 | 11.6 | 5.1 | - | | | | | |
| | | | I-C | N | 26.8 | 99.4 | 15.8 | 99.4 | 26.1 | - | | | | | | | | | | |
| | | | D-C | N | 3.5 | 6.6 | 4.5 | 6.6 | 4.5 | - | | | | | | | | | | |

D.14: Back of sheet 7:

| Est. Volume (mm ³) | Microclimates in °C and % humidity | | | Cont. T Surf. | Cont. T Air | Cont. Hum | Time (24:00) | Comments and Notes |
|--------------------------------|------------------------------------|-------|------|---------------|-------------|-----------|--------------|---------------------------------|
| | Roof | Floor | Cell | | | | | |
| | 32.5 | 31.9 | 31.4 | 32.1 | 32.2 | 89.2 | 13:44 | |
| | 32.1 | 31.5 | 30.6 | 31.3 | 30.7 | 7.3 | 13:47 | |
| | 31.9 | 31.8 | 32.3 | 31.6 | 32.0 | 8.5 | 13:50 | |
| | 31.8 | 31.1 | 32.2 | 31.4 | 31.9 | 8.7 | 13:52 | |
| | 31.6 | 31.3 | 32.3 | 31.1 | 32.1 | 8.9 | 13:55 | |
| | 31.4 | 31.3 | 31.8 | 30.9 | 32.3 | 8.9 | 13:58 | |
| | 31.4 | 31.2 | 30.5 | 30.3 | 31.2 | 9.9 | 14:01 | |
| | 32.7 | 33.4 | 27.7 | 32.8 | 29.6 | 22.2 | 10:47 | |
| | 33.0 | 33.8 | 29.8 | 33.1 | 30.3 | 18.6 | 10:50 | |
| | 32.5 | 32.8 | 31.0 | 32.6 | 30.8 | 17.5 | 10:53 | |
| | 32.9 | 32.7 | 29.3 | 33.4 | 30.8 | 17.8 | 10:56 | |
| | 32.7 | 32.4 | 30.8 | 32.6 | 30.8 | 16.2 | 10:59 | |
| | 33.2 | 32.6 | 30.9 | 33.1 | 31.6 | 16.4 | 11:02 | |
| | 32.3 | 32.7 | 32.3 | 32.9 | 33.3 | 15.1 | 11:05 | |
| | 31.6 | 32.3 | 31.7 | 31.8 | 34.3 | 14.7 | 11:09 | |
| | 33.6 | 34.0 | 32.4 | 33.4 | 30.8 | 15.5 | 11:11 | |
| | 31.3 | 30.8 | 31.9 | 31.0 | 31.2 | 15.6 | 11:15 | |
| | 32.0 | 32.4 | 30.4 | 32.1 | 32.4 | 17.2 | 11:17 | |
| | 32.2 | 32.9 | 29.7 | 32.4 | 30.2 | 18.2 | 11:21 | |
| | 31.4 | 31.1 | 28.8 | 31.4 | 45.4 | 5.7 | 11:27 | |
| | 30.3 | 30.3 | 34.7 | 30.0 | 30.7 | 9.6 | 11:30 | |
| | 31.1 | 30.9 | 34.3 | 30.9 | 34.7 | 12.3 | 11:32 | |
| | 31.2 | 30.9 | 33.7 | 31.7 | 34.3 | 12.7 | 11:35 | |
| | 30.9 | 34.1 | 35.3 | 32.6 | 39.2 | 7.2 | 11:38 | Amul shopped |
| | 30.6 | 30.3 | 40.0 | 31.0 | 38.4 | 7.3 | 11:42 | Hooded but pants were too small |
| | 31.4 | 30.9 | 36.3 | 31.0 | 34.4 | 11.4 | 11:46 | |
| | 30.9 | 30.8 | 35.5 | 30.4 | 37.1 | 12.4 | 11:49 | |
| | 30.6 | 30.1 | 37.8 | 30.3 | 37.4 | 8.7 | 11:51 | |
| | 30.3 | 30.1 | 32.6 | 30.6 | 33.4 | 13.5 | 12:14 | |
| | 29.7 | 20.6 | 38.8 | 29.3 | 35.9 | 9.5 | 12:17 | |
| | 29.6 | 30.6 | 40.8 | 30.8 | 40.0 | 8.5 | 12:19 | |
| | 30.7 | 29.9 | 37.8 | 28.3 | 40.9 | 8.2 | 12:22 | Sabbath in cell |
| | 30.2 | 30.3 | 41.3 | 30.2 | 40.0 | 6.6 | 12:27 | Hooded but pants too small |
| | 30.4 | 30.4 | 47.7 | 30.3 | 43.4 | 5.7 | 12:30 | |